Hydraulic Variable Valve Actuation on a Single Cylinder Engine

by

Mohammad Sharif Siddiqui

A thesis
presented to the University of Waterloo
in fulfillment of the
thesis requirement for the degree of
Masters of Applied Science
in
Mechanical and Mechatronics Engineering

Waterloo, Ontario, Canada, 2017

I hereby declare that I am the sole author of this thesis. This is a true copy of the thesis, including any required final revisions, as accepted by my examiners.

I understand that my thesis may be made electronically available to the public.

Abstract

The combustion characteristics in an engine cylinder can greatly change over a range of speeds and loads. However, conventional engines fix the timing and amount of intake and exhaust, which can lead to higher emissions, wasted fuel, and lower power output. This thesis studies the application of a hydraulics based variable valve actuation system to change the valves' lift and timing on a single cylinder spark ignition engine. In addition to controlling the valve actuation, a hydraulics based design has the advantage of protecting against engine failure in cases of electrical power loss, reverting the system to behave as a conventional camshaft valve train.

The research extends the previous iterations of the hydraulics design to prevent leakage, retain pressure, and reliably open and close the engine valves. A hydraulic cylinder is used to replace the conventional cam where pressurized fluid opens, and spring force closes, the engine valve. The pressurized fluid is supplied to, or removed from, the cylinder using rotary spool valves coupled to the engine crankshaft. Additionally, the system is modelled in Simulink to determine the effect of system pressure, flow area, and spring rate on the resulting valve profile.

After modelling the system's performance for achieving variable lift and timing, the system was designed, manufactured, and tested on a single cylinder engine with the aid of a dynamometer. Experimental results for valve lift showed good agreement with the simulation models. Majority of the tests were performed using manual control, followed by experiments with active control of the system pressure to reach a desired valve lift. The lift controller is able to achieve the desired valve actuation in under 2 seconds with active pressure feedback. Lastly, the ability of the hydraulic variable valve system as a viable alternative is shown by achieving combustion at 1500 RPM engine idle speed.

Acknowledgements

I would like to thank my supervisor Dr. Amir Khajepour for providing guidance and an environment encouraging creativity and responsibility.

I would also like to thank Jeff Graansma and Jeremy Reddekopp for their help in assembling, troubleshooting, and testing of my variable valve project. Their expertise and efficiency is crucial to the success of most projects in our lab. Additionally, I would like to thank Navid Milani and Yangtao Li for their guidance in the design and thesis writing process of my project. I would also like to thank ODG for supplying the equipment needed for this project.

Lastly, I would like to acknowledge my fellow graduate students and researchers in the MVSL. They have always made the lab a friendly and rich learning environment.

Dedication

This thesis is dedicated to my grandmother.

Table of Contents

List of Tables

List of Figures

List of Abbreviations

BDC bottom dead center 5

HVVA hydraulic variable valve actuation 3, 73, 79, 82

RSV rotary spool valve 14

TDC top dead center 5

VVA variable valve actuation 3, 19

VVT variable valve timing 5

List of Symbols

A_{ex} Area of exhaust valve opening[mm^2]. 33

A_p Cushion device hydraulic piston area [m^2]. 31

A_{SV} Spool valve flow area [m^2]. 35

C_p Heat capacity at constant pressure [kJ/kg*K]. 33

C_v Heat capacity at constant volume [kJ/kg*K]. 33

D_1 Inner diameter of cushion device where the hydraulic cylinder moves [mm]. 46

D_2 Outer diameter of hydraulic oil cylinder moving inside the cushion device [mm]. 46

ΔV_a Change in accumulator volume [L]. 48

$F_{damping}$ Cushion device damping force [N]. 31

$F_{friction}$ Friction force [N]. 31

F_{gas} Engine cylinder gas force [N]. 31

$F_{preload}$ Valve spring preload force [N]. 31

K Engine valve spring rate [N/mm]. 31

N_e Engine crankshaft pulley - number of teeth. 26, 27

N_{ps} Phase shifter pulley - number of teeth. 26, 27

N_r Ring gear - number of teeth in planetary gearbox. 27

N_s Sun gear number of teeth in planetary gearbox. 27

P_{1a} Accumulator pre-charge pressure [psi]. 48

P_{2a} System operating pressure [psi]. 48

P_2 Pressure in the hydraulic cylinder [psi]. 31, 36

P_{3a} Maximum system pressure [psi]. 48

P_{cyl} Engine cylinder pressure [psi]. 32

P_{high} High pressure: the maximum allowed pressure in the system, also the working pressure created by the pump and accumulator [psi]. 36

P_{low} Low pressure point of the system, assumed to be atmospheric pressure [psi]. 36

Q_{LHV} Lower heating value for gasoline fuel [MJ/kg]. 35

Q_n Flow rate per valve without the use of an accumulator [gpm]. 46

V_{1a} Pump flow rate with the aid of an accumulator [L/min]. 46

R Gas constant: used in the ideal gas law, also known as the Boltzman constant. 32

T_{cyl} Temperature of engine cylinder gas [K]. 32

T Time for one full engine cycle - 720 CA°[s]. 46

U_{cyl} Internal energy of the cylinder gas. 32

V_{1a} Accumulator initial volume- at pre-charge pressure [L]. 46

V_{cyl} Volume of engine cylinder [m^3]. 32

V_n Hydraulic cylinder volume displaced for one valve cycle [L/valve]. 46

ΔT_f Change in temperature causing valve components to over-constrain [C°]. 22

h_{cyl} Enthalpy of the cylinder gas. 32

κ Ratio of heat capacity at constant pressure (Cp) to heat capacity at constant volume (Cv). 48

l_{rod} Piston rod length [mm]. 32

l_v Engine valve lift distance [mm]. 46

λ_l Lead angle of worm gear [deg]. 28

l length of port on rotating spool [mm]. 35

m_{cyl} Mass of the engine cylinder gas [kg]. 32

m_{ex} Mass of gas escaping the engine cylinder once the exhaust valve opens [kg]. 32

$m_{f,b}$ Mass of burnt fuel in cylinder [kg]. 35

m_f Mass of fuel in cylinder[kg]. 35

μ_s Coefficient of static friction between steel and bronze. 28

m Moving mass of hydraulic oil piston cylinder and engine valve [kg]. 31

ϕ_c Spool casing port angle [deg]. 35

ϕ_s Spool port angle [deg]. 35

r_{cs} Radius of crank shaft [mm]. 32

r_s radius of rotating spool [mm]. 35

θ_{cs} Crankshaft angle [CA°]. 32

θ_c Angle between spool outer casing port and reference line [deg]. 35

θ_s Angle between fluid port on rotating spool and reference line [deg]. 35

ω_c Rotational speed of planet carrier in gearbox [RPM]. 27

ω_e Rotational speed of engine, same as 'N' [RPM]. 27

ω_r Rotational speed of outer ring gear in planetary gearbox [RPM]. 27

ω_{sun} Rotational speed of sun gear in gearbox [RPM]. 27

ω_s Rotational speed of rotary spool valve [RPM]. 27

x_b Mass fraction of burnt fuel. 35

$\boldsymbol{x}$ Engine valve lift [mm]. 31

y Vertical displacement of engine cylinder piston [mm]. 32

Chapter 1

Introduction

1.1 Motivation

Traditional engine design has had to balance power output, engine emissions, and fuel economy. Moreover, the fuel economy of an engine is inversely related to the performance, forcing the designers to prioritize one at the expense of the other. Finally, with increasingly stringent environmental restrictions on engine emissions and the emergence of electric vehicles, there is a need for combustion engines to pollute less and provide comparable amounts of power.

Even with a drastic 75% reduction in small gas powered vehicles, the vehicular demand for oil is projected to go from 10 million to 7.5 million barrels a day by 2050, as shown in Figure 1.1 [1]. Futhermore, projections by the U.S Environmental Protection Agency show that cars manufactured in the model year 2016 are unlikely to meet the emissions targets by 2025 [2]. These projections and trends show a future demand will exist for cars that consume oil and produce fewer emissions. Moreover, car manufacturers will seek to improve their engine designs to produce more power, gain higher fuel economy, and do so without adding weight as shown by the trends in Figure 1.2. Therefore, advancement in engine technology seeks to not increase weight or size, reduce emissions, increase fuel economy, and overall power output.

Conventional engine designs involve cam-follower mechanisms that fix the timing and lift profile of engine valves, usually to maximize torque at a certain engine speed, even though the combustion characteristics vary with engine speed and load. Therefore, innovation in combustion engine design involves achieving the optimum point of providing

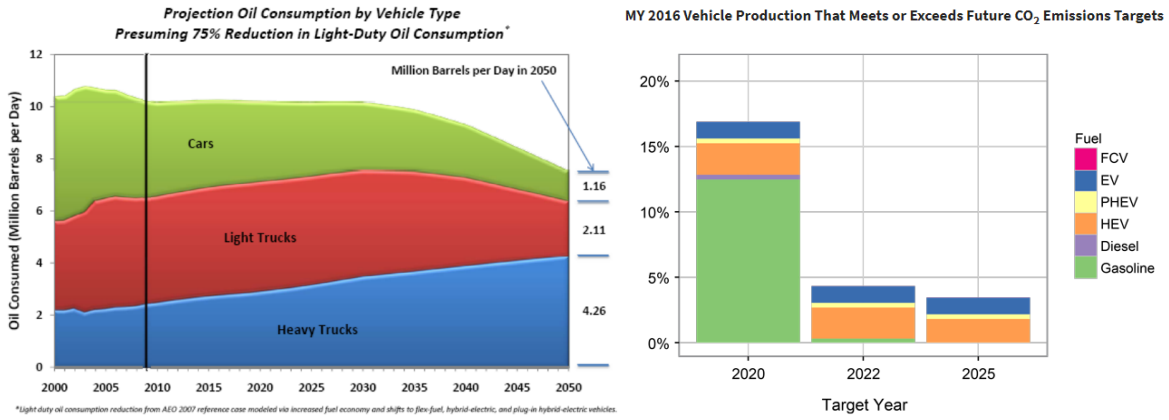

(a) Oil demand projections by vehicle type [1] **(b)** Environmental pass rate projections of vehicles [2]

Figure 1.1: Contrast demand on oil by vehicle type and the vehicle's likelihood of passing future environmental regulations [1] [2]

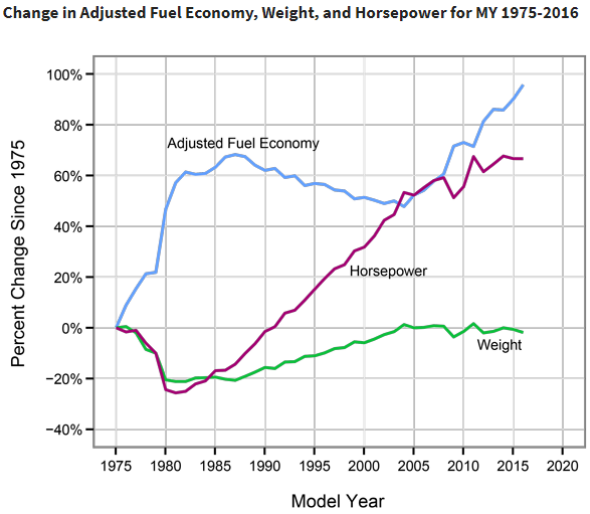

Figure 1.2: Observed trend of rising fuel economy, engine output, and stable weight of cars over four decades, reproduced from EPA [2]

maximum torque, or producing the fewest possible emissions, at any given engine speed. One method to accomplish this, is to alter the intake and exhaust valve lift and timing. Furthermore, active control of the valves can allow the engine to switch between performance and lowering emissions as desired. In this chapter, an overview of advantages from variable valve actuation (VVA) technology is presented, followed by the structure of this thesis to develop the VVA system.

1.2 Thesis Outline

The objective of this project is to further develop the hydraulic variable valve actuation (HVVA) technology by adapting it on an engine to obtain combustion. The HVVA design is carried on from the work of M. Pournazeri in the thesis 'Development of a New Fully Flexible Hydraulic Variable Valve Actuation System' [11]. Current state of technology is reviewed in Chapter 2 to highlight the possible areas of improvement. Additionally, a review of previous setups is provided in Chapter 3, this review provides a basis for the new system design in Section 3.2.

A prototype of the design is initially tested on a separate bench, developed by Chermesnok [12], in Section 5.2. The full manufactured system is then assembled on an engine test bench and experimental setup covered in Chapter 4. The dSpace and Simulink environment is used to connect all components and develop the control logic for operating the system in Section 4.2. The system is tested on the engine without combustion in Section 5.3. Finally, in Section 5.4, the HVVA system is used to obtain combustion at engine idle speed and controlled for desired valve lift.

Chapter 2

Literature Review

2.1 Conventional Engine Valve Control

An internal combustion engine operates by introducing fuel into a combustion chamber, compressing said fuel until combustion to extract power, and expelling the waste products. The intake valve opens to introduce the air/fuel mixture into the chamber and the exhaust valve opens to expel the combustion products. Traditionally, both valves are controlled by a pear shaped cam that runs on a camshaft. This connection sets both valves to a fixed timing of opening and closing intervals. A general arrangement of this valve control is given in Figure 2.1.

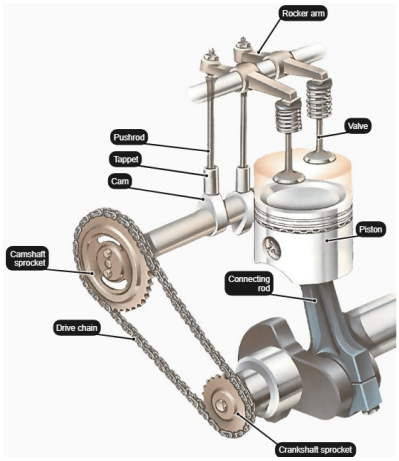

Figure 2.1: Conventional valve timing system using cam mechanism [3]

The standard valve lift profile, or the motion each engine valve goes through in a combustion cycle, with the corresponding piston position is shown in Figure 2.2. The picture also shows the piston position inside the engine cylinder, top dead center (TDC) referring to the highest position of the piston, and bottom dead center (BDC) to the lowest position of the piston. Note that the intake and exhaust valves only open once for every two rotations of the engine crankshaft, showing the need for a 2:1 reduction between the valve cycle and engine cycle. Furthermore, each valve opens and closes gradually because the shape of the cam changes gradually. Finally, this representation of an engine cycle shows valve profiles that are likely tuned for performance at one speed. In order to obtain higher power outputs or fewer emissions, at different engine speeds and loads, the valve profiles will have to change. These changes can include varying the valve timing by advancing or delaying valve profiles to the left or right in Figure 2.2, or changing their total lift.

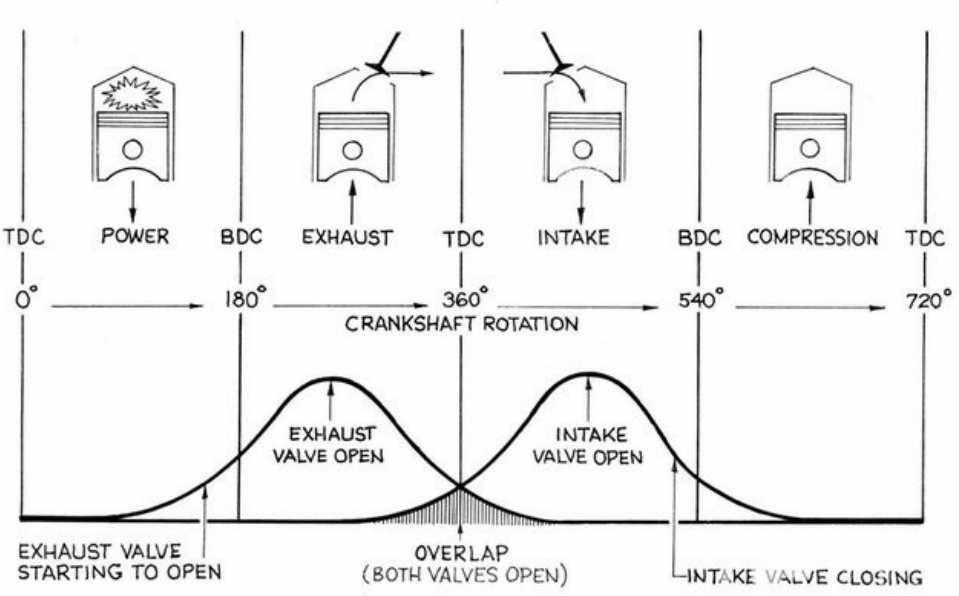

Figure 2.2: Intake and exhaust valve cycles for four stroke engine [4]

As previously mentioned, controlling variable valve timing (VVT), lift, or both can be done by several methods. These methods are best explained as divided into cam and cam-less systems, which are further separated by each technique's actuation method: electric, hydraulic, pneumatic, or some combination of the three. A few of these methods are shown in Figure 2.3 and explained below to address their benefits and limitations.

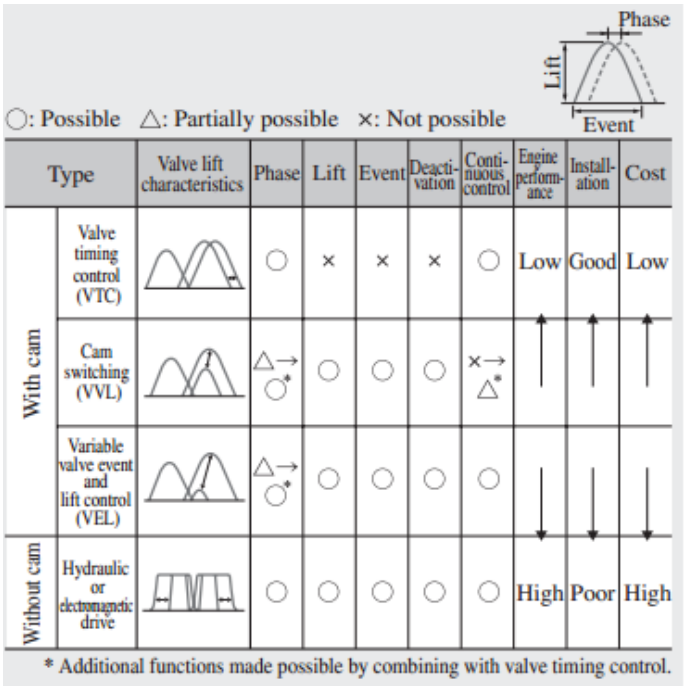

Type		Valve lift characteristics	Phase	Lift	Event	Deacti-vation	Conti-nuous control	Engine perform-ance	Install-ation	Cost
With cam	Valve timing control (VTC)		○	×	×	×	○	Low	Good	Low
	Cam switching (VVL)		△→○	○	○	○	×→△*	↑	↑	↑
	Variable valve event and lift control (VEL)		△→○	○	○	○	○	↓	↓	↓
Without cam	Hydraulic or electromagnetic drive		○	○	○	○	○	High	Poor	High

* Additional functions made possible by combining with valve timing control.

Figure 2.3: Different types of VVA systems and their ability to phase valve timing, change event length, or valve lift [5]

2.2 Variable Valve Actuation Technology

2.2.1 Cam Phasing Methods

Mivec

The Mitsubishi Innovative Valve timing Electronic Control (MIVEC) system is a hydraulic based cam phaser. The system was first used in 1992 by Mitsubishi and has continued to evolve with its use in the Japanese Outlander in 2012 [6]. The system's ability to control the valve timing is shown in Figure 2.4. The outer sprocket is connected to the crankshaft and the cam shaft is connected to the inner body. Introducing fluid to either the advance or retardation chamber changes the angle of rotation between the camshaft and crankshaft and therefore changes the valve timing. A drawback of this system is its limited ability to vary the timing as shown in the figure by "phase angle".

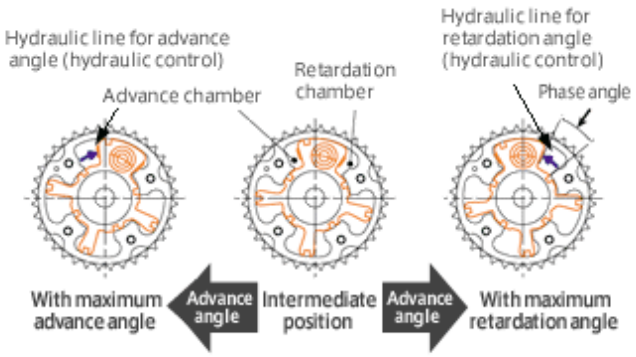

Figure 2.4: Mitsubishi Innovative Valve timing Electronic Control (MIVEC) system [6]

Vanos

A cam phasing technique to adjust the valve timing is the VANOS system developed by BMW [7]. The ability of the VANOS system to change valve timing is presented in Figure 2.5. The system uses a helical gear to connect the standard camshaft to a hydraulic piston. A controller (ECU) signals the solenoid to introduce high pressure oil flow to either side of the hydraulic piston, causing the piston to move axially. Due to the helical gear, any linear motion of the hydraulic piston causes rotation of camshaft which advances or delays the valve timing. However, the system does not allow for any change to the valve lift.

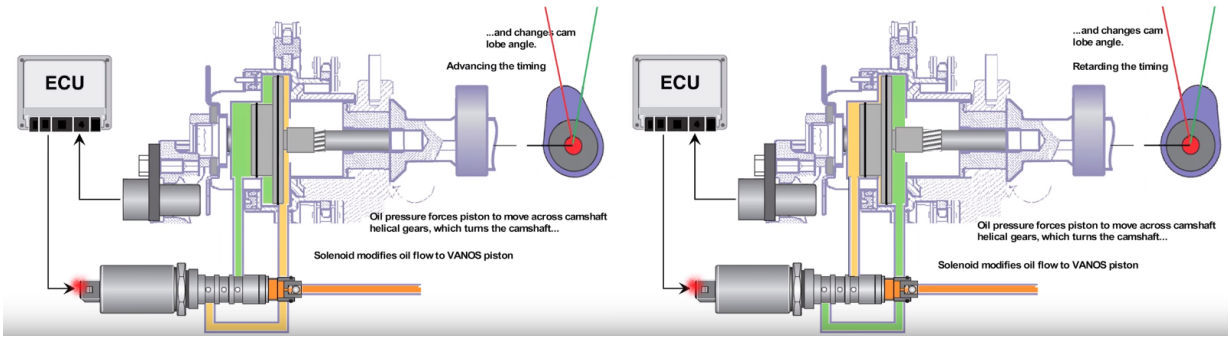

(a) Advanced timing **(b)** Retarding timing

Figure 2.5: Vanos System showing hydraulics use to vary valve timing [7]

2.2.2 Cam Switching Methods

Valvetronic

A variable valve lift method developed by BMW is the valvetronic system. This system is often used in combination with their VANOS setup to also provide variable valve timing. The valvetronic system is shown achieving different valve lifts in Figure 2.6. The conventional cam and rocker arm system is interrupted here by two intermediary arms shown in red. The original cam, pictured on the right in each snapshot, is pushing against the intermediary arm. This intermediate arm can pivot on its centre based on the setting of a secondary cam above that is electronically rotated. Note that the orignal cam is shown in the "fully open" or max height setting as it is pushing at the tip of its lobe. However, the setting of the secondary cam pulls the intermediate arm further down and increases the maximum possible lift.

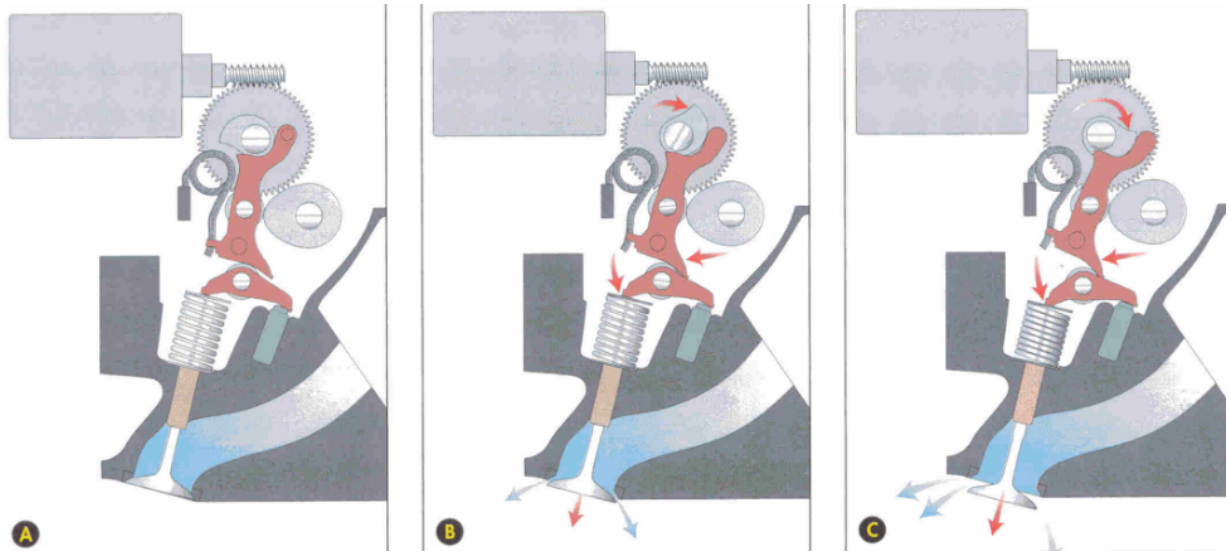

Figure 2.6: Valvetronic system showing valve lift adjustability [8]

Variable Valve Event and Lift

Another multi-link system, similar to the valvetronic model, is Nissan's variable valve event and lift (VVEL) mechanism. An overview of the VVEL mechanism is presented in Figure 2.7. Similar to the valvetronic system, the VVEL design inserts intermediary rocker and

a secondary camshaft between the standard camshaft and the engine valves. The rocker transmits the rotation from one camshaft to another, thereby allowing the engine valves to open. The rocker can be driven by an electronic actuator to different heights, allowing the system to change the overall engine valve lift. Note that the system requires few additional parts to the standard engine but does not provide the ability to change valve timing.

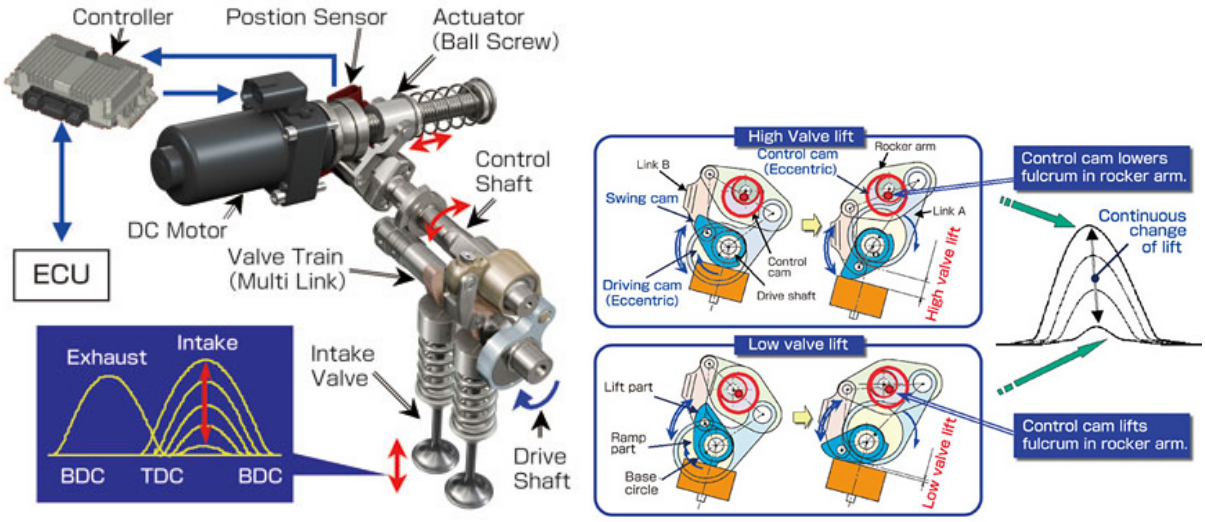

Figure 2.7: Variable Valve Event and Lift (VVEL) system [8]

2.2.3 Camless Methods

Free Valve Technology

Developed by Koenigsegg's sister company, the camless valve system called FreeValve technology is presented in Figure 2.8. The system uses electro-pneumatic actuation to open the engine valves, hydraulics to provide damping and hold the valve at the required position, and pneumatic springs to close the valves. The air springs allow adjustment of the closing force to optimize the spring rate for each engine speed and load requirement. Furthermore, since the system involves a separate actuator for each valve supplied by a common rail, selectively closing ports in the rail allows for cylinder deactivation. However, the high cost of implementation and high frequency of operation for electrical actuators are the largest deterrents to the system.

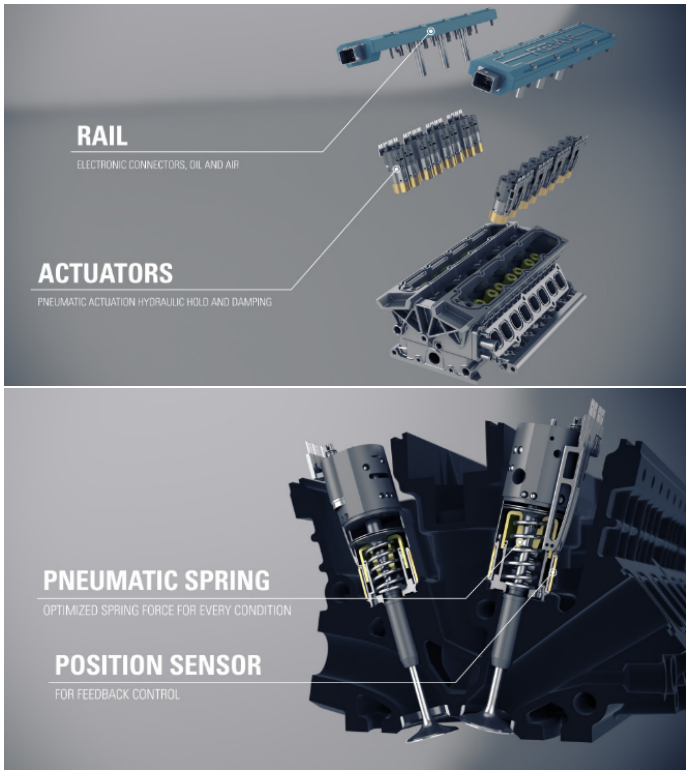

Figure 2.8: Free Valve System using electro-pneumatic actuation and hydraulic damping to control and hold the valve lift [9]

Electro-mechanical Valve Train

Electro-mechanical valve control consists of two magnets and two springs as shown in Figure 2.9. The top closing electromagnet is energized to ensure the valve stays closed. When no voltage is supplied to the electromagnets, the valve is left to float in a neutral position due to the spring forces. Applying a voltage to the bottom electromagnet moves the actuator down and holds it against the spring force. A safety issue with this system is relying on electrical power to ensure valves stay closed, any loss of power can cause the valves to float. Furthermore, the system offers no means of damping or controlling the speed of the engine valve when it closes against its seat in the cylinder head. This can result in early wear of the engine valves and possible engine failure.

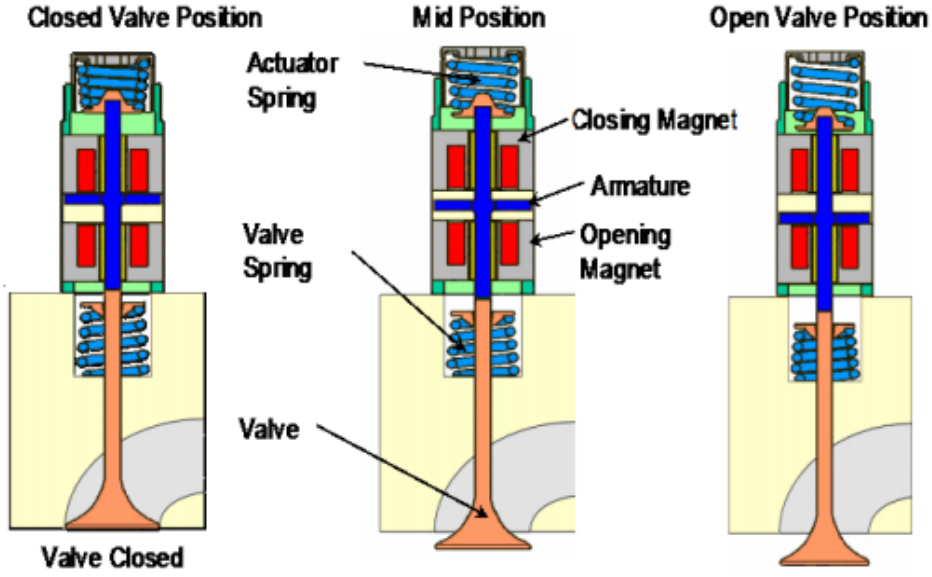

Figure 2.9: Electromechanical valve train actuator [10]

Chapter 3

Variable Valve Actuation System Design

This chapter contains a review of the HVVA system's previous iterations made in the Mechatronics Vehicles Systems Laboratory. Following the review, a new design is explained and mathematically modelled in Simulink.

3.1 Previous Design Review

The initial design concept for a HVVA system, working on a single valve engine, is shown in Figure 3.1 developed by M. Pournazeri [11]. Pournazeri used a hydrualic cylinder to actuate the engine valve. A rotary spool valve, as shown in Figure 3.2, connected to the high pressure line would pressurize the hydraulic cylinder causing the valve to open. A second rotary spool valve, connected to the reservoir, would relieve the pressure in the hydraulic cylinder causing the engine valve to close.

In order to change the valve timing, the spool valves connected to the engine crankshaft through a device termed the "phase shifter". This shifter allowed the valves to change their angular relation to the angle of the crank shaft. This ability to change the spool valve angle, in comparison to the crank shaft angle, or "phase shifting", was done by rotating the spool valves from an additional input. Therefore, the system had a fixed setting where the engine crank shaft would act as one input to turn the spool valves, and an additional input allowing modification of the spool valves' angles causing the engine valve timing to advance or delay. The phase shifting and rotary spool valve assembly developed by M. Chermesnok is shown in Figure 3.3.

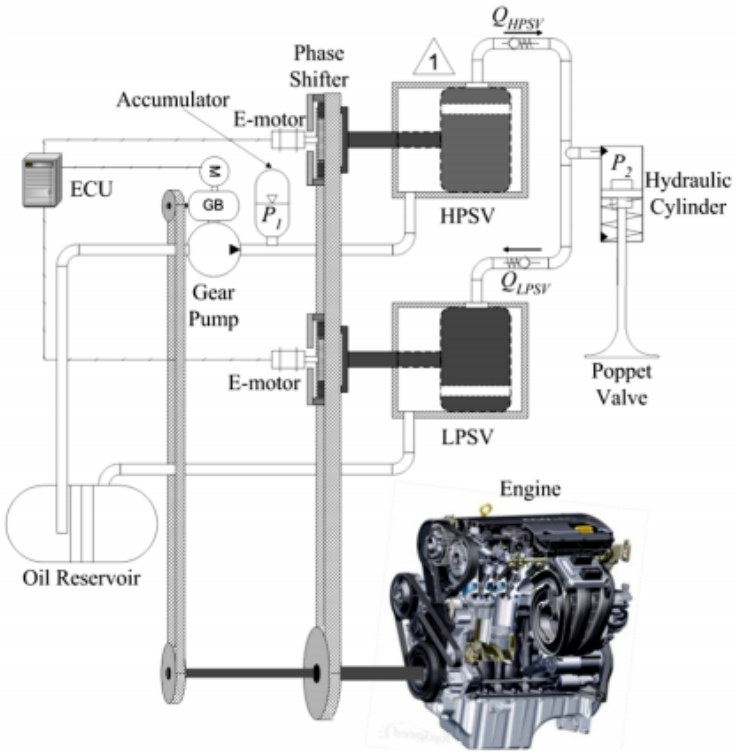

Figure 3.1: Pournazeri's HVVA schematic for single valve operation [11]

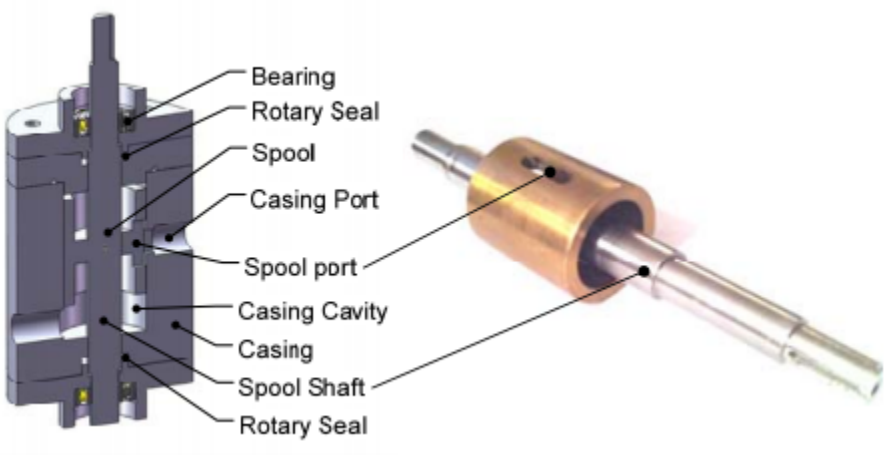

Figure 3.2: Pournazeri's rotary spool valve design [11]

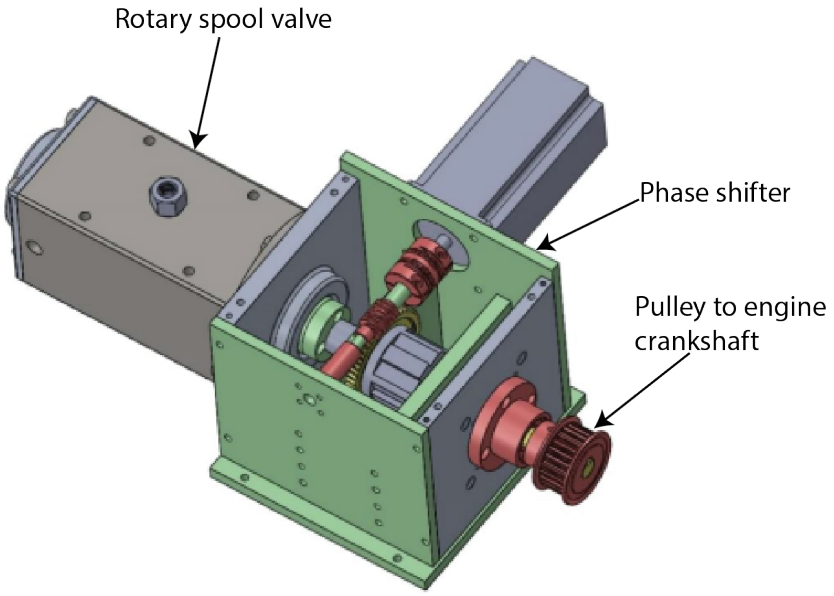

Figure 3.3: Chermesnok's spool valve and phase shifter assembly [12]

3.1.1 Spool Valve

The rotary spool valve (RSV) design, or spool valve for short, developed by Chermesnok was able to spin at an engine speed of 1000 RPM and transmit a pressure of 1000 psi to the hydraulic cylinders. However, the spool valve design suffered from excessive leakage, early failure of radial seals, and high friction due to manufacturing issues.

The assembled spool valve is shown in Figure 3.4, it has one input port where the high or low pressure line can connect and 4 ports to connect hydraulic cylinders. It is meant for a 4 cylinder engine; however, output ports can be blocked allowing the spool valve to function for a smaller engine. The rotary spool shaft in Chermesnok's HVVA system is shown in Figure 3.5. Note that a four cylinder engine has each subsequent cylinder fire 180 CA°after the previous one. Since the spool valve is geared to spin at half the engine speed, the ports on the shaft are 90°out of phase from one another. The middle of the shaft has a groove and several openings, allowing fluid to flow inside the shaft at any angular position. A section view of the spool valve is given in Figure 3.6. The section view shows one port on the spool shaft align with an opening on the casing. In a high pressure valve the fluid will flow from the input port to inside the spool shaft and out through the casing port to a hydraulic cylinder in order to lift an engine valve.

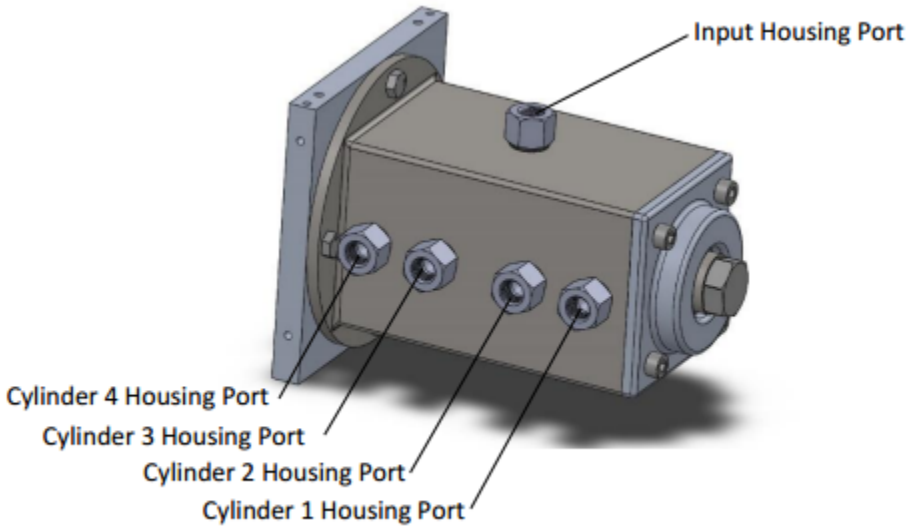

Figure 3.4: Chermesnok's rotary spool valve design [12]

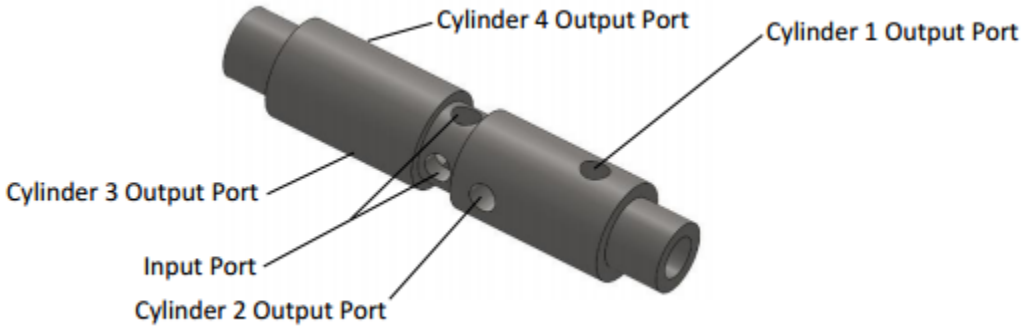

Figure 3.5: Chermesnok's rotary spool shaft with four outputs and a center input groove[12]

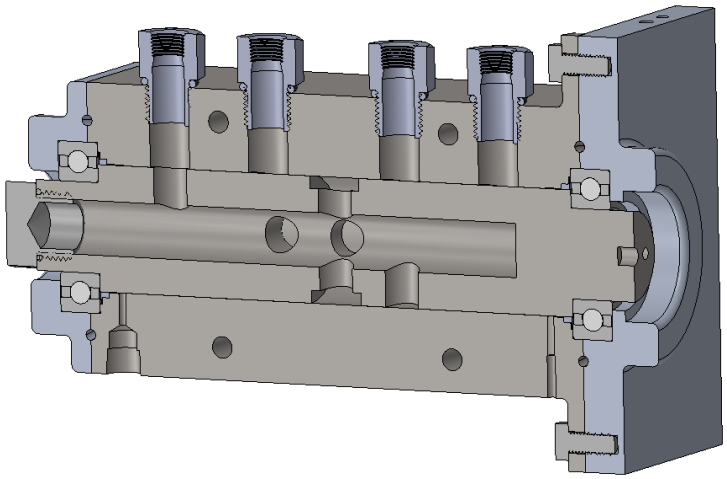

Figure 3.6: Section view of Chermesnok's rotary spool valve design showing allignment of one output port [12]

The sealing issue with the spool valve design was mainly leakage from the spool valve to the environment, not the internal leakage from one port to another. It is important to note that there are no seals separating any housing port from another port on the outer casing. Therefore, the only way to prevent premature valve lift or closing is to have a very narrow gap between the spool shaft and the outer casing, there by limiting the radial leakage when the ports are not alligned, and axial leakage between the ports of different cylinders. Moreover, the radial seals at the outer edges of the spool valve had to retain high pressure, tolerate high oil temperatures, and allow for high speed rotation. In Chermesnok's design, large diameter radial seals were chosen, leading to high tangential velocities and larger areas requiring precise manufacturing tolerances.

The design in these spool valves has to support the shaft at two ends, as done by the bearings in Chermesnok's valve. Additionally, the gap between the valve shaft and outer casing has to be on the order of a few thousands of an inch to prevent excessive leakage. Any issues in shaft axial run out or concentricity forces the shaft to rub against the outer casing, causing the shaft to be over-constrained. In this condition, where the shaft has more than two supports, the torque required to turn the spool valve becomes excessively large. Additionally, the rubbing friction causes the entire assembly's temperature to rise, leading to possible degradation or premature failure of the radial seals.

Rotary Union

Chermesnok based his spool valve design on a conventional rotary union. This type of union allows for fluid flow between parts in rotating machinery as shown in Figure 3.7. The stator, or outer casing, is connected to the fixed supply while the ports on the rotor connect to the lines on the rotating machinery. Grooves cut into the stator allow for flow between ports that are angularly misaligned. Eliminating the groove creates a custom rotary union, which allows for flow only when the ports are aligned as done by Chermesnok's design.

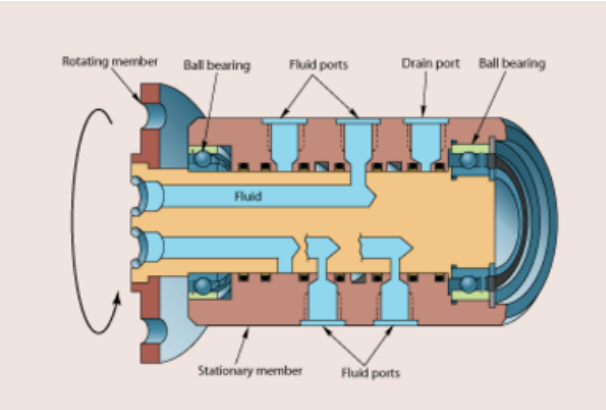

Figure 3.7: Section view of rotary union depicting fluid flow between a stator and rotor [13]

3.1.2 Phase Shifter

The phase shifter used by Chermesnok is shown in Figure 3.8. The phase shifter relied on a small differential which is prone to overheating. Normal operation of a differential involves turning the outer body and only when one side has to spin at a different rate are the internal gears forced to turn against each other. However, in Chermesnok's application, the internal gears are constantly turning while the outer body is only moved for phase shifting purposes by a worm gear. Therefore, the differential's body temperature would rise above 100 C°within 5 minutes of operation which can break down the internal gears and eventually cause damage to the nearby bearings as well.

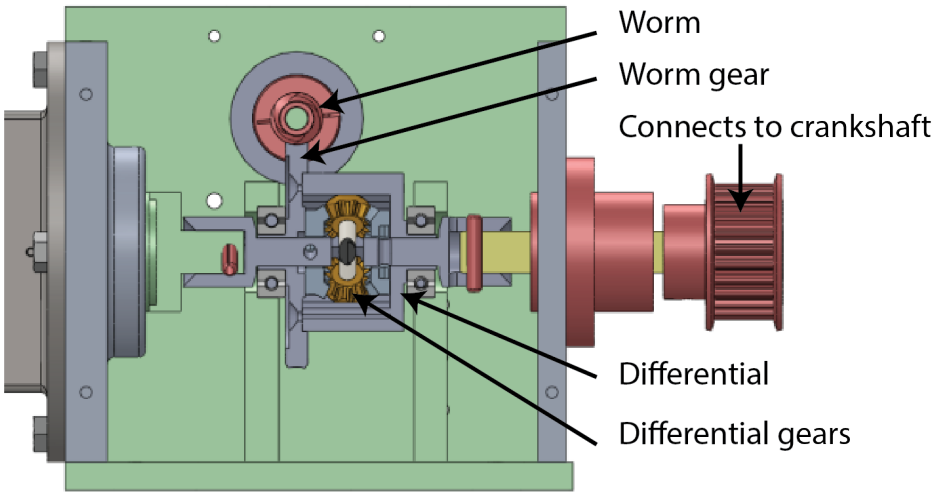

Figure 3.8: Chermesnok's phase shifter design [12]

3.1.3 Cushion Device

Chermesnok's cushion device is shown in Figure 3.9. Flow through the main orifice and the check valve would cause the cushion assembly cylinder to move down and open the engine valve. When the engine valve has to close, the hydraulic fluid initially goes through the main orifice until the cylinder cushion geometry blocks the main orifice path. At this point, the flow cannot move through the check valve and is severely restricted in the main orifice path; therefore, the flow has to primarily go through the hydraulic cushion path. In this cushioning path, the adjustment screw controls the flow port size and can be varied to change the pressure needed to retract the cylinder. This cushioning effect allows the valve to slow down near the end of its closing motion and impact the valve seat at an acceptable speed. The ideal valve closing speed to prevent damage to engine valves is estimated to be below 100 mm/s [14].

The issues noted with Chermesnok's cushion device include the inability to dampen the closing speed to below 150 mm/s, no method of adjusting the cushion block's height to account for engine mounting, and only supporting the cylinder at the singular seal allowing the cylinder to tilt and not move smoothly.

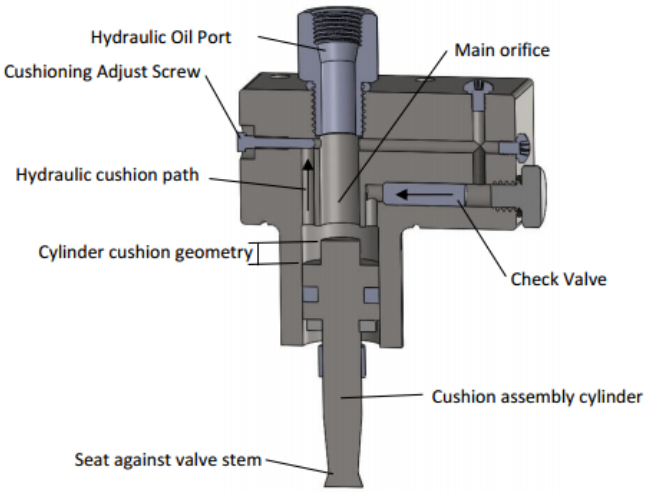

Figure 3.9: Chermesnok's cushion device design [12]

3.2 New VVA Design

The new VVA design is meant to be the next iteration, improving upon the designs of Pournazeri and Chermesnok [11][12] covered in the previous section. The new design combines the slotted port spool valve design of Pournazeri with the use of radial seals and through hole design of Chermesnok. Additionally, a design criteria is formed to improve on the previous iterations. The criteria mainly specifies that the system have low leakage, ability to withstand high termperatures and engine vibration, and low friction for smooth operation. This chapter shows the developement of the new VVA design along with its core components: the spool valve, phase shifter, and cushion device. Following that, a mathematical model is constructed to conduct a parametric study and show the most relevant parameters of the design. The final success of the design is gauged by the HVVA design's ability to work on an internal combustion engine as demonstrated in chapter 5.

New Design Criteria and Model

- Rotary spool valve capable of turning with low friction.
- Spool valves able to hold pressure without leaking into hydraulic cylinder or out to atmosphere.

- System allows for consistent phasing without over heating.
- Hydraulic cylinder must be mounted easily on an engine.
- Hydraulic cylinder has to provide a damping force during valve closing to prevent damage from excessive closing speeds.
- System has to withstand high temperatures from engine combustion, heated hydraulic oil, and friction.
- HVVA system capable of high run times without failure due to mechanical or thermal issues.

A full assembly of the spool valve combined with a phase shifter is shown in Figure 3.10. This single unit, with two hydraulic ports shown, is capable of acting as a high or low pressure rotary spool valve for an engine valve. Therefore, for a single engine cylinder with an intake and exhaust valve, four rotary valve units will be needed. Two spool valves will provide high and low pressure for the intake and an additional two for the exhaust. For a multi-cylinder engine, the system will only need additional ports on the spool valves, not more valve units.

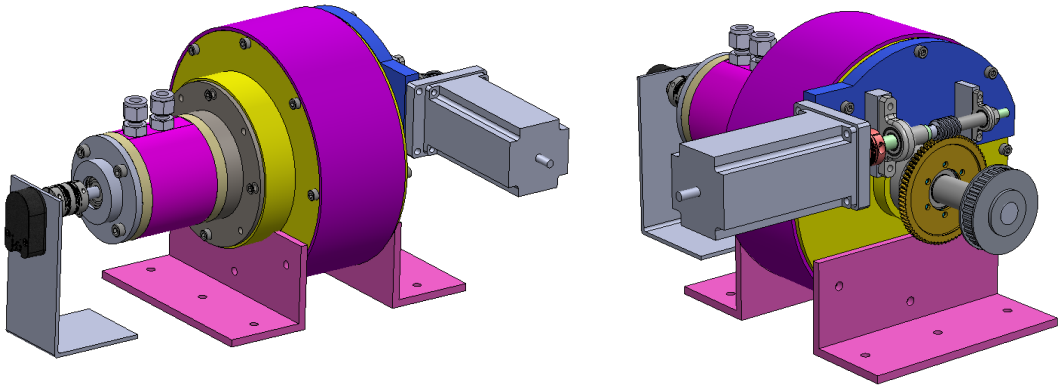

Figure 3.10: New HVVA rotary spool valve and phase shifter assembly

A section view of the VVA assembly is presented in Figure 3.11. The engine crankshaft is connected through a timing belt to the assembly pulley for a 2:1 ratio with the rotary spool valve, this ensures that for 720 CA°the spool valve only completes one rotation. The figure shows the input from the pulley goes into the sun gear, the sun gear turns the planet gears, which rotate the planet carrier, and the carrier spins the spool valve shaft. Additional details of the spool valve and phase shifter are given below.

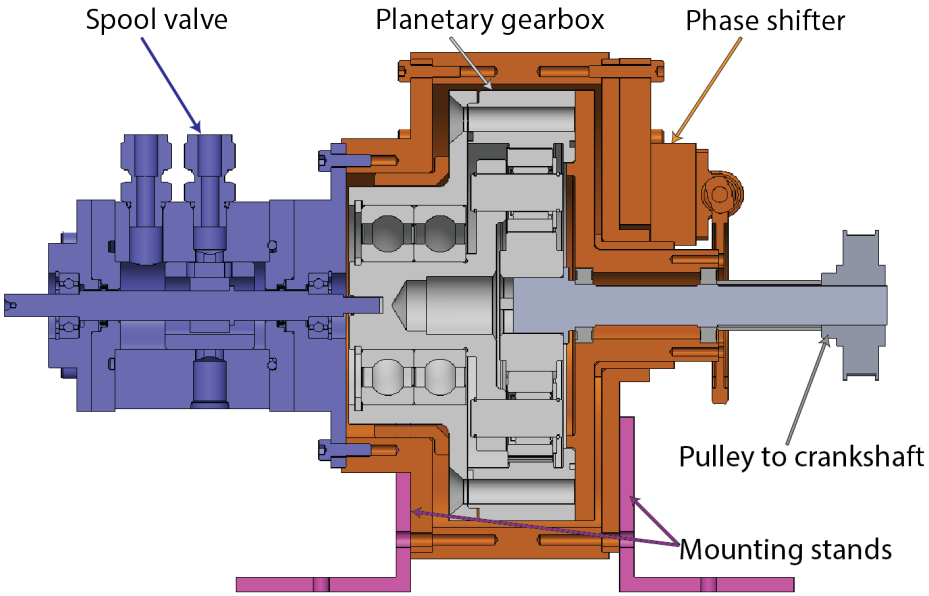

Figure 3.11: Section view of combined phase shifter and spool valve assembly

3.2.1 Spool Valve

The new rotary spool valve RSV design, or spool valve for short, is a combination of the concepts used by Pournazeri [11] and by Chermesnok [12]. An assembled spool valve section view is shown in Figure 3.12 and additional views showing how it functions are given in Figure 3.13.

The spool valve outer casing, is hollow to aid in machining and assembly. The thru hole bore allows the casing to be honed in order to achieve the smooth surface and tight tolerance required to prevent leakage. The rounded outer casing also has flats where the hydraulic ports are located, these allow for the sealed fittings to work without leaking and reduces the angular error between in line fittings, , see section 5.2 for more details. The rotational input to the valve is through the flat machined in the shaft end that allows it to be driven from the phase shifter output.

In contrast to the larger length spool design, a small spool length is used to more easily attain the manufacturing tolerances required between the outer casing (stator) and rotating spool (rotor). Moreover, the tight tolerances between the rotor and stator has to be met along the same axis where the rotors shaft is pressed into bearings. Since the shaft should only be constrained at two locations, not achieving the required tolerances risks

over-constraining the system. Therefore, to overcome the difficulty of machining a long rotor to precise dimensions, a smaller length spool is used. If additional ports are required they can also be added radially instead of axially, as recommended by Chermesnok [12].

The ability of the spool valve to allow or block as shown in Figure 3.13 is for a single intake or exhaust valve. The bottom blocked port can be used when the system is for a two cylinder engine where the second cylinder operates 360 CA°out of phase from the first. Additional ports can be machined in for an engine with more cylinders.

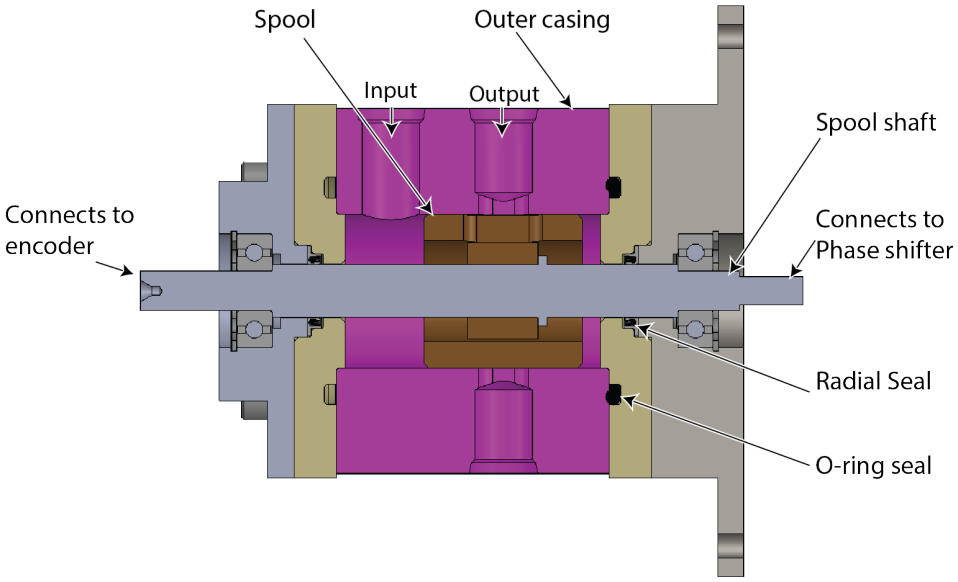

Figure 3.12: Section view of spool valve assembly

Thermal Expansion

In addition to manufacturing tolerances, the system is designed to withstand changes in volume with temperature fluctuations. As the hydraulic oil rises in temperature from passing over the engine head during combustion, the sytem is assumed to reach temperatures of approximately 100 C°. Therefore, a change from room temperature of approximately $\Delta T = 75\ C^{\circ}$ must not excessively expand the bronze spool. The critical case, or failing temperature change ΔT_f, causes the spool outer diameter to jam against the inner diameter of the valve outer casing. Another example of a critical temperature is when the bronze spool's inner diameter expands and loses contact with the spool shaft, or is no

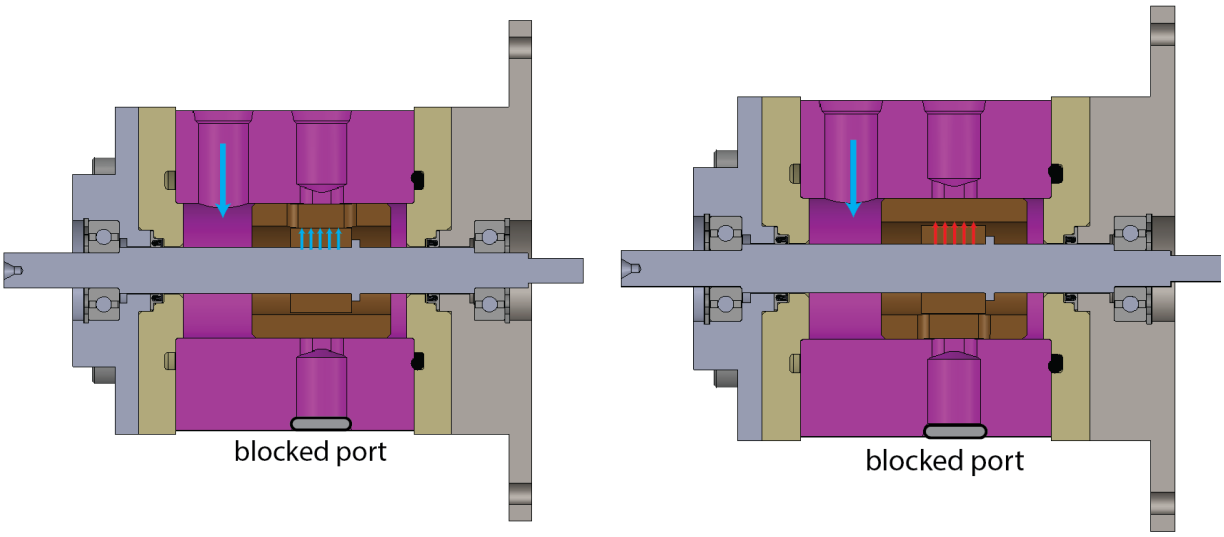

(a) Top output port open **(b)** Top output port closed

Figure 3.13: Rotary spool valve shown with open and closed output for the top port, blue and red arrows show allowed and blocked flow, bottom port is assumed to be plugged

longer press fitted on the shaft. The latter case occurs at a higher temperature change and is addressed by using a set screw to fix the bronze spool to the spool shaft. The material choice of steel for the spool shaft and bronze for the spool are justified with regards to thermal expansion, as shown in equations 3.1 and 3.2.

The thermal expansions are given as α_{bronze} and α_{steel} from Callister[15]. The difference between the original spool diameter, $D_o = 35mm$, and the inner diameter of the casing, $ID_c = 35.07mm$, is set by the maximum gap of 0.003 inches to prevent internal leakage. Similarly, the diameter of the spool shaft, $D_{shaft} = 12mm$, and inner diameter of the spool, ID_{spool}, are chosen to match with commercially available radial seals.

$$
\begin{aligned}
D_o &= 35mm \qquad \alpha_{bronze} = \alpha_b = 22 \times 10^{-6} m/mC^\circ \\
ID_c &= D_o(\Delta T_f \alpha_b + 1) \\
\Delta T_f &= \frac{\frac{ID_c}{D_o} - 1}{\alpha_b} \\
\Delta T_f &= \frac{\frac{35.07mm}{35mm} - 1}{22 \times 10^{-6} m/mC} \\
\Delta T_f &= 91\ C^\circ
\end{aligned}
\tag{3.1}
$$

$$
\begin{aligned}
D_{shaft} &= 12mm \qquad \alpha_{steel} = \alpha_s = 15 \times 10^{-6} m/mC^\circ \\
ID_{spool} &< 12mm \qquad \alpha_{bronze} = \alpha_b = 22 \times 10^{-6} m/mC^\circ \\
min.\ press\ fit\ = 0.02mm &= 12((\Delta T_f \alpha_b + 1) - (\Delta T_f \alpha_s + 1)) \\
0.02 &= 12 \Delta T_f (\alpha_b - \alpha_s) \\
\Delta T_f &= 238\ C^\circ
\end{aligned}
\tag{3.2}
$$

3.2.2 Phase Shifter

As stated earlier, the purpose of the phase shifter is two-fold. First, the phase shifter has to connect the engine crankshaft to the spool valve, ensuring that the engine valves can open and close at a set timing. Second, the phase shifter has to be able to modify the rotation of the spool valve with respect to the rotation of the crankshaft, thus allowing the system to advance or delay the valve timing. To modify the spool valve rotation, the shifter accepts two inputs, one from the engine, and the other from a servo motor. This arrangement of two inputs to the phase shifter, with one output to the spool valve, is shown in Figure 3.14.

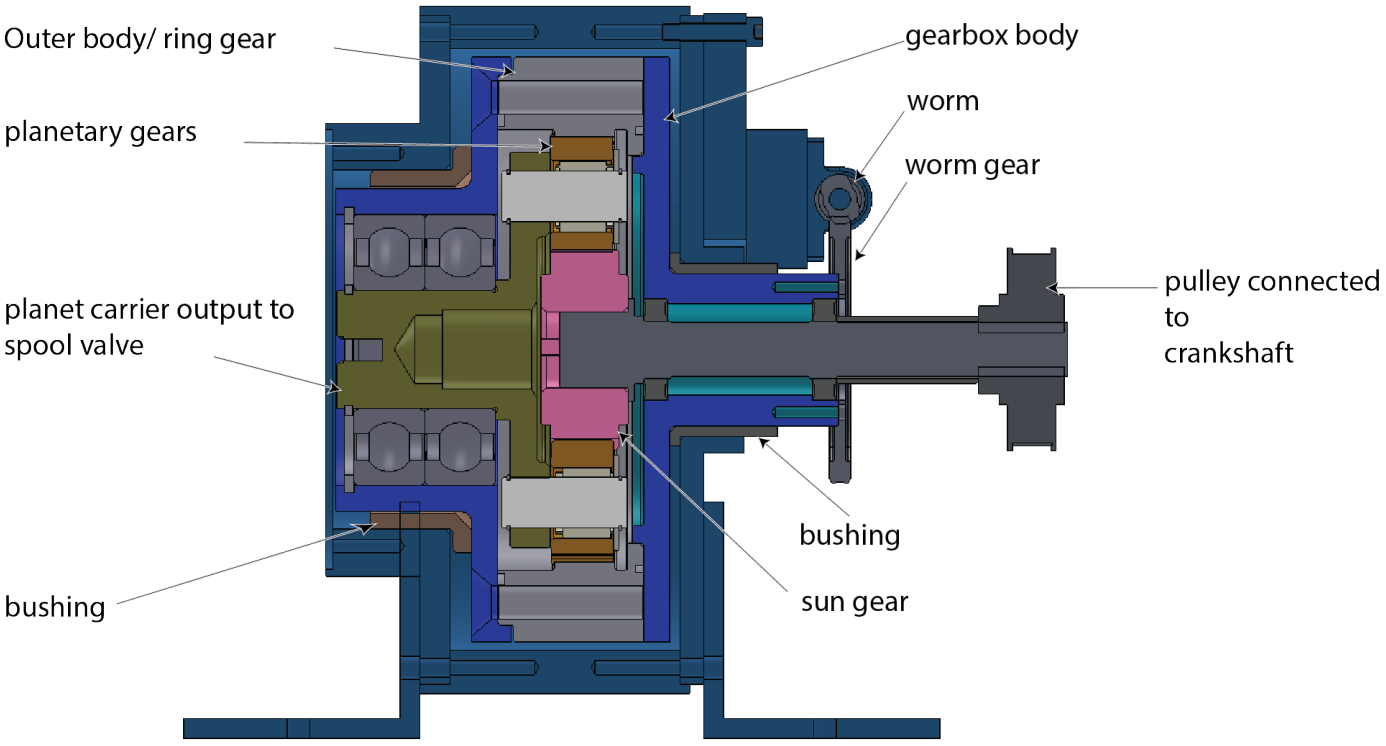

Figure 3.14: Section view of phase shifter showing connection from pulley input to sun gear and worm drive to ring gear

The two separate inputs allow the HVVA system to produce the variable timing effect, by modifying the conventional engine input by the additional input from the servo. While holding the ring gear fixed, the phase shifter takes the engine input through the sun gear and uses it to spin the planet carrier. Input from the servo is transmitted through the

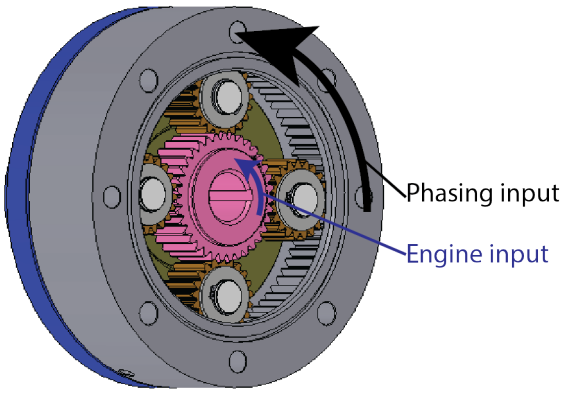

Figure 3.15: Planetary gearbox with inputs from engine crankshaft to sun gear and servo motor to outer ring gear

worm gear, connect to the gearbox body, allowing the whole gearbox to spin on bushings. The servo spinning the gearbox, equivalent to spinning the ring gear, changes the gear ratio between the engine input and planetary carrier output as shown in equation 3.4 and depicted in Figure 3.15. This results in an angle change between the engine rotation and spool rotation, thereby allowing the valve timing and duration to vary.

The pulleys on the engine crank shaft and the phase shifter create a 2:1 ratio between the rotation of the crankshaft and the spool valve. are The number of teeth on the crankshaft and phase shifter pulleys, N_e and N_{ps}, are found using equation 3.3.

$$
\begin{aligned}
\omega_{carrier} &= \frac{1}{2}\,\omega_e = \omega_s \\
\frac{\omega_{sun}}{\omega_{carrier}} &= 1 + \frac{N_r}{N_s} \\
\omega_{carrier} &= \frac{\omega_{sun}}{1 + \dfrac{N_r}{N_s}} \\
\omega_e &= \frac{2\ \omega_{sun}}{1 + \dfrac{N_r}{N_s}} \\
\omega_e &= \frac{2}{1 + \dfrac{79}{35}}\,\omega_{sun} \\
\omega_e &= \frac{35}{57}\,\omega_{sun} \\
N_e\ \omega_e &= N_{ps}\omega_{sun} \\
N_e &= 57 \qquad N_{ps} = 35
\end{aligned}
\tag{3.3}
$$

where ω_c, ω_e, ω_s, ω_r, and ω_{sun} are the rotational speeds of the planet carrier, the engine crank shaft, the spool valve, the ring gear, and the sun gear respectively. Similarly, the variables N_r, N_s, N_e, and N_{ps} are the pulley sizes, or number of teeth on the pulley, for the ring gear, the sun gear, the engine crankshaft pulley, and the phase shifter pulley.

$$
\begin{aligned}
N_s\omega_{sun} + N_r\omega_r &= (N_s + N_r)\omega_c \\
\cancel{N_s}\frac{57}{\cancel{35}}\,\omega_e + N_r\omega_r &= (N_s + N_r)\omega_s \\
\omega_s &= \frac{57\ \omega_e + N_r\omega_r}{N_s + N_r} \\
when\ \omega_r = 0 \qquad \omega_s &= \frac{57\ \omega_e}{35 + 79} = \frac{1}{2}\,\omega_e \\
when\ \omega_r \neq 0 \qquad \omega_s &= \frac{57\ \omega_e + 79\ \omega_r}{114}
\end{aligned}
\tag{3.4}
$$

Worm Gear Design

The phase shifter rotates the planetary gearbox through a worm drive to change the valve timing, the worm drive provides a 60:1 reduction allowing for a small servo torque to rotate the gearbox. Moreover, the worm gear is chosen to prevent back driving when the ring gear is supposed to be held fixed. This locking against back driving is done by the design guide in Shigley's [16] and shown in equation 3.5, where λ_l and μ_s are the lead angle of the worm gear and the static coefficient of friction between the steel and bronze gears. The value for λ_l is given by the manufacturer to be 4.46°, and the coefficient of friction μ_s is 0.16 according to [17].

$$
\begin{aligned}
tan(\lambda_l) &< \mu_s \\
tan(4.46) = 0.078 &< 0.16\ (back\ drive\ safe)
\end{aligned}
\tag{3.5}
$$

Note that the phase shifter is larger than it needs to be to accommodate the gearboxes donated to the lab by ODG. The phase shifter can be reduced in size without affecting functionality as long as the components are rated for speeds of at least 4000 RPM and adequately lubricated.

3.2.3 Cushion Device

The assembly responsible for actuating the engine valves, called the cushion assembly, and is mounted on to the engine head with a modified cover as shown in Figure 3.16. The modified cover includes jacking screws to raise the entire assembly against the engine head to limit the maximum valve lift.

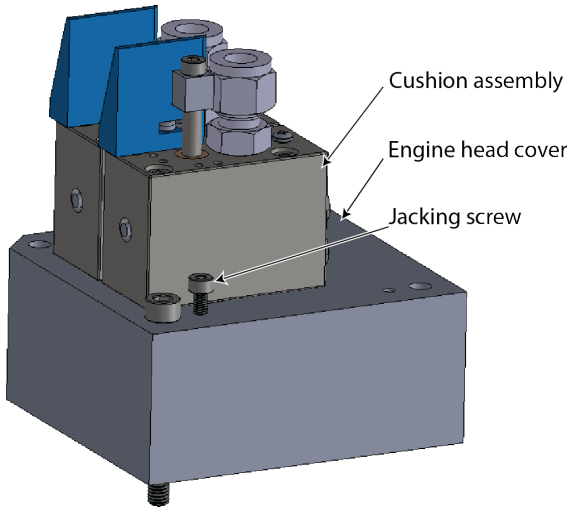

Figure 3.16: Modified engine cover with cushion device assembly

The cushion assembly's components are shown in detail in Figure 3.17. The assembly contains the hydraulic cylinder, called the 'oil cylinder piston', that uses high pressure fluid to open the engine valve and is closed shut by the valve spring when the pressure is reduced. Differences between the new cushion assembly and the previous one, reviewed in section 3.1.3, include the following:

- Modifying the design to appropriately detect valve lift during engine operation
- Adding an additional seal and support to the piston
- Changing the flow path to no longer align with the piston
- Changing the seal installation to ensure proper operation
- Resizing tolerances and dimensions to ensure smooth actuation and damping function.

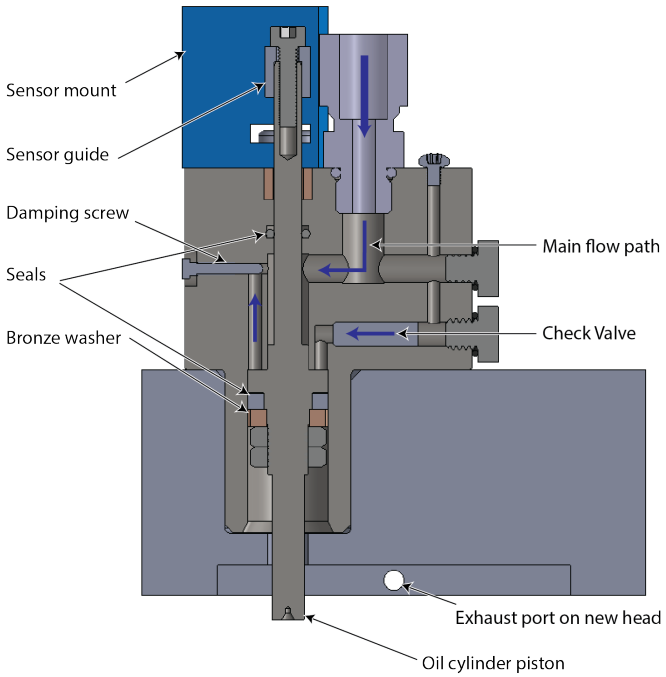

Figure 3.17: Section view of cushion device assembly showing components necessary for sealing fluid, damping valve closing speed, and sensing linear position

The previous design used a linear sensor to detect the piston and engine valve motion *below* the cushion assembly on a test bench. However, in an actual engine mount, the space below the cushion assembly is very limited. Moreover, for experimental purposes, the system has to easily observe valve lift and be modifiable without significant maintenance. Therefore, the design uses a sensor *above* the cushion assembly with a modified oil cylinder piston. The modification involves elongating the piston so it is seen moving up and down during engine operation. This design allows for easy sensor access and calibration along with visual proof of engine valve motion.

In order to elongate the cylinder piston, an additional seal is inserted in the design near the top of the cushion assembly. While adding another seal raises overall friction, the seals provide two points of support, ensuring the piston moves axially in comparison to the previous single seal design. The former single seal design is suspected to have reduced damping functionality by not properly closing in each stroke. Additionally, changing the piston's length requires moving the flow path to a new location as shown in the assembly figure. The new design requires higher pressures for valve lift in comparison to the previous design because the change in flow path creates an additional fluid resistance, and the

reduction in hydraulic piston area necessitates higher pressure to generate the same force.

The large seal on the piston is easier to install without incurring damage unlike the previous design. The seal is pressed against the piston and then held fixed by tightening a bronze washer beneath the seal. Previously, the seal was simply elongated over a groove in the cylinder, possibly causing damage and reducing its total lifespan. Finally, the new design addresses the issues with inadequate damping and sealing of the previous cushion assembly, by using tighter tolerances in the check valve and idle screw regions and smoother surface finishes where the piston glides against the seals.

3.3 Mathematical Modelling

The equations used to simulate the system are adapted from the work by Pournazeri [11] which determines the force balance in the cushion device, or hydraulic cylinder, using the pressure inside the engine cylinder, and the flow rates from the rotary spool valves.

Hydraulic Cylinder

The force balance on the moving mass, m, is given in equation 3.6 where: $\boldsymbol{x}$ and K are the engine valve lift and spring rate; $F_{friction}$, $F_{preload}$, $F_{damping}$, and F_{gas} are the forces of friction, spring preload, system damping, and engine cylinder gas force; finally, A_p and P_2 are the hydraulic area and pressure in the cushion device.

$$m\ddot{\boldsymbol{x}} = -K\boldsymbol{x} - F_{preload} - sign\left(\dot{\boldsymbol{x}}\right) F_{friction} - F_{gas} - F_{damping} + A_p P_2 \tag{3.6}$$

Pressure inside the hydraulic cylinder P_2 is found by relating the change in pressure to the change in volume for a compressible fluid: $\Delta P = \beta \Delta V / V$. Dividing both sides by the change in time results in an equation relating the change in pressure over time to the change in volume over time, the latter can be expressed as a sum of flow in and out from the high and low pressure valves as well as any surface boundary changes. This is combined to produce the pressure equation 3.7 seen below:

$$\frac{dP_2}{dt} = \frac{\beta}{V_{2,0} + A_p \boldsymbol{x}} \Big(Q_{hp} - Q_{lp} - A_p \dot{\boldsymbol{x}} \Big) \tag{3.7}$$

In-Cylinder Pressure Models

The gas inside the engine cylinder is approximated as an ideal gas of one uniform composition. Higher order models assume a burned and unburned portion of the gas but this is omitted for simplicity. The omission is justified by the in-cylinder pressure rapidly decreasing once the exhaust valve opens, and the purpose of determining this pressure is to find the gas force on the exhaust valve $F_{gas} = P_{cyl}A_{valve}$ where P_{cyl} is the cylinder pressure determined by equation 3.8:

$$P_{cyl} = \frac{m_{cyl}RT_{cyl}}{V_{cyl}} \tag{3.8}$$

Where; m_{cyl}, R, T_{cyl}, and V_{cyl} are the mass of the engine cylinder gas, the ideal gas constant, temperature of the gas, and the volume of the combustion cylinder. The engine cylinder volume is found by the mechanics of the piston motion as shown in equations 3.9 and 3.10:

$$V_{cyl} = A_{piston}y + V_{cyl,0} \tag{3.9}$$

$$y = r_{cs} + l_{rod} - r_{cs}\cos(\theta_{cs}) - \sqrt{l_{rod}^2 - r_{cs}^2 sin^2(\theta_{cs})} \tag{3.10}$$

Where; y, l_{rod}, r_{cs}, and θ_{cs} are the piston displacement, length of the piston connecting rod, radius of the crankshaft, and the crankshaft angle. An energy balance is performed on the cylinder shown in equation 3.11. In this equation, U_{cyl}, h_{cyl}, m_{ex}, Q, and W are the internal energy and enthalpy of the cylinder gas, the mass of gas escaping the cylinder, heat transfer into the gas, and work being done by the gas to the surroundings.

$$\frac{dU_{cyl}}{dt} = -\dot{m}_{ex}h_{cyl} + \frac{dQ}{dt} - \frac{dW}{dt} \tag{3.11}$$

The work by the gas on its surroundings is shown in equation 3.12 where the speed of the vertial piston displacement $\dot{y}$ is given by equation 3.13:

$$\frac{dW}{dt} = P_{cyl}\frac{dV_{cyl}}{dt} = P_{cyl}A_{piston}\dot{y} \tag{3.12}$$

$$\dot{y} = r_{cs}\dot{\theta}_{cs}\sin(\theta_{cs}) + r_{cs}^2\dot{\theta}_{cs}\sin(\theta_{cs})\cos(\theta_{cs})\left(l_{rod}^2 - r_{cs}^2 sin^2(\theta_{cs})\right)^{-1/2} \tag{3.13}$$

The internal energy is expanded using the product rule for derivatives in equation 3.14. The rate of change of the cylinder gas mass with respect to time, dm_{cyl}/dt is equivalent to the rate of mass leaving the cylinder.

$$\frac{dU_{cyl}}{dt} = \frac{d}{dt}(m_{cyl}u_{cyl}) = u_{cyl}\frac{dm_{cyl}}{dt} + m_{cyl}\frac{du_{cyl}}{dt} = m_{Cyl}\frac{du_{Cyl}}{dt} - u_{Cyl}\dot{m}_{ex} \tag{3.14}$$

Assuming constant heat capacities over time and temperature the internal energy and enthalpy are found using equations 3.15 and 3.16, where C_p and C_v are the capacities at constant pressure and volume.

$$\frac{du_{cyl}}{dt} = C_v\frac{dT_{cyl}}{dt} \tag{3.15}$$

$$\frac{dh_{cyl}}{dt} = C_p\frac{dT_{cyl}}{dt} \tag{3.16}$$

The above equations are combined to find the temperature of the cylinder gas using 3.17:

$$\frac{dT_{cyl}}{dt} = \frac{1}{m_{cyl}C_v}\Big(u_{cyl}\dot{m}_{ex} - \dot{m}_{ex}h_{cyl} + \frac{dQ}{dt} - P_{cyl}A_{piston}\dot{y}\Big) \tag{3.17}$$

The mass leaving the engine cylinder is calculated using equation 3.18 [18]. Where, C_d and C_m are flow coefficients found using Manring [18], and A_{ex} is the area of exhaust valve opening determined using equation 3.19.

$$\dot{m}_{ex} = \frac{-dm_{cyl}}{dt} = C_dC_mP_{cyl}A_{ex}\sqrt{\frac{1}{T_{cyl}}} \tag{3.18}$$

$$A_{ex} = 2\pi r_{valve}\boldsymbol{x} \tag{3.19}$$

Cylinder Pressure With Combustion

A modified in-cylinder pressure model is developed below that assumes no heat loss to the surroundings, minimal heat generated by the fuel (lower heating value), and using the

standard Wiebbe function to approximate the progression of fuel burnt [19]. This model relates the combustion to the engine crankshaft angle instead of performing the calculations on a time basis. See equation 3.20 for a reformulation of the first law with respect to crank angle.

$$\frac{dU_{cyl}}{d\theta} = -\dot{m}_{ex}h_{cyl} + \frac{dQ}{d\theta} - \frac{dW}{d\theta} \tag{3.20}$$

Using constant heat capacity with volume and modeling the work as change in pressure and volume, the internal energy and work done is calculated by equation 3.21.

$$\frac{dU_{cyl}}{d\theta} + \frac{dW}{d\theta} = P\frac{dV}{d\theta} + \frac{d}{d\theta}(mc_vT) \tag{3.21}$$

Since the cylinder contents are treated as an ideal gas, logarithmic differentiation is applied to the ideal gas equation 3.8 with constant mass and gas constant to yield equation 3.22.

$$\frac{dP}{P} + \frac{dV}{V} = \frac{dT}{T} \tag{3.22}$$

The above equations are combined to produce equation 3.23, and the heat capacity ratio κ is used to further simplify and produce equation 3.24.

$$\frac{dU_{cyl}}{d\theta} + \frac{dW}{d\theta} = c_v\left(\frac{PV}{R}\right)\frac{\frac{dP}{P} + \frac{dV}{V}}{d\theta} + P\frac{dV}{d\theta} \tag{3.23}$$

$$\frac{dU_{cyl}}{d\theta} + \frac{dW}{d\theta} = \left(\frac{1}{\kappa - 1}\right)V\frac{dP}{d\theta} + \left(\frac{\kappa}{\kappa - 1}\right)P\frac{dV}{d\theta} \tag{3.24}$$

Rearranging the energy balance in terms of differential heat release and substituting in equation 3.24 gives the following:

$$\frac{dQ}{d\theta} = \dot{m}_{ex}h_{cyl} + \frac{dU_{cyl}}{d\theta} + \frac{dW}{d\theta} \tag{3.25}$$

$$\frac{dQ}{d\theta} = \left(\frac{1}{\kappa - 1}\right) V \frac{dP}{d\theta} + \left(\frac{\kappa}{\kappa - 1}\right) P \frac{dV}{d\theta} + \dot{m}_{ex} h_{cyl} \tag{3.26}$$

Isolating and simplifying for the pressure gradient results in equation 3.27.

$$\frac{dP}{d\theta} = \left(\frac{\kappa - 1}{V}\right) \left(\frac{dQ}{d\theta} - \dot{m}_{ex} h_{cyl}\right) + \left(\frac{\kappa}{V}\right) P \frac{dV}{d\theta} \tag{3.27}$$

The minimum amount of heat release possible is determined in equation 3.28, where Q_{LHV} is the lower heating value of the gasoline used and $m_{f,b}$ is the mass of burnt fuel.

$$\left(\frac{dQ}{d\theta}\right)_{min} = Q_{LHV} \frac{dm_{f,b}}{d\theta} \tag{3.28}$$

Burned fuel mass is determined using equation 3.29 where m_f is the total fuel mass and x_b is the burnt fuel fraction determined by the Wiebbe function shown in equation 3.30. Here the constants used are $a = 2\ and m = 5$.

$$\frac{dm_{f,b}}{d\theta} = m_f \frac{dx_b}{d\theta} \tag{3.29}$$

$$x_b = 1 - exp\left[-a\left(\frac{\theta - \theta_o}{\Delta\theta}\right)^{m+1}\right] \tag{3.30}$$

Rotary Spool Valves

In order to calculate the flow rate from the spool valves, the opening area A_{SV} has to be determined using equation 3.31. The variables for this equation are shown in Figure 3.18, where θ_s and θ_c are the angles between the reference line and the ports on rotating spool and outer casing, ϕ_c and ϕ_s are the angles of opening on the spool and casing, r_s and l are the radius of the spool and length of the port.

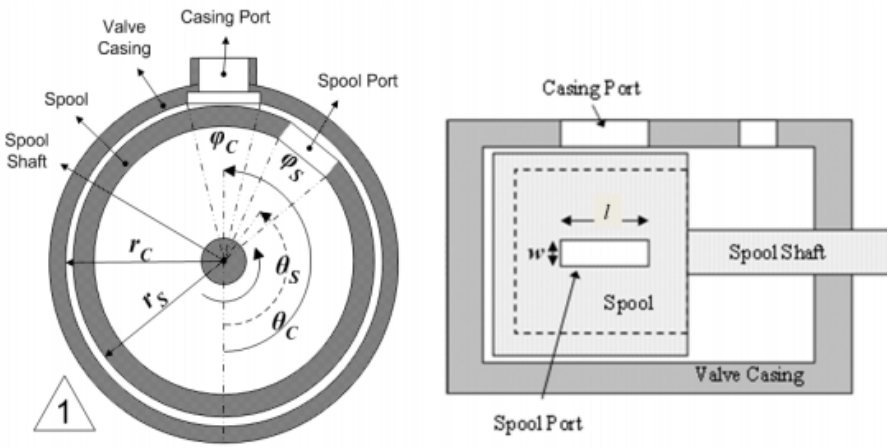

Figure 3.18: Geometry of rotary spool valves [11]

$$A_{SV} = \begin{cases} 0 & \theta_s \leq \left(\theta_c - \dfrac{\phi_c + \phi_s}{2}\right) \\ lr_s min\left(\phi_s, \theta_s - \theta_c + \dfrac{\phi_s + \phi_c}{2}\right) & \left(\theta_c + \dfrac{\phi_c - \phi_s}{2}\right) \geq \theta_s \geq \left(\theta_c - \dfrac{\phi_c + \phi_s}{2}\right) \\ lr_s min\left(\phi_c, \theta_c - \theta_s + \dfrac{\phi_s + \phi_c}{2}\right) & \left(\theta_c + \dfrac{\phi_c + \phi_s}{2}\right) \geq \theta_s \geq \left(\theta_c + \dfrac{\phi_c - \phi_s}{2}\right) \\ 0 & \theta_s \geq \left(\theta_c + \dfrac{\phi_c + \phi_s}{2}\right) \end{cases} \tag{3.31}$$

ΔP refers to the difference in pressure across the spool valve. In the high pressure spool valve case, assuming negligible losses in the pipes and fittings, the pressure inside the spool valve is P_{high} provided by the pump and accumulator. The spool valve outlet pressure is approximated as the hydraulic cylinder pressure P_2. However, in the low pressure spool valve case, the pressure inside the rotary valve is equivalent to the hydraulic cylinder pressure P_2, and the outlet port pressure is reservoir or low pressure P_{low}. Using the opening area found in equation 3.31 with the flow through an orifice model, the flow rate in the spool valves can be approximated by equations 3.32 and 3.33.

$$Q_{hp} = \begin{cases} A_{SV} C \sqrt{2 \dfrac{P_{hp,in} - P_{hp,out}}{\rho}} & P_{hp,in} \geq P_{hp,out} \text{ and } A_{SV} \neq 0 \\ 0 & else \end{cases} \tag{3.32}$$

$$Q_{lp} = \begin{cases} A_{SV} C \sqrt{2 \dfrac{(P_{lp,in} - P_{lp,out})}{\rho}} & P_{lp,in} \geq P_{lp,out} \text{ and } A_{SV} \neq 0 \\ 0 & else \end{cases} \tag{3.33}$$

In addition to the flow when the spool and outer casing ports are aligned, flow from leakage is expected as shown by Pournazeri's model in Figure 3.19. This leakage flow through the small gap between the spool outer diameter and casing inner diameter is approximated by simplifying the Navier Stokes equations [20]. The simplifying assumptions are: fluid is incompressible, flow is uniform over θ or only varies axially and radially, the velocity of the fluid is zero at the outer casing walls and equivalent to the spool velocity at the spool wall. The leakage flow rates in the axial and radial directions of the spool valves are given in equations 3.34 and 3.35.

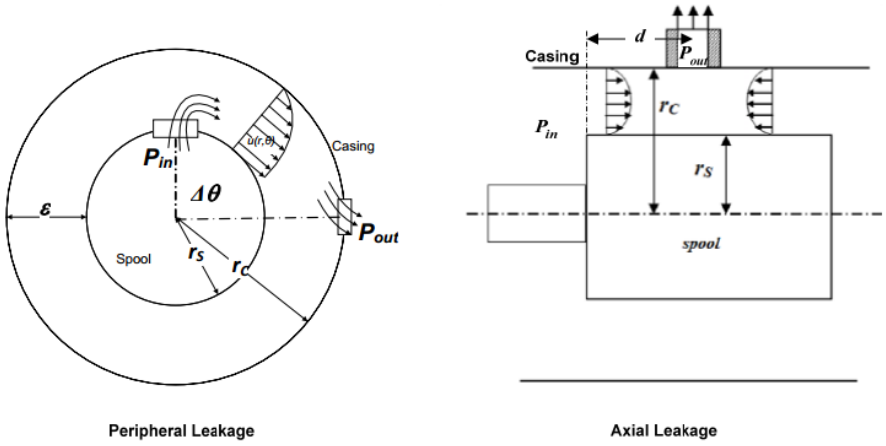

Figure 3.19: Axial and radial leakage in spool valves [11]

$$Q_{leak,a} = (r_s + r_c)\,\phi_c \left(\frac{(r_c^3 - r_s^3)\,(\Delta P)}{12\mu d} + C_{1,a}\,(r_c\,(\ln r_c - 1) - r_s\,(\ln r_s - 1)) + C_{2,a}\,(r_c - r_s) \right) \tag{3.34}$$

$$C_{1,a} = \frac{-\,(r_c^2 - r_s^2)\,\Delta P}{4\mu d\ \ln(r_c/r_s)}$$

$$C_{2,a} = \frac{-\,r_c^2 \Delta P}{4\mu d} - C_{1,a} \ln(r_c)$$

$$Q_{leak,r} = l \left(\frac{\Delta P\,(r_c^2 - r_s^2)}{2\mu\Delta\theta} + C_{1,r}\,(r_c\,(\ln r_c - 1) - r_s\,(\ln r_s - 1)) + C_{2,r}\,(r_c - r_s) \right) \tag{3.35}$$

$$C_{1,r} = \frac{-\,r_s\dot{\theta}_s\Delta\theta + (r_c - r_s)\,\Delta P}{\mu\Delta\theta \ln(r_c/r_s)}$$

$$C_{2,r} = \frac{-\,r_c \Delta P}{\mu\Delta\theta} - C_{1,r} \ln(r_c)$$

Pressure Losses

Resistance to flow in the hydraulic tubes results in pressure loss that is calculated using techniques detailed by Fox and McDonald [20]. Simulations not accounting for pressure loss produce a maximum flow rate that stays within the laminar flow regime. Assuming incompressible flow inside the tubes, the Reynold's number criteria is met for laminar flow: $Re = \rho v D/\mu < 10^5$. Using the friction factor $f = 64/Re$ and simplifying all the fittings and tube length into an equivalent length, L_e, the loss in pressure is described by equation 3.36.

$$\Delta P = \frac{128\mu L_e Q}{\pi D^4} \tag{3.36}$$

3.4 Simulation Results

The engine valve lift results from the mathematical model are presented in this section using the parameters in Table 3.1. The code and simulink model used to generate the results are given in Appendix A.

Table 3.1: Simulation model parameters

Symbols and Values					
A_{piston}	0.0064 cm^2	V_{c0}	20 cc	r_{cs}	27 mm
l_{rod}	83.9 mm	r_v	12.5 mm		
β	17000 bar	ρ	850 kg/m^3	μ	0.051 Ns/m^2
K_{spring}	20 N/mm	$x_{preload}$	3 mm		
m	0.1 kg	$V_{2,0}$	5.72e-5 m^3	A_p	173.55 mm^2
C_d	0.6	l	8 mm	d	18mm
ϕ_c	20 deg	ϕ_s	20 deg	r_s	15 mm
r_c	15.01 mm	Q_{LHV}	43.4 MJ/kg	$\Delta\theta$	50°
P_o	101 kPa	k	1.4	R	287
C_v	717.5 J/kgK	C_p	1004.5 J/kgK	$T_{cyl,o}$	1000 K
spool valve offset	100°	F_{fric}	70 N	C_{damp}	142 Ns/m

Models results are given below in Figure 3.20 for different pressures and distances between the high and low pressure spool valves. The model uses an engine speed of N= 1000 rpm with spring rate k= 20 N/mm. Figure a) shows that increasing the system, or high, pressure results in larger valve lifts as expected. Furthermore, higher pressures are expected to open the valves earlier and close later in comparison to the low pressures. Note that the spool valve ports have a total opening angle of 40°and are rotating at half the speed of the engine crankshaft; therefore, the opening and closing of the engine valves lasts 80CA°. Figure b) shows the effect of changing the valve duration, or reducing the distance between the high and low pressure spool valves. Depending on the system pressure, reducing the angular distance between the spool valves can result in decreased lift due to the overlap between high and low pressure spool valve openings.

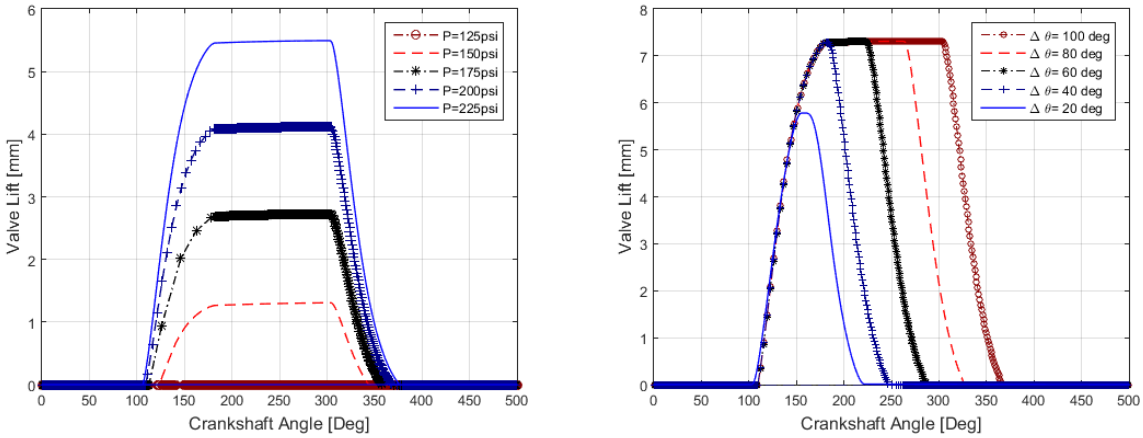

(a) Changing system pressure

(b) Varying angular distance between high and low pressure valves at P=250 psi

Figure 3.20: Engine valve lift simulations at N = 1000 rpm

Simulations varying the spring rate of the engine valve are given in Figure 3.21 at a constant high pressure of P= 250 psi and engine speed of N= 1000 rpm. The results are as expected for the valve lift to decrease as the spring rate increases. This shows the pump energy that can be wasted if the spring rate is unnecessarily high and thereby limiting the valve lift.

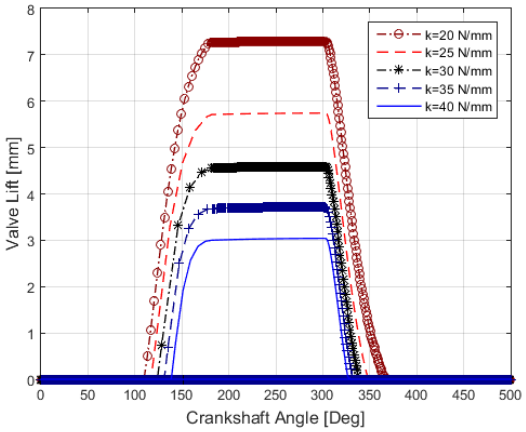

Figure 3.21: Simulations with different engine valve spring rates at system pressure P = 250 psi

Results for changing the spool valve port opening size are given in Figure 3.22 at a constant speed of N= 1000 rpm and pressure P= 250 psi. The port sizes are changed by varying the opening angles from 10°to 30°. Small port angles can result in "valve float" as shown by the $\phi_s = 10$ results where the valve lift does not return to 0 mm. This floating occurs because the low pressure valve spool does not remain open long enough to relieve the pressure in the hydraulic cylinder. To ensure valve float does not occur, a stiffer spring can be used, or a larger opening in the low pressure spool valve.

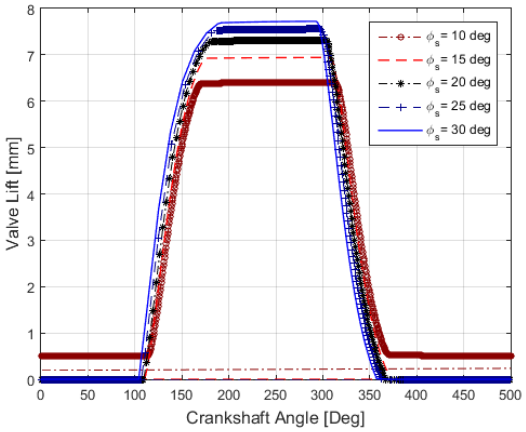

Figure 3.22: Simulations with different spool valve port opening angles at system pressure P = 250 psi

Valve lift simulations at different engine speeds are shown in Figure 3.23. The simulations use two engine valve spring rates of k = 20 and 30 N/mm at high pressure P = 250 psi. The lower spring rate causes the valves to float at N $\geq$ 1500 rpm. The higher speeds lower the time in which the spring has to shut the engine valve; therefore, stiffer springs are required as shown in Figure 3.23b) for k= 30N/mm.

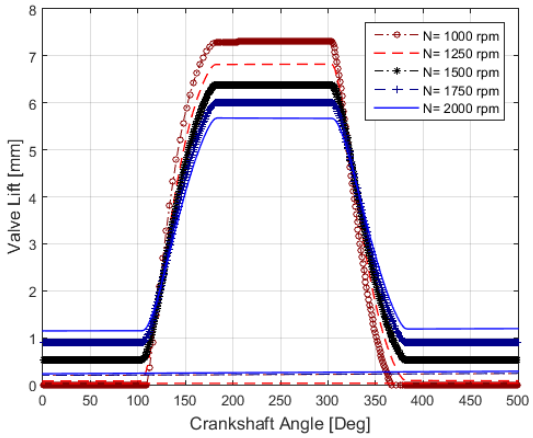

(a) k = 20 N/mm engine valve spring

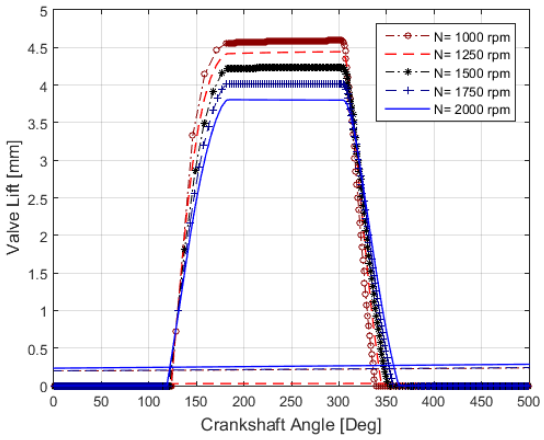

(b) k = 30 N/mm engine valve spring

Figure 3.23: Engine valve lift simulations at system pressure P = 250 psi

Chapter 4

Experimental System

This chapter shows the experimental design for testing the HVVA system. Specifcally, how the VVA system was assembled as well as controlled using dSpace and Simulink.

4.1 Experiment Frame Assembly

The HVVA system connects to a small single cylinder engine, a Honda GX-200, as shown in Figure 4.1. This configuration allows the engine to be driven by a dynamometer, not pictured, at a fixed speed. The system is divided into its mechanical, hydraulic, and electrical layouts as detailed in the sections that follow.

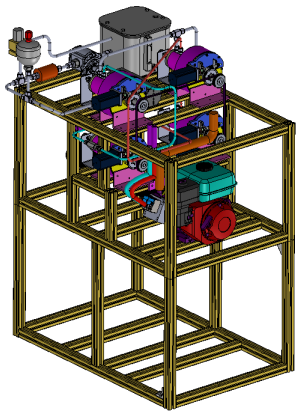

Figure 4.1: HVVA engine test bench

4.1.1 Mechanical Assembly

The test assembly without the structural frame is presented in Figure 4.2. This assembly shows the engines connection to the dynamometer, its ability to vent outside the system, the HVVA connection on to the engine head, as well as the tubing connections and hydraulic equipment necessary for the rotary spool valves. Starting from the bottom right, the engine is shown connected to a large drive shaft that couples the engine crankshaft to a dynamometer. The fuel intake system is left unchanged while orange tubing replaces the exhaust system to vent engine emissions safely outside of the lab environment. A modified engine head cover is shown with cushion devices over each engine valve. The fluid necessary to move the engine valves flows through the blue tubing for the exhaust valve and red tubing for the intake valve. The engine crankshaft drives each rotary spool valve through a timing belt system, while the phase shifters allows for valve timing adjustments in the spool valves. The rotary spool valve assemblies are shown with low pressure valves on top of the high pressure valves, in an effort to reduce piping distance between the cushion devices and high pressure spool valves. Lastly, gray tubing is shown connecting the spool valves to the reservoir, pump, relief valve, and accumulator.

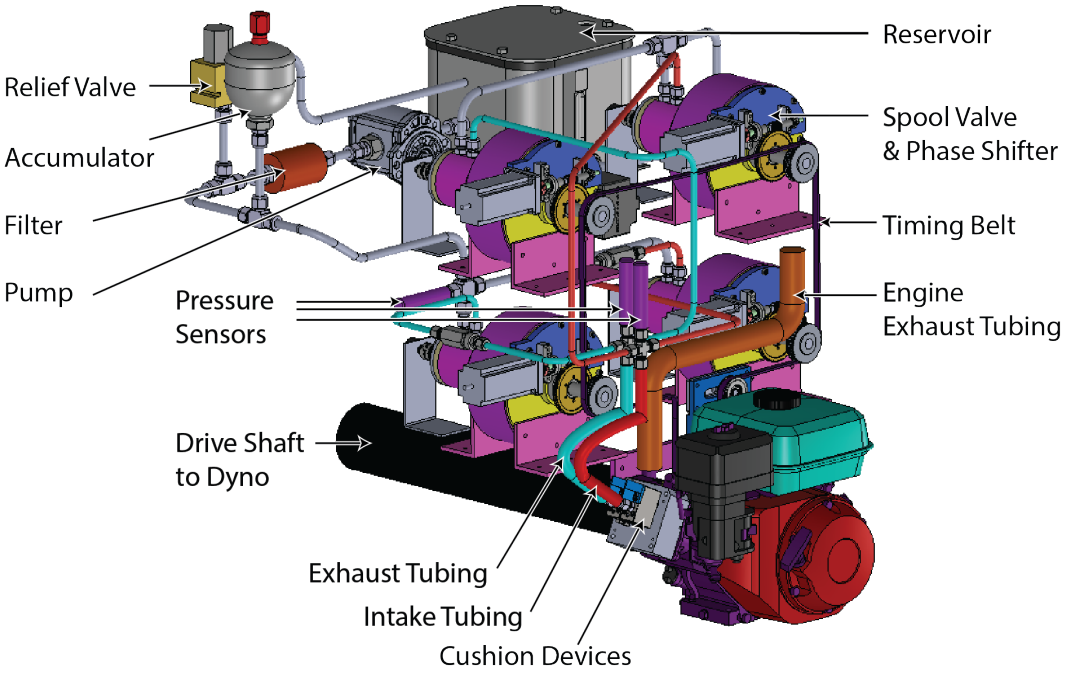

Figure 4.2: HVVA engine test bench without structural frame

4.1.2 Hydraulic Assembly

The hydraulic layout of the experimental system is shown in Figure 4.3. The system pumps hydraulic fluid, out of a reservoir, through a filter, and into a junction where it flows into both high pressure spool valves (HPSVs). Before the junction where the intake fluid flow splits into two, there is an gas-charged accumulator that stores additional fluid to aid the pump flow and a pressure sensor that describes the "system pressure". Furthermore, there is a relief valve immediately after the filter that is set to the maximum operating pressure. If the system exceeds this pressure, the relief vale opens to divert the flow back to the reservoir, thereby preventing components downstream from ever exceeding the maximum pressure. Each high pressure spool valve, once opened, pass fluid to a cushion device that sits above an engine valve. The cushion devices are shown with an adjustable cushion or damping setting. Pressure sensors mount above each cushion device to record the hydraulic cylinder pressure acting on each engine valve. When the low pressure spool valves open, fluid from the cushion device drains back to the reservoir.

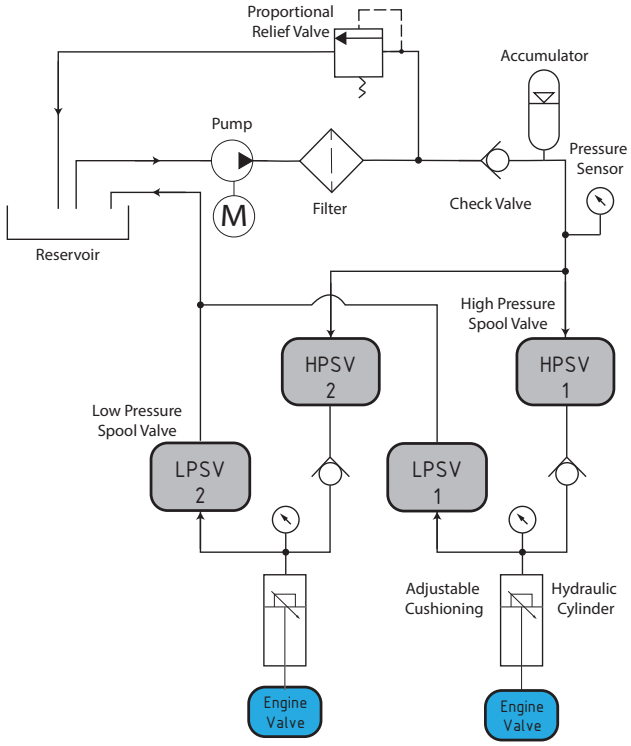

Figure 4.3: Hydraulic layout of HVVA experimental setup

Pump and Accumulator

The HVVA system uses an accumulator to reduce the required speed of the pump, stabilize the system pressure, and provide shock absorption against pressure spikes. General guidelines suggest the accumulator pre-charge pressure be 0.4-0.8 times the operating pressure to augment the pump and to absorb pressure spikes [21]. Using an assumption of 400 psi operating pressure, the pre-charge is set to 250 psi. In order to size the accumulator, the required flow rate *without* an accumulator is found below in equation 4.1. In this equation, V_n is the volume displaced inside the cushion device for each engine valve opening, D_1 is the cushion device ID, D_2 is the hydraulic cylinder OD, l_v is the engine valve max lift, T is the time for one engine cycle, and Q_n is the flow rate required per valve. The values from the calculation are given in Table 4.1 using a maximum valve lift of 7 mm.

$$\begin{aligned} V_n &= \frac{\pi}{4}(D_1^2 - D_2^2)l_v \\ V = nV_n &= \frac{n\pi}{4}(D_1^2 - D_2^2)l_v \\ t_{spool} = t_s &= N\frac{360°percycle}{40°portopening} \\ T &= 60\frac{s}{min} \times \frac{2}{N}\frac{min}{rev} \\ Q_n &= \frac{V_n}{t_s} \end{aligned} \tag{4.1}$$

The lowest allowable pump speed is attained by distributing the required flow rate for engine valve lift over the entirety of the engine cycle. This concept is demonstrated in Figure 4.4. **Note:** the old pump only worked to open engine valves, the new pump fills the accumulator when the engine valves are closed. The new pump flow rate, V_{1a}, and initial accumulator size, V_{1a}, are found using equations 4.2. The other variables are described and their values collected in Table 4.2.

Table 4.1: Flow rate requirement by pump without the use of an accumulator - solutions to equations 4.1

Description	Variable	Value
Cushion Device ID	D_1	15.875 mm
Piston Shaft OD	D_2	5.5 mm
Distance Travel	l_v	7 mm
Volume displaced per valve	V_n	0.001225 L/valve
Engine Speed	N	3600 RPM
Time spool port is open	t_s	$\approx 0.003704\ s$
Total time for cycle	T	0.0333 s
Flow rate per valve	Q_n	5.27 gpm

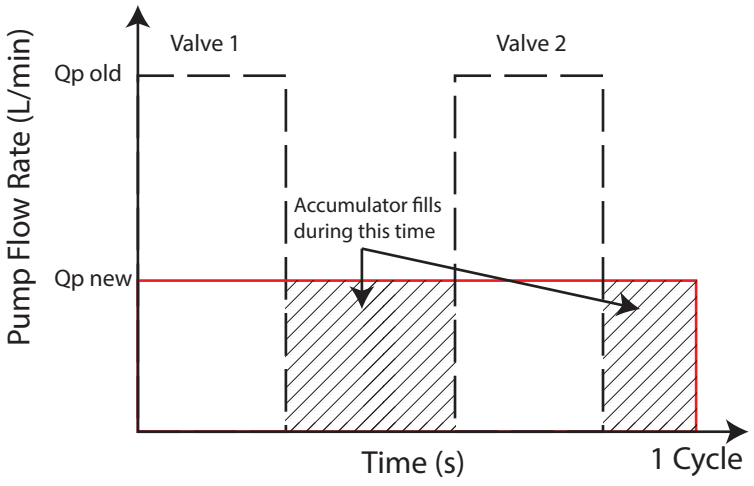

Figure 4.4: Pump flow rates with and without the aid of an accumulator

$$
\begin{aligned}
&New\ pump\ flow\ rate: \\
&\qquad Q_p = \frac{Q_n \times 2t_s}{T} \\
&Accumulator\ change\ in\ volume: \\
&\qquad \Delta V_a = Q_p \times (T - nt_s) \\
&Sizing\ accumulator: \\
&\qquad P_2 = 400\ psi \qquad P_3 = 1000\ psi \\
&\qquad P_1 = 0.5 \times P_2 \qquad P_2 = 200\ psi \\
&\qquad V_{1a} = \frac{\Delta V_a}{\left(\frac{P_1}{P_2}\right)^{\frac{1}{k}} - \left(\frac{P_1}{P_3}\right)^{\frac{1}{k}}}
\end{aligned}
\tag{4.2}
$$

Table 4.2: Accumulator sizing and new pump flow rate - solutions to equations 4.2

Description	**Variable**	**Value**
Nitrogen gas - heat capacity ratio	κ	1.4
New pump flow rate	Q_p	4.417 L/min
Change in accumulator Volume	ΔV_a	0.0019086 L
Operating system pressure	P_{2a}	$\approx 400\ psi$
Maximum system pressure	P_{3a}	1000 psi
Pre-charge accumulator pressure	P_{1a}	250 psi
Accumulator initial volume	V_{1a}	$\approx 0.00652\ L$

The maximum accumulator size is $V_{max} = V_{1a} + \Delta V \approx 0.009L\ or\ 0.003gal$, this justified the use of an accumulator with a 0.026 gal capacity. In addition to the accumulator sizing, the pump and its motor were considered appropriate for the experiment using assumptions about the pump displacement and efficiency. The pump has a displacement

of approximately $V_D \approx 0.4\ in^3/rev$ and the overall efficiency is $\eta \approx 70\%$, a conservative estimate according to 'Fluid Systems Theory' [21]. The pump motor speed for a 7 mm valve lift is found to be $N_{pump} = 965\ rpm$ using equation 4.3. This speed is considerably less than the maximum pump rated speed of 4000 rpm.

$$N = \frac{Q}{\eta V_D} \tag{4.3}$$

Pressure Control Valve

The system uses a proportional relief valve as a safety relief-valve. The original intent of the valve, shown in Figure 4.5, was to adjust the system pressure and hold it steady while setting the pump to run at a high speed, ensuring an adequate flow rate. The pressure could be changed by sending a PWM signal to the valve, which changes the allowed pressure drop across the valve before it fully opens. Therefore, allowing the valve to change the maximum system pressure [22]. However, the experimental design changed to control the pressure by varying the pump speed and using the pressure control valve as a safety measure to ensure the system never surpassed a maximum pressure of 1000 psi. The safety limit is chosen to be below the pressure rating for the seals and fittings used in the experiment.

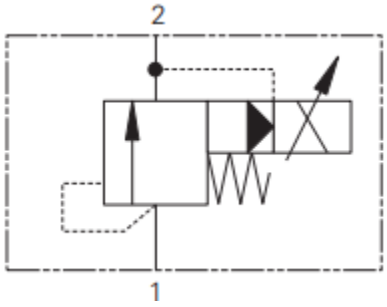

Figure 4.5: Pressure relief valve with proportional control

4.1.3 Electrical Assembly

The electrical layout of the system is shown in Figure 4.6. The layout shows the sensors, encoders, and actuators connecting to the controller cards. More information about the controller is given in section 4.2. Electrical control of the system involves digital and analog

sensor measurements, control of servo and stepper motors, and monitoring rotary encoder outputs. The digital input/output card controls the phase shifting motor and adjusts the maximum system pressure setting on the safety relief valve. The analog input card records the pressure and valve displacement sensor outputs. The analog output controls the dynamometer and pump servo motor. Lastly, the encoder card takes the readings from the spool valves and engine crankshaft rotary encoders. Duplicate parts are not given in the layout; for instance, only one pressure sensor is shown connecting to the DS-2003 analog input card where as the actual system has two pressure sensors connecting to the DS-2003 card. Similarly, only one stepper driver, phase shifter, spool valve, and rotary encoder are shown when the actual assembly contains four of each.

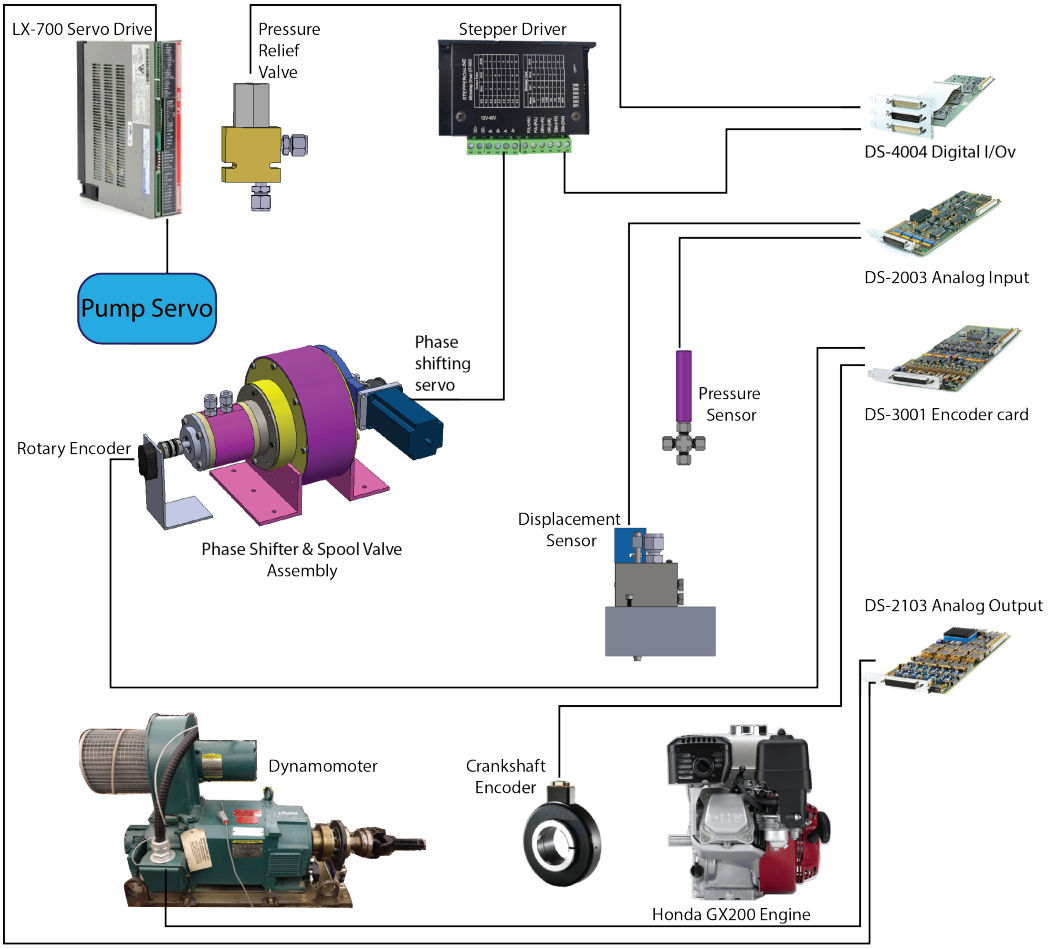

Figure 4.6: Electrical layout of HVVA experimental setup

The analog sensor used to measure engine valve displacement is shown in Figure 4.7. The sensor works on the inductive principle, outputting a 0-5 V signal when a metal piece moves along it's sensing range. Lack of a separate ground wire prevents filtering out noise during experiments as the sensor uses the ground for a reference 0 V signal. Since the sensor is a custom design, furture experiments should use a 4 wire sensor to improve the signal to noise quality of the sensor.

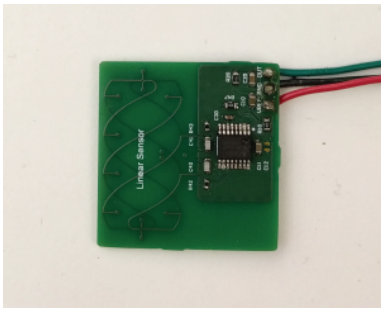

Figure 4.7: Linear displacement sensor with 0 to 5V output for 10 mm range

Calibration of the sensor is given in Figure 4.8 using linear, polynomial, and spline interpolation. Calibrating the sensor showed the non-linear voltage output of the sensor, especially in the 0-2 mm range. By moving the metal piece that is detected by the sensor over the linear region only, displacement sensor non-linearities are accounted for in the experiments.

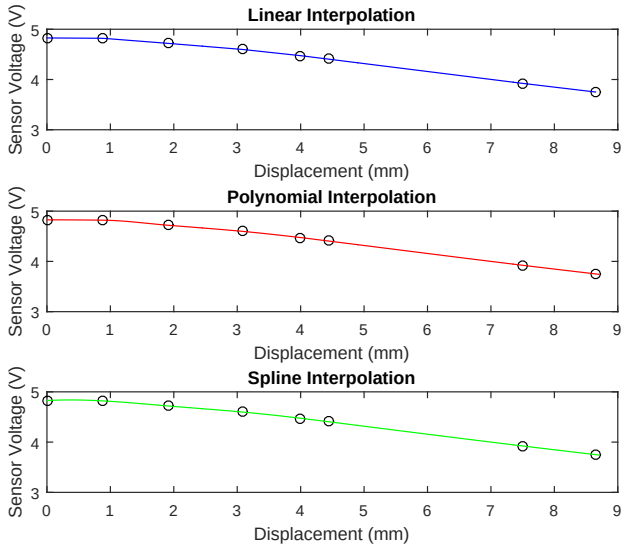

Figure 4.8: Valve displacement sensor output calibration curve showing non-linear behaviour near the zero displacement end

4.2 Hardware Control and Simulink Interfacing

The control logic and communication layout between the dSpace controller and electrical hardware is done through a Simulink program. The layout consists of dividing the signals, from sensors and to actuators, into inputs and outputs. These signals are represented in the program as analog or digital depending on the dSpace card that is used for the signal. This section further explores the logic used in each section of the analog and digital signals. Additionally, the controls used for safety measures are shown in this section. Finally, the user interface is presented, allowing monitoring and manipulation of the simulink program done through a program called ControlDesk.

The top level of the simulink program is separated into the inputs and outputs of the experimental system as shown in Figure 4.9. Expansion of the input subsystem is shown for the analog signals in Figure 4.10. The analog input card, dSpace DS2002, records the speed of the pump servo motor, pressure readings for the system and each engine valve hydraulic cylinder, and the torque measurements from the dynamometer. These input signals are then routed to their respective sub-systems as shown by the blocks for temperature and

valve lift sensors. Before the signals can be used for monitoring and control purposes they are conditioned using amplification and filtering techniques. Conditioning of an input signal is shown in Figure 4.11 for the intake valve pressure sensor. Unmodified, or "raw", sensor signal is first conditioned using a moving average filter and then amplified, according to its calibration curve, to obtain the actual pressure reading. Moving average filtering uses a delay line, taking 150 samples, which are then averaged to a single value using a matlab block.

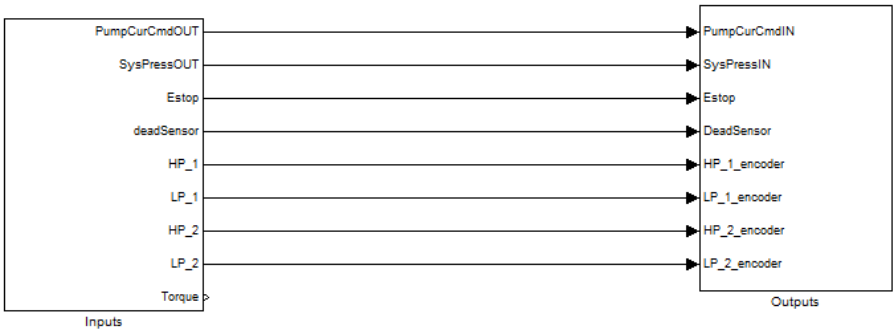

Figure 4.9: Main inputs and outputs in high level of Simulink control model

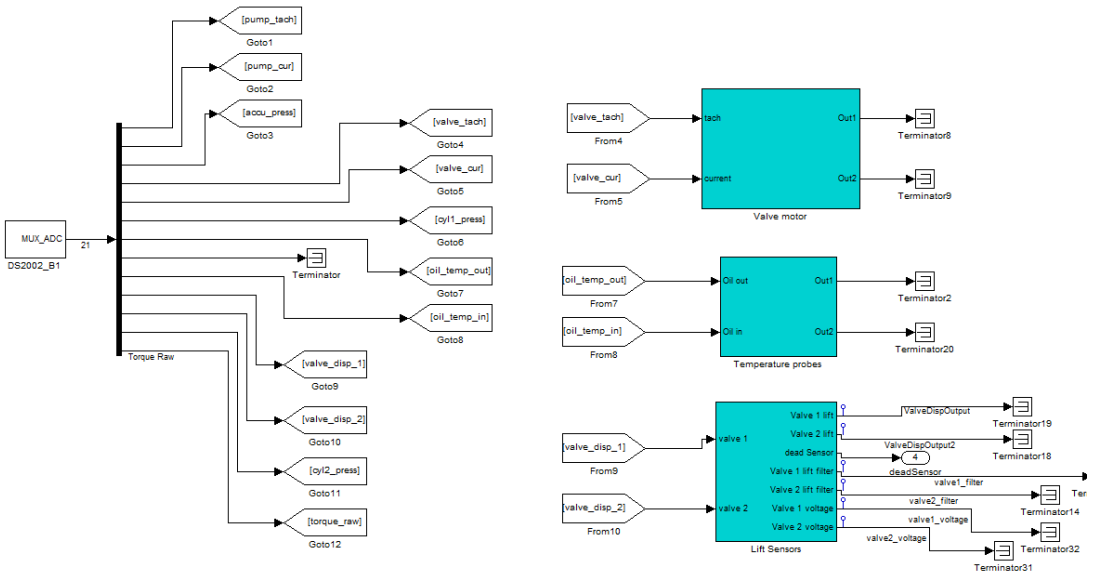

Figure 4.10: Analog input modules

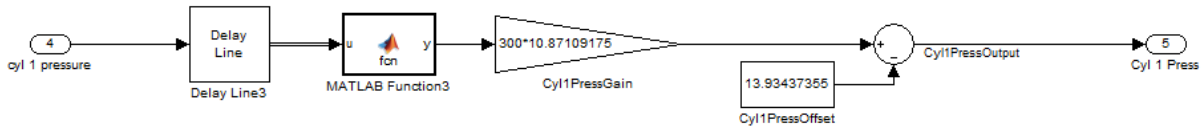

Figure 4.11: Conditioning input signals to reduce noise or decrease lag in the dSpace controller

Signals from the rotary encoders are recorded using the dSpace DS3001 card as shown in Figure 4.12. Similar to the analog input conditioning, the encoder signals are amplified to produce the actual spool valve angles. The angular outputs from the high and low pressure spool valves are also subtracted to produce the angular duration during which the engine valves should remain open. Furthermore, the DS3001 card includes an index block which resets the encoder value once the index is detected. Therefore, the encoders loop back to 0°after each rotation and are calibrated after the first rotation each time the system is rebooted.

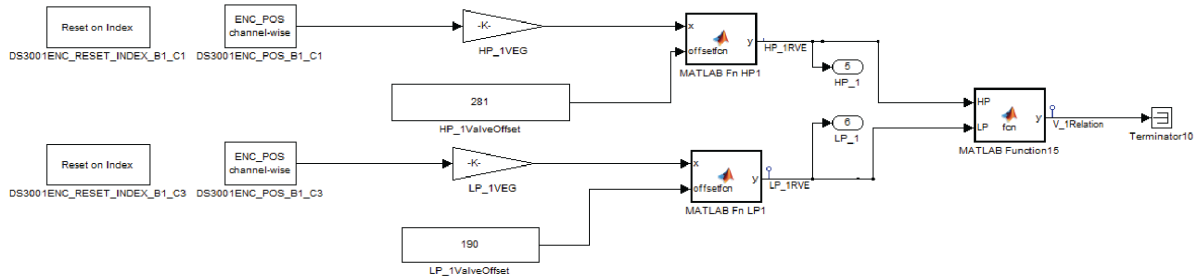

Figure 4.12: Encoder inputs from the high and low pressure rotary spool valves and the conditioning method to obtain spool valve angles

Analog output controls the pump and dynamometer speeds as shown in Figure 4.13 using the DS2103 card. Rate limiter blocks are used to ensure the speeds smoothly ramp up at 100 rpm/s to prevent damage to the mechanical parts.

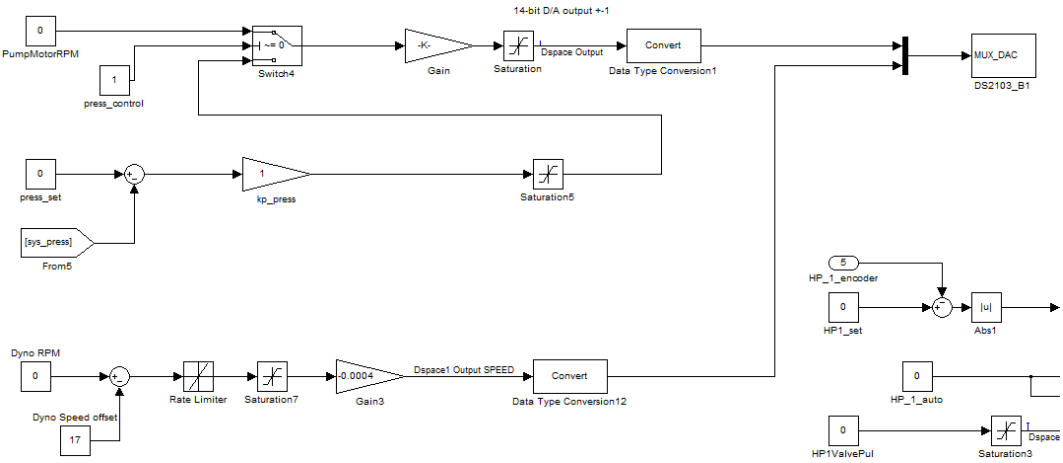

Figure 4.13: Pump motor and dyno control

Digital I/Os

Communication involving digital inputs and outputs is done using the DS4004 card. The digital card allows for high/low signals to indicate an "on" or "off" setting and PWM signals that can digitally mimic analog signals. Use of these signal types to control the proportional relief valve and phase shifting stepper motors is shown in Figure 4.14. Switiching between high (1) and low (0) changes the stepper motor direction and the pressure duty cycle changes the setting at which the pressure relief valve opens (0.5 x max pressure = new max pressure setting). The digital outputs are all limited between 0 and 1 using saturation blocks.

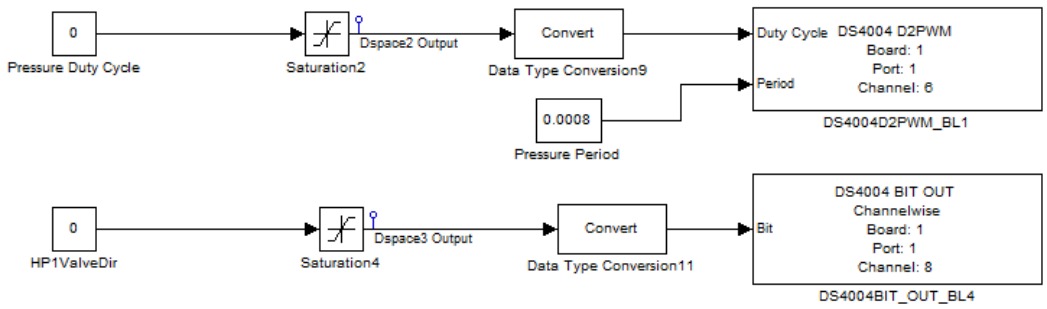

Figure 4.14: Proportional relief valve and stepper motor direction control using PWM and high/low signals

Safety Measures

Safety measures are implemented through a "set-reset" switch that shuts down the pump motor, effectively reducing the system pressure to prevent valve actuation, and therefore disabling engine combustion. The switch is triggered in the following cases: exceeding a maximum allowable system pressure or pump motor current, if the displacement sensors are in a fault state, and if the pump stop button in ControlDesk or the physical Estop button has been pressed. These safety measures are shown in Figure 4.15.

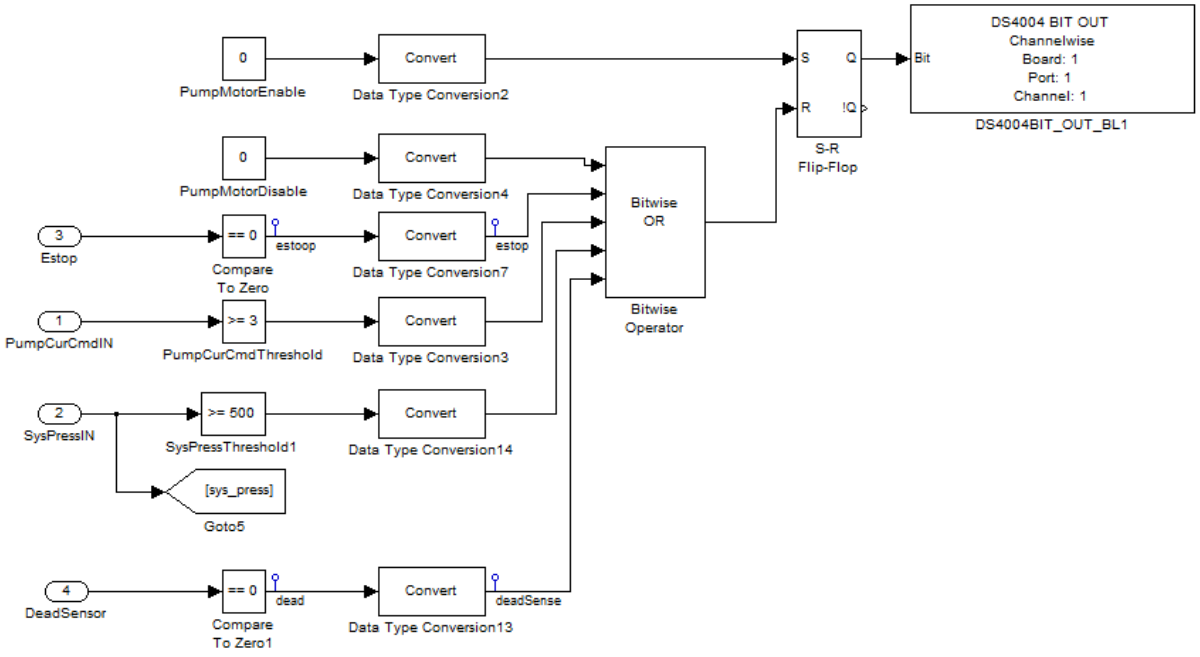

Figure 4.15: Safety control for pump and dynamometer motors

User Interface

The dSpace system compiled the Simulink program and allowed visual access and control over the inputs and outputs. The user interface for the controller was created in ControlDesk and a sample of it is shown in Figure 4.16. Green and red lEDs indicate whether the pump, sensors, or spark plug are active or inactive. The user has control over starting the pump, setting the pump speed, system pressure, and desired valve lift. The interface

lets users observe the pressures in the system, lift of each valve in both the original and filtered signal, as well as the duration of each valve, and crank angle.

Figure 4.16: Control Desk user input interface allowing manual control of pump, lift target, combustion start and read outs of pressures and valve lifts

User ability to monitor and set each spool valve's anglular position is shown in Figure 4.17. The angles refer to the spool port aligning perfectly with the outer casing port at 0°and move in the same direction as the engine crankshaft output.

Lastly, the ability to select between manual, open loop, and closed loop control of the system to reach a desired valve lift is presented in Figure 4.18. The open loop control uses a look-up table of pressure needed to achieve a desired lift for a given engine speed, where as the closed loop control monitors the system pressure and adjusts to reach the desired valve lift. The Simulink programming to accomplish this is given in Section 5.4.1.

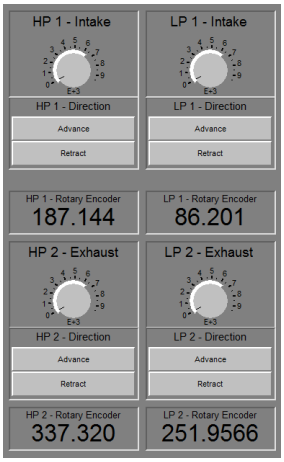

Figure 4.17: Spool valve encoder measurements and manual phasing controls, HP1 refers to high pressure for intake and LP2 refers to low pressure for exhaust

Figure 4.18: User interface for selecting manual, open loop, or close loop PID control to reach a desired valve lift for an engine speed

Chapter 5

Experimental Results and Discussion

This chapter contains a brief overview of how tests were conducted, followed by the first series of experiments on a test bench excluding the use of an engine. After that, the experiments involving an engine are done using the assembly developed in Chapter 4. Initially, these engine experiments are done without combustion to ensure the system is operating as expected before introducing the possibility of engine back or after fire and possible piston-valve collisions. Following that, combustion tests are conducted on the engine with a controller to achieve a desired valve lift. Finally, the system is dis-assembled for post-testing examination of the relevant parts.

5.1 Methodology for Collecting Results

The testing process has the following steps:

1. Start the dSpace controller and power on all the components *except for the dynamometer*.
2. Manually rotate the crankshaft twice to reset all the encoders.
3. Bring piston to TDC by rotating the crank shaft with no fluid flow in the system.
4. Move the spool valves to the desired angles by phase shifting.
5. Allow fluid to flow through the system by starting the pump.

6. Start the dynamometer and slowly ramp up the engine speed for the desired test.

7. Build up the pressure for the desired amount of lift.

Note that this testing process is only relevant for the engine tests since there is no dynamometer used on the test bench experiments in section 5.2. In those experiments, the system has to be rotated twice to ensure all the encoders are reset.

5.2 Engine-less Tests

Initial component testing was conducted using a test bench, seen in Figure 5.1. A servomotor, elevated above the spool valves, emulated the engine output. Additional details about the test bench can be found in the work by Chermesnok [12]. The bench allowed one set of the spool valve, phase shifter, and cushion device to be tested. A single valve was actuated by the cushion device assembly, with the new spool valve providing the high pressure, and a previously designed spool valve, see Chermesnok's design 3.1, providing the low pressure side. Engine-less tests were done to validate the assemblies for basic functional requirements, and to address design flaws before additional manufacturing. Furthermore, the test bench eliminated the complexity of engine tests which would require four functioning sets of spool valves and two cushion device assemblies.

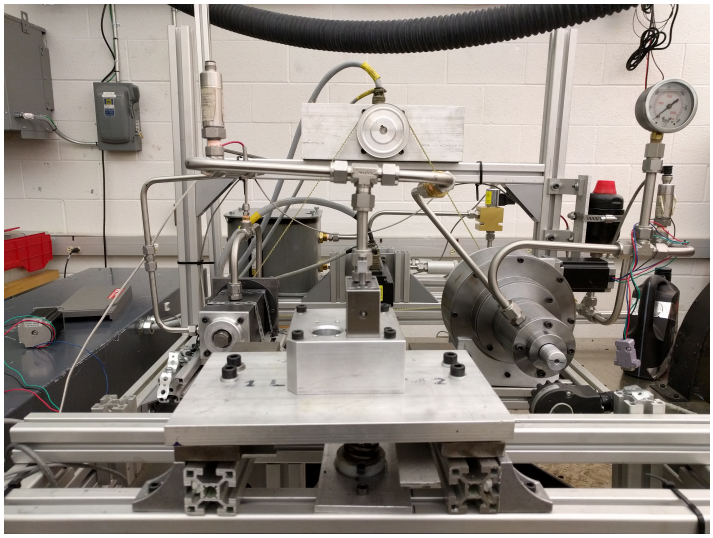

Figure 5.1: Test bench used to validate parts for functional requirements without the use of an engine

The test bench experiments, using the methods given below, allowed the following design requirements to be validated:

1. *Phase Shifting*

   The new spool valve design was used for the high pressure side of the system and phase shifting allowed the valve event to increase (or decrease) in duration as shown in Figure 5.2. Additionally, the crank angle at which the valve opens could also be changed.

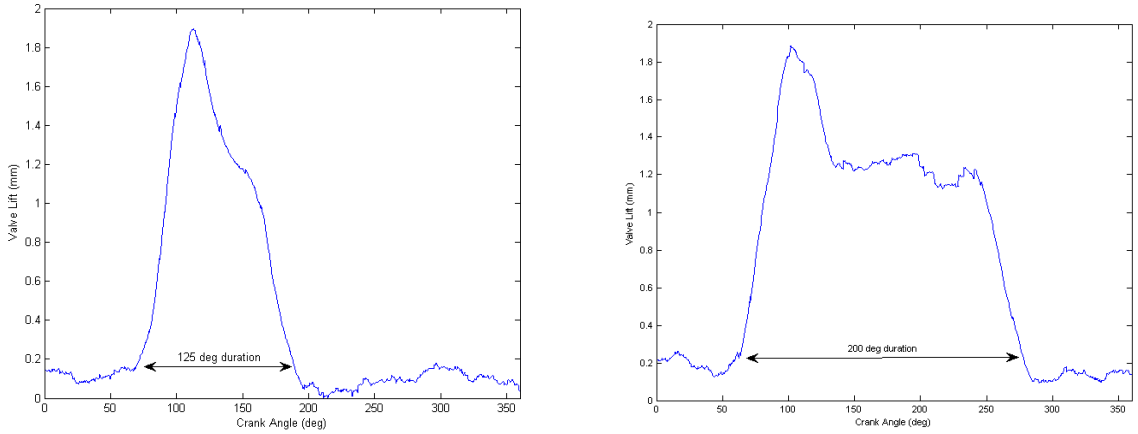

(a) Valve event duration of 125 degrees **(b)** Valve event duration of 200 degrees

Figure 5.2: Phase shifting to change timing of valve event

2. *Valve Lift*

   Changes in valve lift can be accomplished by raising the system pressure. The higher pressure results in a greater force on the hydraulic cylinder, acting against the spring on the test bench, which increases the valve lift.

3. *Adjusting Valve Seating Velocity*

   The damping effect, also called cushioning effect, takes place in the last 4 mm of motion when the valve is closing. The damping mechanism allows for the valve to decelerate to a safe speed before it closes on to the valve seat.

In addition to testing functional requirements, the engine-less tests revealed design issues in the spool valve and cushion device assemblies. The spool valve flow ports required

a flat face to ensure the hydraulic fittings could seal against pressure. These changes were incorporated into the system design before additional manufacturing for the on-engine tests.

Leakage occurred during initial pressurizing from the casing ports. Curvature of the spool casing, preventing the hydraulic fittings from completely sealing the ports as showing in Figure 5.3, was deemed to be the cause. Milling flats around the hydraulic ports, as shown in Figure 5.4, allowed the fittings to seal without additional leakage.

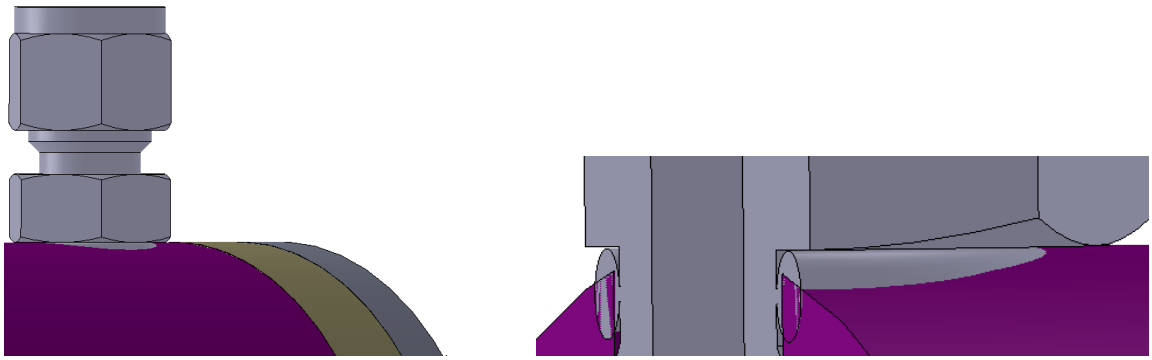

(a) Curvature of spool valve and sealing issue **(b)** Section view showing seals not below the outer casing surface

Figure 5.3: Issues with sealing for spool valve with round outer casing

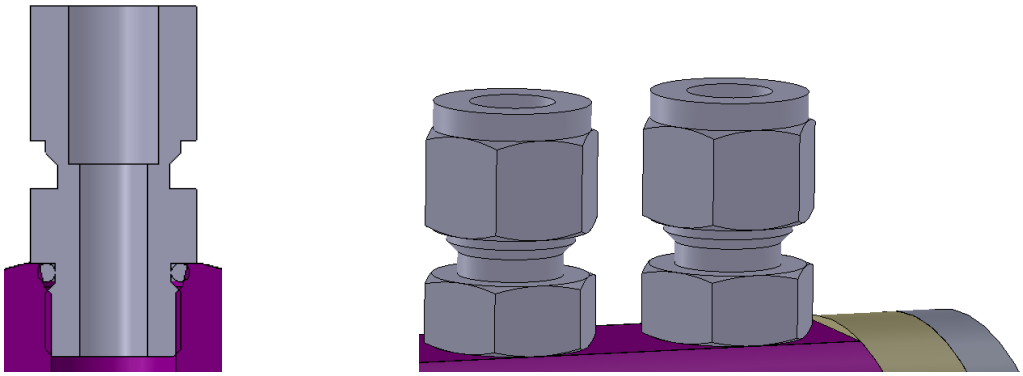

(a) Section view showing the seal resting below the surface **(b)** Hydraulic fittings sitting flush with the flats

Figure 5.4: Adding flats to the spool valve casing prevented the seals from extruding

Manufacturing defects, and tight tolerance requirements, caused the cushion piston to be over constrained. While the intended points of contact at the seals provided the necessary support for the piston, any additional contact around the "damping" region prevented full actuation. Reducing the damping region diameter solved the issue. However, less effective damping was expected during the experiments as a result of widening the flow path in the damping region.

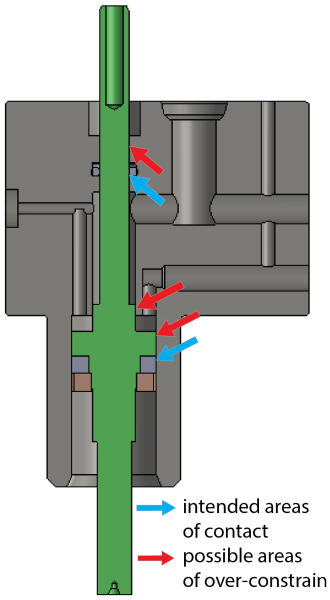

Figure 5.5: Test bench used to validate parts for functional requirements without the use of an engine

The initial design featured an opening only on one side of the spool casing. The design was changed to a fully bored casing as seen in Figure 5.6. The fully open design reduced manufacturing complexity for the casing to be honed. The change allowed a finer finish on the casing, preventing any rough spots where the spool assembly could seize. Furthermore, the spool could be assembled or disassembled from either side of the casing.

Finally, extrusion of the O-rings into the flow gap created a strong bonding force between the parts. Disassembly required prying the seal holder and casing apart, causing possible damage and requiring extraneous effort. Jacking screws were incorporated in to the seal holder design to aid in disassembly without the use of prying tools.

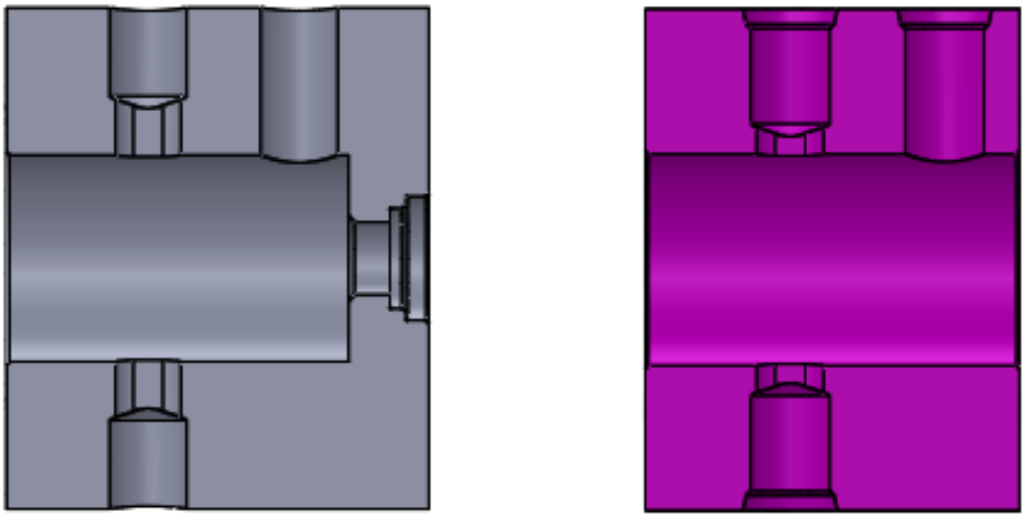

(a) One side open outer casing **(b)** Through hole outer casing

Figure 5.6: Changing the original spool vale outer casing to be a through hole design

5.3 Engine Tests without Combustion

Initial engine tests are done with the *spark plug not connected to the engine*, to characterize the system without combustion. Vibrations caused by pump motor, dynamometer, and fluid motion, and environmental noise picked up by the linear displacement sensors created the need for filtering results. The difference between the original displacement sensor output and filtered output is shown in Figure 5.7. Sensor filtering uses the *moving average method*, replacing each point with an average of 51 sample points distributed symmetrically on each side of the original output point. The moving average filter equation is given in 5.1.

$$x_{avg} = \frac{1}{51}\sum_{i=1}^{51} x_i \tag{5.1}$$

The filtering technique creates a delay of $\frac{n-1}{2}$ samples in the filtered signal. This delay is accounted for by adjusting the time index of each filtered point by the equation 5.2.

$$t_{delay} = \frac{filtering\ delay}{sampling\ rate} = \frac{\frac{51-1}{2}\ samples}{5000\ \frac{samples}{s}} = 0.005\ seconds \tag{5.2}$$

Post processing methods avoided smoothing techniques on output data. If smoothing methods are used, the results appear to change gradually whereas the actual data shows abrupt changes. This discrepancy between smoothed data and actual data can be the difference between low and high seating velocity when the valves close and therefore change the evaluation of the system damping capabilities. Smoothing and filtering techniques often used on noisy data include robust least squares regression and Savitzky-Golay (S-G) filtering [23]. Least squares methods risk making abrupt changes appear gradual where as the S-G filtering uses a polynomial fit which performs poorly at capturing both narrow and wide peaks in data. Depending on test settings, the valve lift duration may contain wide or narrow peaks, making the S-G filtering unsuitable for post-processing.

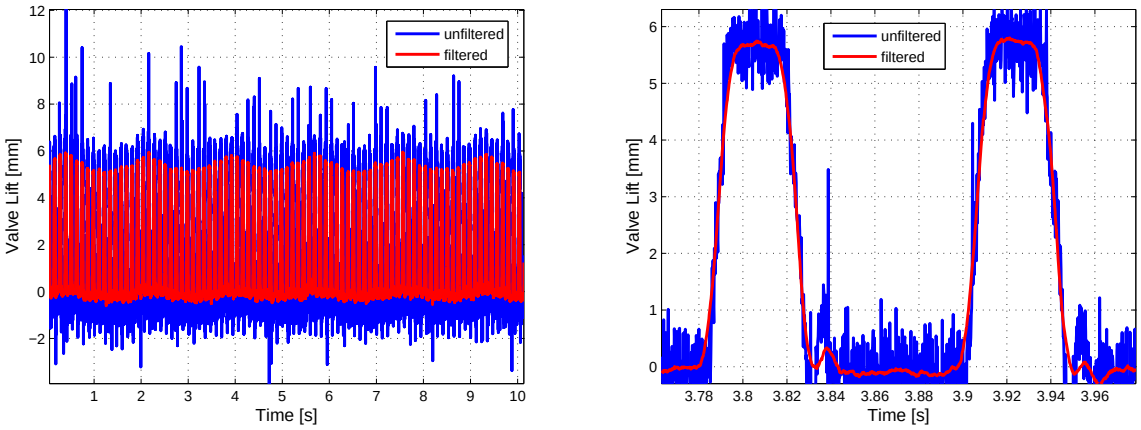

(a) Pressure required

(b) Pump speed required

Figure 5.7: Engine speed 1000 RPM, Pump motor 500 RPM, Average Accumulator pressure = 270 psi. Pressure and pump requirements to achieve a desired valve lift at varying engine speeds 'N'

Sampling rate of the controller was set in the Simulink program. The highest possible rate was chosen where the dSpace controller could operate without performance lag. The objective of the sampling rate was for the sensors' output to show all relevant parts of the valve lift profile. The important parts of the valve lift include the opening or "rising" edge, the constant valve lift palteau, the closing or "falling" edge, and any subsequent valve "bounce" caused by spring surge and impact of valve on its seat. These valve lift profile features are shown in Figure 5.8. Equation 5.3 shows the number of valve displacement samples in the rising or falling portion of a single valve cycle. Number of lift samples $'\eta'$ can be tuned for a given engine speed $'N_e$ and spool valve port opening $'VC'$ by adjusting the

sampling rate of the controller $'f'$. The number of samples for each valve lift cycle are given in Table 5.1 for the minimum, maximum, and idle engine speed. The tabulated values are found for a given spool and casing port opening of 20°each, causing an opening duration of 80°on the crank angle cycle, and with maximum sampling frequency of 5000 Hz. Note that the dSpace controller has to compensate for tracking additional signals by lowering the sampling rate, therefore future projects with multi-cylinder engines or more sensors will likely require a lower sampling rate and produce lower precision in valve displacement measurements.

$$\begin{aligned} \frac{Valve\ cycle\ degrees}{360\ \frac{cycle}{rev}} &= valve\ cycle\ [rev] = VC[rev] \\ VC\ [rev] = \frac{80^\circ}{\frac{360^\circ}{rev}} &= 0.222 rev \\ \eta\ [samples] &= VC\ [rev] \times \frac{2}{N_e}\ \left[\frac{min}{rev}\right] \times \frac{60\ s}{min} \times \frac{f\ samples}{s} \\ \eta\ [samples] &= \frac{120\ VC\ f}{N_e} \end{aligned} \tag{5.3}$$

Table 5.1: Valve lift samples for engine speed

	Engine Speed	Lift Samples η
$N_{e,min}$	1000	133
$N_{e,idle}$	1500	88
$N_{e,max}$	3600	37

Moreover, a slight valve "bounce" is seen at the end of Figure 5.8a) after the valve closes. This bounce also occurs in conventional cam following valve profiles as shown by the work of Richard Stone in Figure 5.8b) [24]. It is ideal to minimize this valve bounce which can cause unintentional intake charge or exhaust gas motion.

Encoders have a value of 0°when the spool and casing ports align completely. Since the ports *start* aligning 20°before the 0°point, and stay partially aligned for 20°afterwards, hydraulic fluid is allowed to flow through for a total of 40°in each spool valve rotation. Due to a 2:1 ratio, the spool valve opening corresponds to 80°of opening interval on the engine side. This agrees with experimental results in Figure 5.9 showing valve lift starting approximately 40°before HPSV fully opens and valve closing 40°before LPSV fully opens.

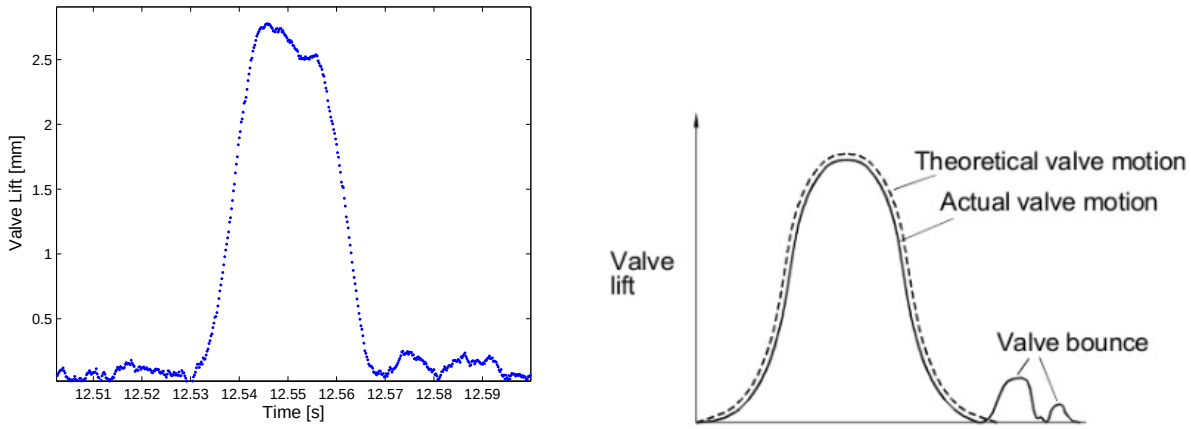

(a) Valve lift sampling through dSpace system **(b)** Theoretical and actual valve motion showing often disregarded "valve bounce" [24]

Figure 5.8: Valve lift profile showing adequate sampling rate to observe valve opening and closing as well as "valve bounce" phenomenon

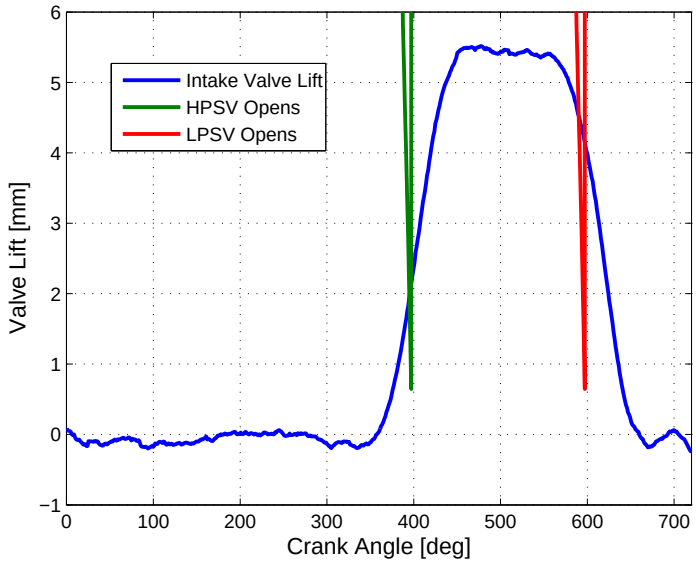

Figure 5.9: Opening and closing of engine valve in relation to the high and low pressure spool valves opening

The ability of the HVVA system to control the valve lift height without changing the duration of valve opening is shown in Figure 5.10. The magnitude of the valve lift can change by altering the hydraulic pressure in the system, the exhaust valve shows a decrease in lift from approximately 5.2 mm to 2.5 mm for a pressure change of 277 psi to 160 psi. Changing system pressure also affects the speed of valve lift and return as seen by different slopes during the rising and falling portions the lift profile. The slower rate of ascent, or descent, can be explained by equation 3.6. Decreasing the force of pressure without changing any other force would result in slower acceleration during the opening phase and result in less return force from the spring, causing a slower descent acceleration.

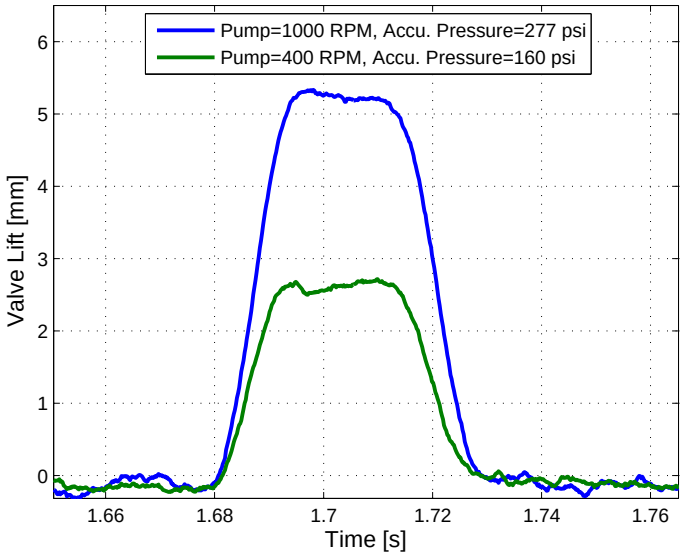

Figure 5.10: Varying the amount of valve lift by changing hydraulic pressure at engine speed $N_e = 1000RPM$

Majority of experimental tests used the valve opening intervals shown in Figure 5.11a). This test shows a final lift of 5.5 mm and the opening intervals given in Table 5.2 to closely match valve lifts from the original test engine as seen in Figure 5.11b). Even though the HPSV for the exhaust valve was set to open at 100 CA°, the results show the valve opening approximately 40 CA°before. This early valve lift occurs due to partial opening of the spool valve as mentioned earlier. The main differences between the HVVA and cam profile are the overlap durations and the speed of valve motion. The original, or unmodified, engine used a cam to control the valve lift and therefore shows a gradual change in lift profile,

or slower valve motion, requiring 120 CA°from maximum lift to close completely, whereas the HVVA system closes within 80 CA°, less if higher pressure is used. Furthermore, the overlap between the intake and exhaust valves shown in the cam profile is avoided in the HVVA tests by phasing the exhaust valve cycle to occur earlier by 60 CA°. This change of valve timing was done to prevent any large overlaps between the intake and exhaust, since the HVVA system allows quicker opening and closing, and to prevent any possible collision of the valves with the piston at TDC.

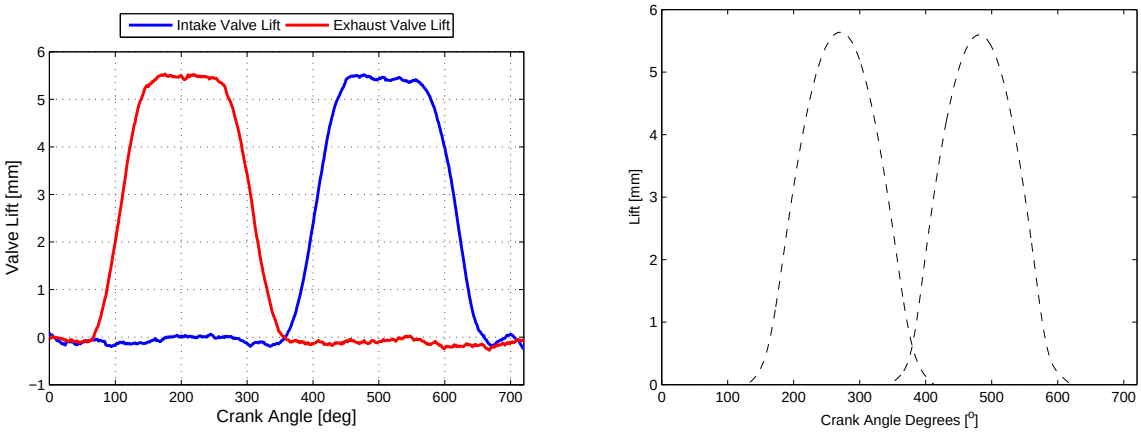

(a) HVVA intake and exhaust lift profiles **(b)** Original cam lift profiles [25]

Figure 5.11: Comparison between HVVA and conventional cam valve lift profiles

Table 5.2: Valve opening settings for lift comparison between HVVA and cam profile

Angle	HP_e	LP_e	HP_i	LP_i
Spool Valve	50	150	200	300
Crank Shaft	100	300	400	600

In experiments aiming for a low valve lift, range of 1-3 mm, a discrepancy is found between the intake and exhaust valve lifts as shown in Figure 5.12. This discrepancy in valve lifts is due to differences in friction of each cushion device, different tubing lengths from the reservoir to each valve, manufacturing differences in each spool valve, and most importantly, an inconsistent high pressure source for each spool valve.

Changes in cushion device friction can occur from varying seal compression. Slight deviations of the cushion device bore, even within tolerance of one to three thousands

of an inch, can change the compression of the seals. Moreover, radial run-out along the path of piston travel can vary seal compression. Finally, friction can increase from any contact of the piston and cushion device bore, as mentioned in section 3.2.3, especially in the damping region where the gap is smaller than three thousands of an inch.

The hydraulic oil flow from the reservoir is split between the intake and exhaust cushion devices. However, there are more hydraulic resistances in the path of the intake valve cushion device. These resistances include, longer tubes, more tubing bends, and additional sensors in comparison to the exhaust valve hydraulic path.

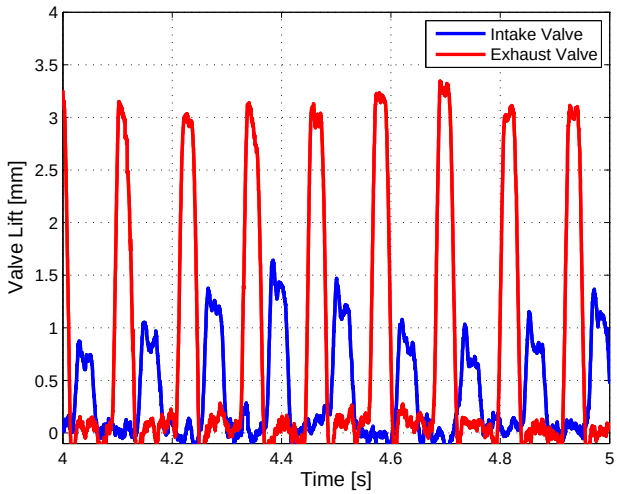

Figure 5.12: Discrepancy between intake and exhaust valve opening when aiming for low valve lifts

The most important reason for lift discrepancy between the intake and exhaust valves is the inconsistent pressure source for each valve. The changing pressure source refers to deviations in accumulator pressure as seen in Figure 5.13. Results of normalized lift show the exhaust valve opening before the intake valve; moreover, the accumulator pressure falls to cause the exhaust valve to open and rises to a high pressure again before the intake valve opens. However, *the initial accumulator pressure for the intake valve is less than it was for the exhaust valve.* This difference in accumulator pressure provides a higher pressure force for the exhaust valve than it does for the intake valve as shown in Figure 5.13b). The discrepancy in valve lifts does not exist at higher pump speeds where the accumulator is able to "recharge", however this solution will not allow for low valve lifts in the 0-3 mm range.

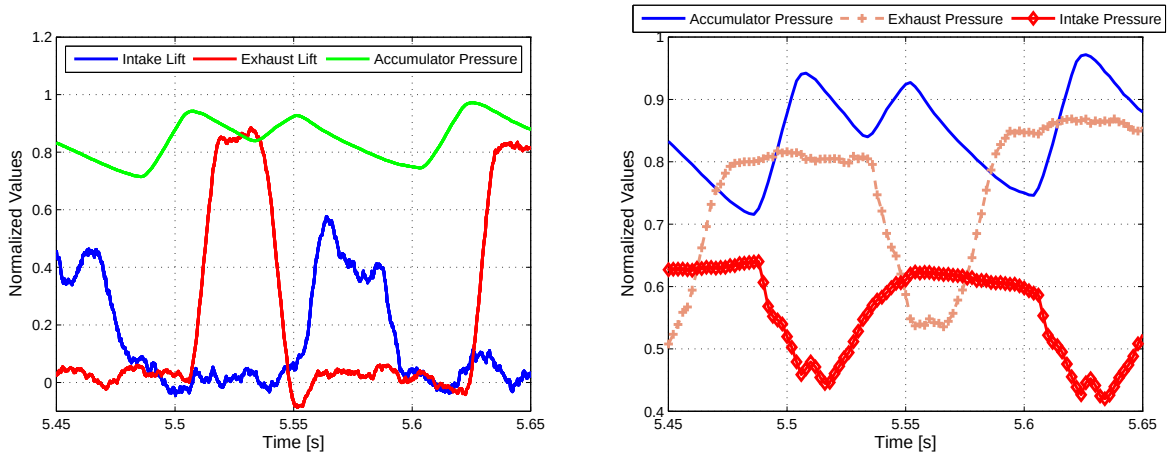

(a) valve lifts compared to accumulator pressure **(b)** valve pressures compared to accumulator pressure

Figure 5.13: Normalized comparison of exhaust and intake lifts and pressure against deviations in accumulator pressure

The valve "floating" case is seen in Figure 5.14 where the valve is unable to close after opening. The inability to close the valve occurs for two reasons: a low spring rate and the opening in the LPSV. Weaker valve springs at higher engine and pump speeds are unable to push out enough pressurized fluid before the LPSV closes, this result agrees with the simulations in section 3.4. However, a weak spring can push the fluid out if the LPSV opening interval is enlarged. Additionally, the experiment shows oscillations in the valve lift profile, these are caused by the valve starting each cycle at a slightly different lift and therefore a changed spring force "preload" affecting the overall dynamics each lift cycle.

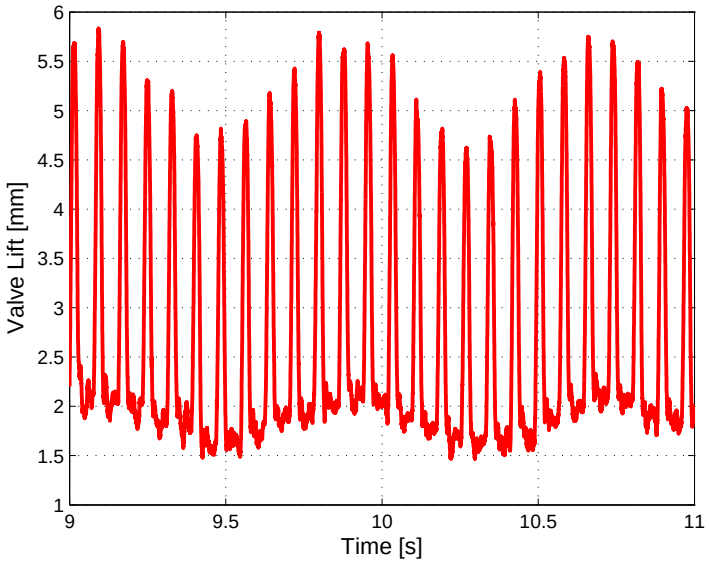

Figure 5.14: Valve "float" case at engine speed $N_e = 1500RPM$ and pump motor $N_p = 600RPM$

5.4 Engine Tests with Combustion

5.4.1 Performance of Valve Lift Controller

To achieve a consistent, desired valve lift, experiments used a feedback system with a PD controller. The system controlled for average accumulator pressure, over a two second period, that had corresponded to a specific lift in the user controlled experiments. This accumulator pressure to valve lift relation, and the corresponding pump speed required for accumulator pressure, are shown in Figure 5.15. The control system, allowing a switch between manual user control, open loop control using only previously attained data, and closed loop control using accumulator pressure as feedback are shown in Figure 5.16. An important distinction to make is that the feedback system controlled for an accumulator pressure matching the desired valve lift, not for the valve lift directly. The pressure control was chosen because the pressure transducers offered a low noise to signal ratio, were calibrated and certified by manufacturer, and were generally more robust than the linear displacement sensors.

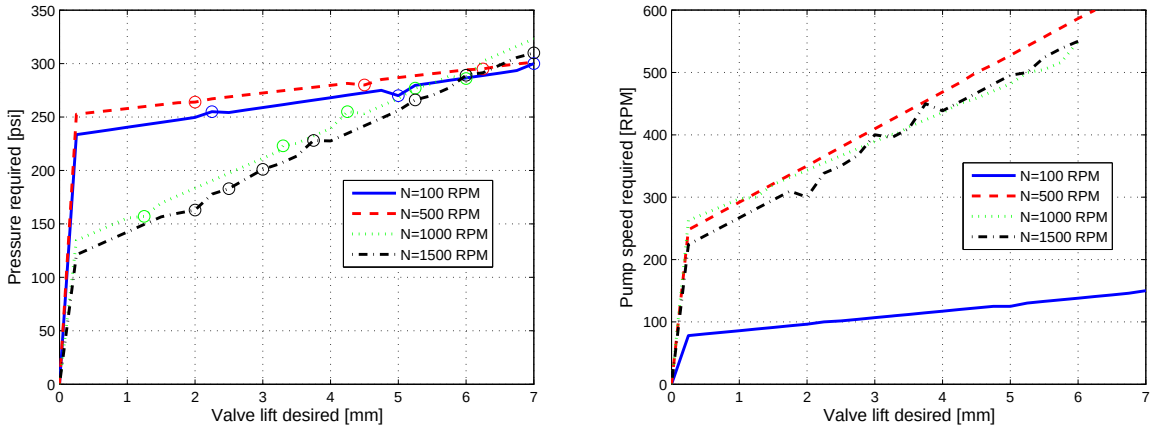

(a) Pressure required

(b) Pump speed required

Figure 5.15: Pressure and pump requirements to achieve a desired valve lift at varying engine speeds 'N'

Controller tuning used an experimental approach of slowly increasing the gains, starting with K_p, then K_d, and finally K_i. The experimental tuning avoided using the classical methods such as Ziegler-Nichols (ZN). Not using these methods is justified because the required stability limit response was not readily observable in a time limit imposed to conserve computer memory and limit post processing time. Moreover, The HVVA experimental system lacks the linear, single-pole dominated response that is ideal for the ZN method [26]. Finally, the experimental tuning achieved a response with less than 5% error within two seconds, showing a fast and accurate response that justifies the experimental method. Progression of testing different gains are shown in Figure 5.17, these results show the error and time required to reach a valve lift of 2 mm at an engine speed of 1500 RPM for three gain settings. *Experimental best gain settings were:* $K_p = 1.5$ *and* $K_d = 1.25$.

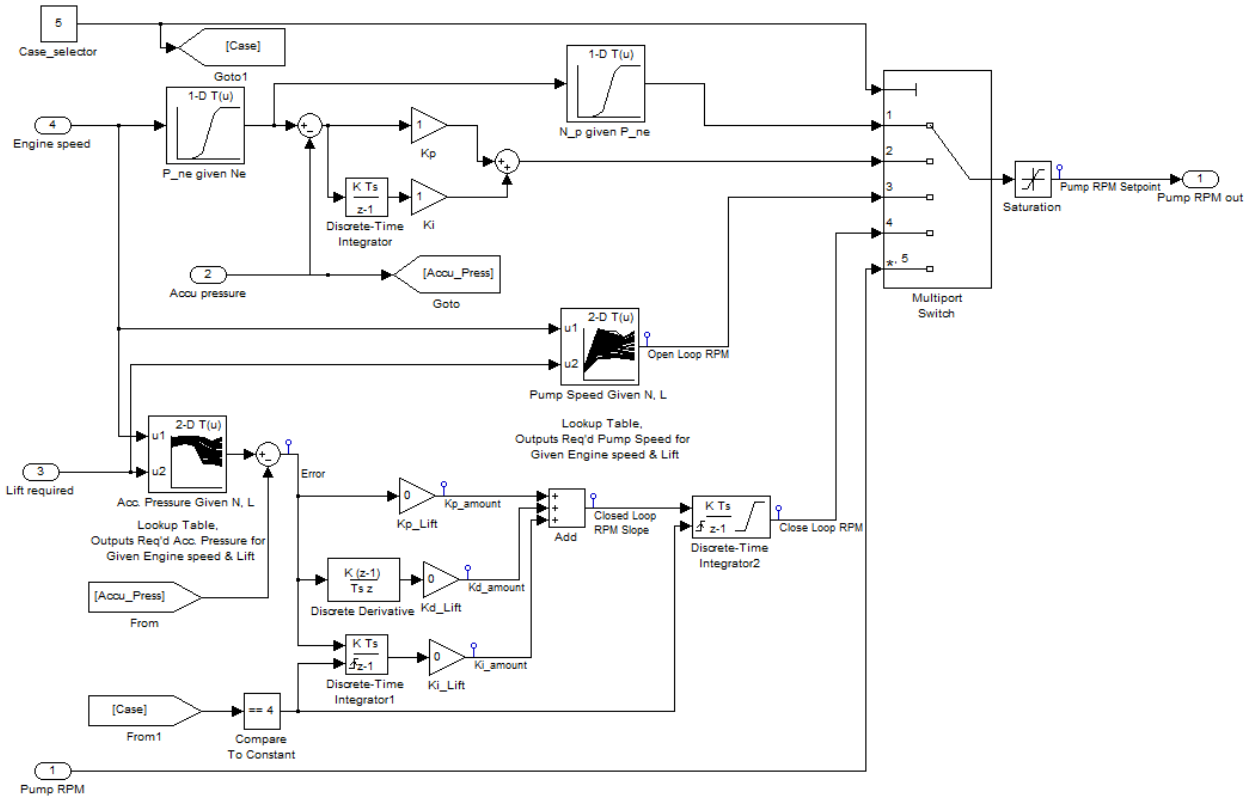

Figure 5.16: Controlling Valve lift by adjusting pump motor RPM through PID control system

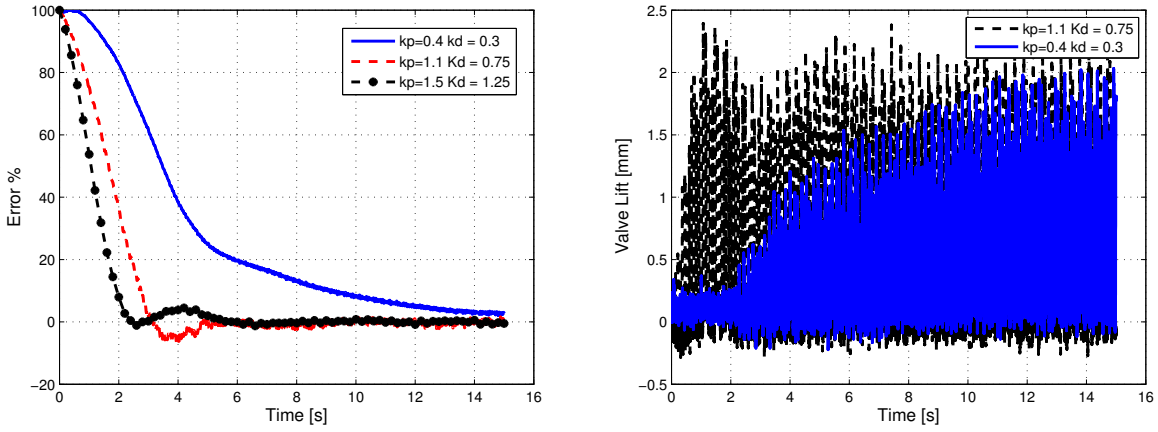

(a) Error between required and actual system pressure

(b) Response of controllers to reach 2 mm valve lift

Figure 5.17: Comparison of error and response for different valve lift controller parameters

Engine Combustion - Torque Results

Torque produced from combustion at an engine speed of 1000 rpm and valve lift of 3 mm is shown in Figure 5.18. The first figure shows a consistent profile for the torque generated at the dynamometer with a positive value indicating torque output from the engine and a negative value for torque required by the dyanmometer to maintain the speed. The magnified torque output profile shows the presence of a positive output during combustion, and a required torque input for compression and pumping losses during the exhaust stage.

After changing to stiffer springs (k=30 N/mm) to counter the presence of valve float at 1500 rpm, the recorded torque output of a single engine cycle at 1500 rpm is presented in Figure 5.19. Note the values have been scaled to allow for a visual comparison. The cycle consists of the following: combustion, pumping loss, exhaust valve opening and closing, followed by intake valve opening and closing, compression of the intake charge, and finally combustion once again. The valve timing allows the crankshaft to turn approximately 180 CA°before opening the exhaust valve, this wait time causes the pumping loss torque shown as “compression before exhaust”.

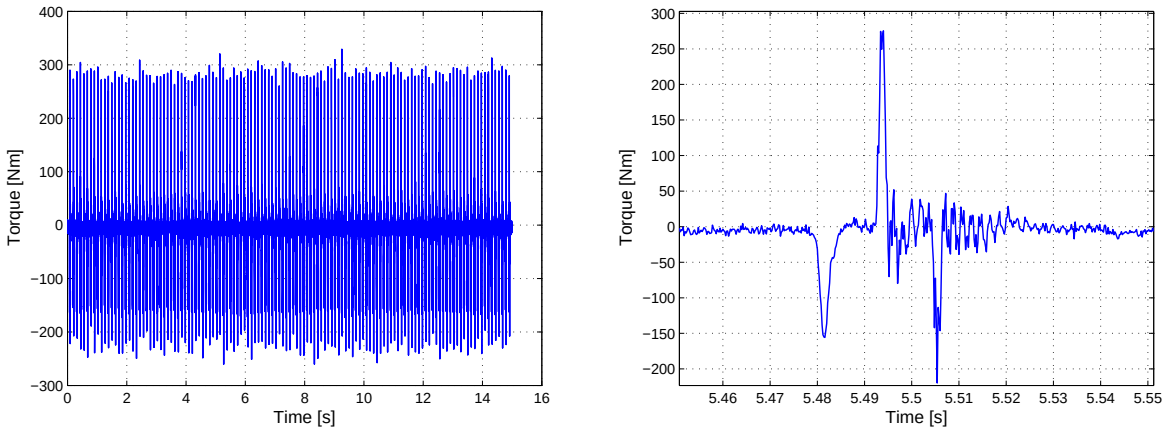

(a) Torque output of engine at 1000 rpm

(b) Torque measurements over a single engine cycle (720 CA°)

Figure 5.18: Resulting torque from combustion for single cylinder engine at 1000 rpm

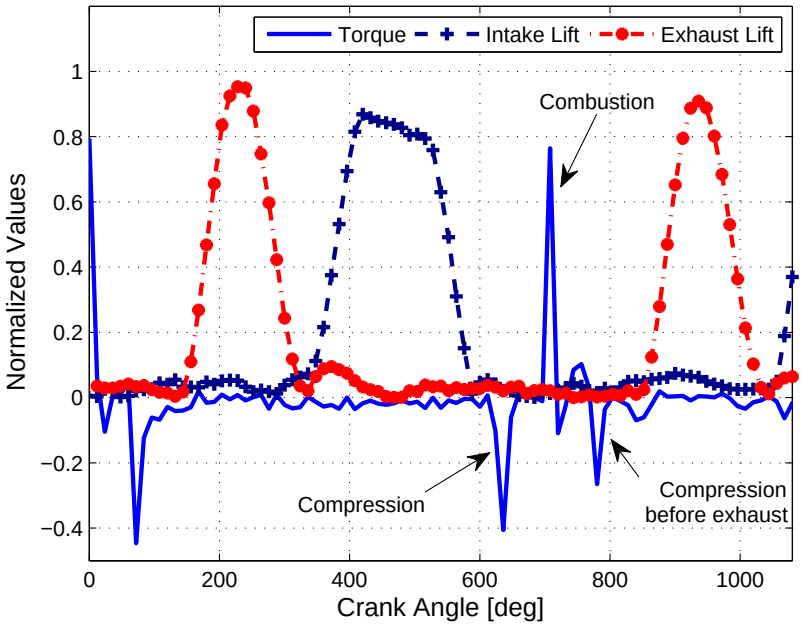

Figure 5.19: Examining torque in relation to intake and exhaust valve lift at 1500 rpm

5.4.2 Comparison of Experimental and Simulation Results

A comparison of the results from experiments and the mathematical model developed in section 3.3 is shown in Figure 5.20. This comparison allows for validation of the simulation model in the low to idle engine speeds ranging between 1000 and 1500 rpm. The experimental results show an error of +/- 6% in comparison to the simulations during the valve steady lift region. However, the areas where the valve is opening or closing show good agreement with the simulations for the low 1000 rpm speed only. In the case of N=1500 rpm, the experimental results show increased damping in the opening and closing sections, causing the simulation to be off by 30 CA°in predicting when the valve will open and close. Therefore, future simulations should account for a change in damping with the engine speed, as well as the damping effects taking place in two different regions. A steady damping force can be expected to occur throughout the motion; however, an increased damping force is present due to the cushioning effect when the valve closes. The disparity caused by this increased damping is seen in Figure 5.20b.

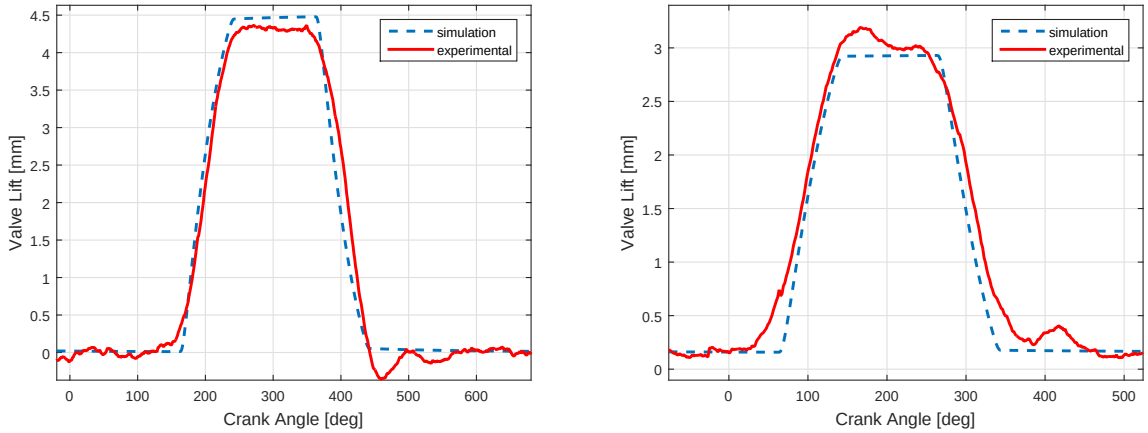

(a) Engine speed 1000 rpm, pressure 250 psi **(b)** Engine speed 1500 rpm, pressure 220 psi

Figure 5.20: Comparison of experimental and simulation results for the intake valve with stiffness k=20 N/mm

5.4.3 Post Combustion Inspection

While replacing the engine valve springs with stiffer springs, the spark plug and valves were inspected for damage and any other notable observations. The spark plug and valves, after combustion testing with $k = 20N/mm$ valve springs, are shown in Figure 5.21. The spark plugs show a dark coating of carbon deposit on the tip indicating dry fouling [27]. Moreover, the dark carbon buildup on the valves shows the engine is running with a high fuel/air ratio. The high fuel/air ratio, or "rich" condition, is because the throttle is held fully open and the HVVA system opens the intake valve rapidly in comparison to the conventional cam system, allowing for a greater intake charge. These conditions of running the engine "rich" and dry fouling on the spark plug can negatively effect combustion efficiency [27].

An electronic fuel injection system can be used in future designs to alter the amount of fuel to air ratio and negate these issues of running a "rich" engine. Lack of damage to the engine valves in Figure 5.21 also shows the effectiveness of the damping system in reducing the seating force on the valves. An important distinction is that the inspection was done after testing with spring stiffness of $k = 20N/mm$ and not after the $k = 30N/mm$ springs, these observations cannot be used to qualify that valves will not sustain damage with stiffer springs.

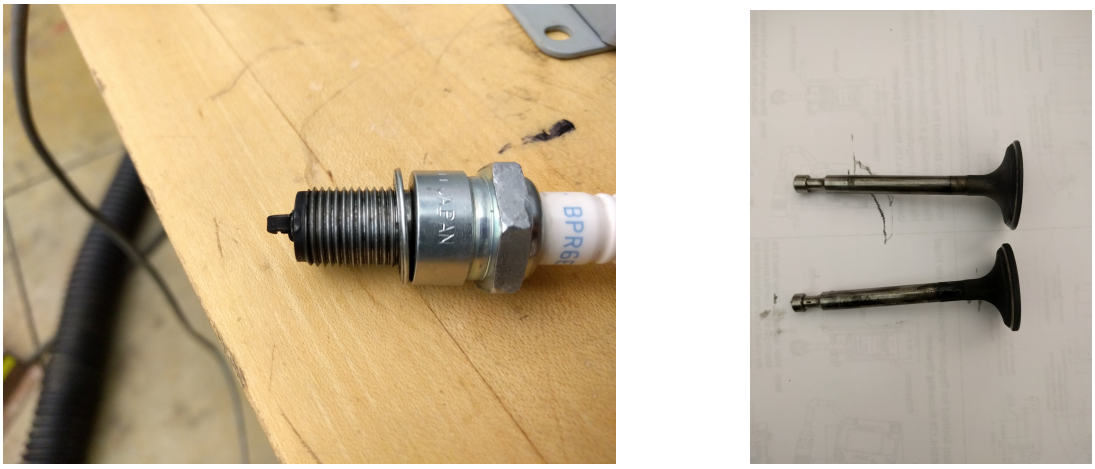

(a) Spark plug with carbon build-up on the tip **(b)** Engine valves showing no damage but large amount of carbon deposits

Figure 5.21: Examination of spark plug and engine valves after combustion testing, blackened valves show evidence of running the engine with a "rich" F/A ratio

During and after combustion testing, leakage was observed as shown in Figure 5.22. The

pictures of leakage are from two different spool valves, and the remaining two experienced no leakage. The leaks are seen happening near the O-ring seals in the spool valve, the blocked port, or the rotary seal. The manufacturing quality of the parts is suspected for causing the small amounts of leakage because they are present in different locations and not occuring in other valves.

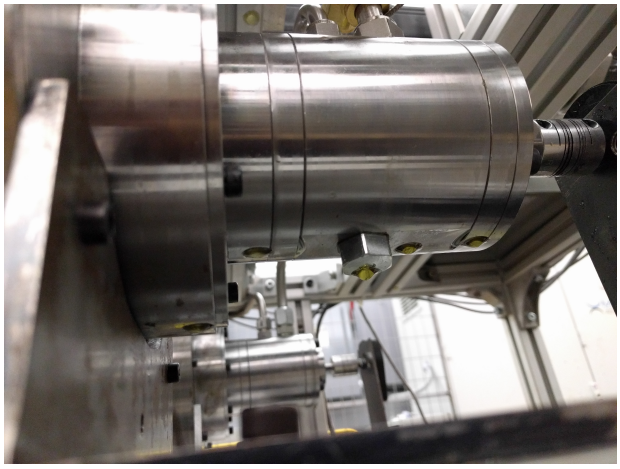

(a) Small droplets of leakage seen at O-ring seals and blocked port location

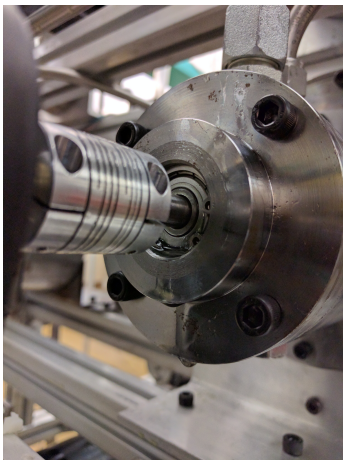

(b) Trail of leakage seen at the rotary seal

Figure 5.22: Observations of leakage at two different spool valves

5.5 Valve Cushion Device Test

While a conventional cam based system gradually opens and closes the valve, slowing the valve speed substantially before it contacts the valve seat, no such speed control inherently exists in a HVVA system. Without sufficient resistive force near the end of a valve lift cycle the excessive closing speed will damage the valve. Therefore, the damping capabilities of the cushion device, provided by the idle screw and check valve acting as a flow control valve, are given in Figure 5.23. High damping corresponds to a fully tightened idle screw which severely restricts return flow, whereas low damping occurs when the idle screw is loosened, allowing a larger flow path. The results of high and low damping in TEST CASE are given in Figure 5.23a), where differences in closing speed are not easy to observe. Expanding the relevant section of the valve lift cycle in Figure 5.23b) shows that the high damping produces a slightly higher resistive effect in comparison to low damping. A crude

approximation examining the change in distance and change in time for the two cases shows a $\frac{\Delta\ 0.1\ mm}{\Delta\ 0.001\ s} \approx 100\ \frac{mm}{s}$ difference.

A better approximation of the damping effect is attained by differentiating the valve lift with respect to time, producing the valve speed profile shown in Figure 5.24 for the high damping case. The numerical differentiation is simply measuring the rate of change between successive points of valve lift in Matlab. However, the "raw" valve speed is shown as a cloud of points to indicate the "noise" that is present when approximating with this method. A moving average filter reduces the noise in the speed curve and is scaled to bound the maximum and minimum lifts, especially near the important valve closing region given in Figure 5.24b). The filtered speed is approximately 10% of it maximum value in the high damping case and 25% of its maximum value in the low damping case. The maximum valve speed, found by numerical differentiation, is $v_{max} = 950\ \frac{mm}{s}$ and the closing speeds are $v_{high\ damping} = 0.1 \times v_{max} = 95\ \frac{mm}{s}$, and $v_{low\ damping} = 240\ \frac{mm}{s}$. Therefore, the cushion device meets the requirement of damping the closing speed to less than 100 mm/s; however, future iterations should aim for further reduction in closing speed.

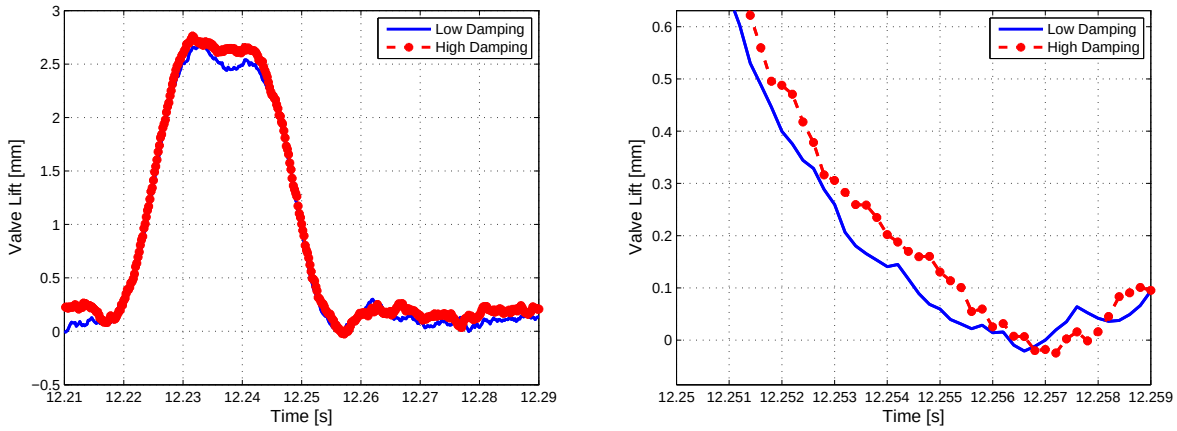

(a) Varying exhaust valve lift by changing the closing speed damping

(b) Damping effect at end of engine valve closing

Figure 5.23: Damping effect provided by cushion device on exhaust valve lift at $N_e = 1000\ RPM$

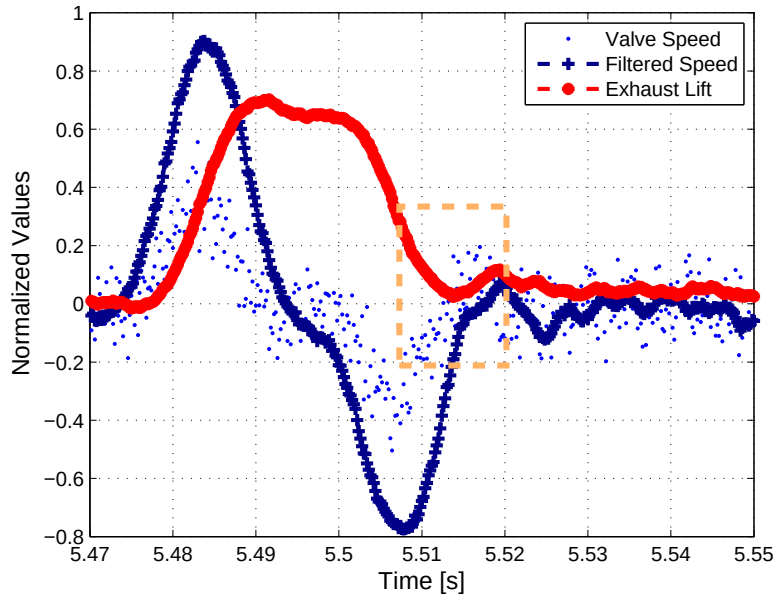

(a) Valve speed produced by numerical differentiation of the exhaust lift profile with *high* damping

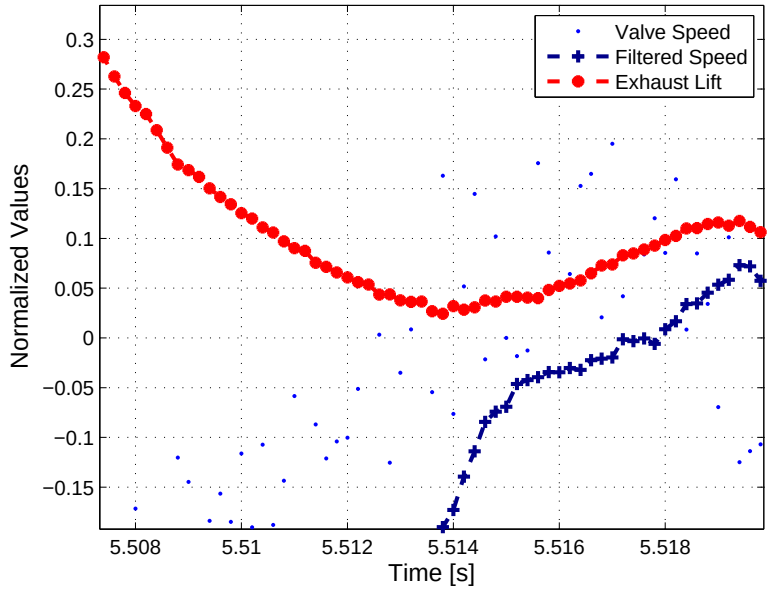

(b) Zoom in of figure a) in the relevant valve closing region

Figure 5.24: Studying the effectiveness of *high* damping when valve closes on exhaust valve lift and speed

Chapter 6

Conclusions And Future Work

6.1 Conclusions

The purpose of this research was to implement a working model of hydraulic variable valve actuation system on a spark ignition engine. In order to justify this research, alternative VVA methods were reviewed to highlight existing solutions and their issues. Commonly, phasing methods allowed limited ability to change valve timing in comparison to a fully variable system. Alternatively, electric and electro-hydraulic methods presented full vva systems. However, these systems either involved a high degree of control complexity, large set-ups with expensive actuators and sensors, or had issues with solenoid frequency of operation at high engine speeds. Therefore, adaption of theHVVA system to an engine presented an opportunity to advance the state of technology in order to improve engine performance and reduce harmful emissions.

After reviewing former designs, the HVVA system was designed, manufactured, and experimented on a 4-stroke single cylinder engine. The system was tested for leakage, ability to retain pressure, actuate the engine valves reliably, and withstand the high temperatures and vibration from combustion. Through the use of a dSpace and Simulink controller, the system showed the ability to vary the valve timing a full 360°and adjust the valve lift up to 7 mm (limit set to prevent valve colliding with engine piston). A controller was made to adjust the lift automatically and the system was connected to a dynamometer in order to set a fixed engine speed and measure torque output.

The system achieved combustion upto engine idle speed of 1500 RPM. Higher speeds were not tested due to time constraints. The system did not overheat, as was the case for

previous designs, and retained pressure of 600 psi over the course of two days. Finally, the system showed robustness by operating for atleast 3 hours a day during the course of experiments. In conclusion, this project advanced the state of engine technology by showing the HVVA system as a functional system, capable of achieving combustion on an engine. Furthermore, this research provided the foundation for additional testing to improve engine performance, reduce emissions, test at higher speeds, or test on multi-cylinder engines.

6.2 Future Work

It is recommended that additional development of the hydraulic VVA system include the following research:

6.2.1 Mechanical Design

Phase shifting

Future design can omit the use of a gearbox to phase shift by having a mechanism that rotates the spool valve body. Without the need for a gearbox, future HVVA systems can be greatly reduced in size and mechanical complexity. However, some form of bearing and pulley shaft coupling will still be needed to transmit torque from the crankshaft to spool valve shaft. Without appropriate bearings and coupling, excessive bending moments will be seen by the spool valve.

Spool valve size

Further reduction in the HVVA assembly is possible by reducing the spool valve size using several strategies.

- First, a smaller radial seal and bearings have to be found in order to shrink the spool valve shaft size.
- Second, the edge spacing around the spool valve fasteners follows the Shigley's guideline [16]. There is at least one screw diameter of space between the pitch circle diameter of the screws and the O-ring, a similar spacing is followed for the screws to the outside edge. However, the screw spacing can be reduced after performing additional analysis to show the spool valve body will not deform under pressure or leak.

- Finally, a smaller spool can be used, reducing the internal cavity in the spool valve. Additional analysis will be needed to justify the spool size; it is recommended to have the internal capacity for a few valve cycles.

Crankshaft connected to pump

To make the HVVA system a viable alternative to conventional VVA methods, the engine output through the crankshaft has to drive the system pump. A separate motor can aid the engine input through a gearbox, but the power has to primarily come from the engine. Therefore, future designs should have the ability to connect the crankshaft to the hydraulic pump.

Engine intake and exhaust modifications

Additional sensors measuring exhaust emissions and a fuel injector controlling the fuel intake should be incorporated into a future design to measure and improve engine performance.

Valve displacement sensor into engine head cover

As recommended by Chermesnok [12], the valve displacement sensor can sit in the engine head cover. A solution can involved recessing the sensor into the head cover and beneath the cushion device. This will protect the sensor electronics from the harsh engine environment and allow for easy access to the sensor.

Radial ports on spool valve

Another recommendation from Chermesnok [12] involves omitting axial ports on the spool valve in favour of radial ports to conserve space and reduce manufacturing complexity, see Figure 6.1 for an example. This configuration can allow the spool valve to rotate at 1:4 speed ratio instead of the current 1:2 ratio with the crankshaft, thereby reducing wear on the components.

6.2.2 Simulations and Controls

Valve lift controller

Currently, the valve lift is controlled by monitoring and adjusting the system pressure. A look-up table stating what lifts are expected, for a given pressure at a given engine speed, is used to set the goal for the controller with accumulator pressure as the feedback. A more accurate controller would adjust the pressure and use the valve displacement sensor reading as the feedback variable. To achieve this, the sensor noise should be minimized and a more robust sensor design used to ensure the feedback reading is accurate.

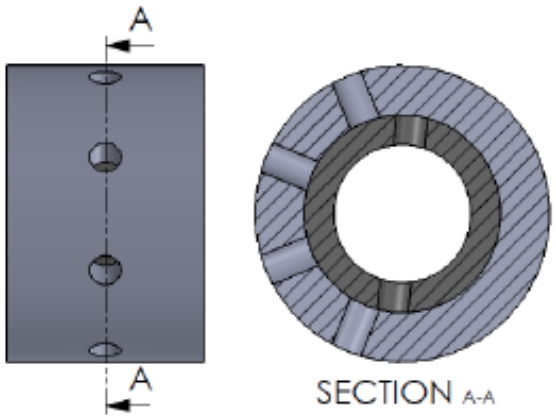

Figure 6.1: Spool valve using radial outputs instead of axial output as depicted by Chermesnok [12]

Simulate C_d of spool valves

A more thorough analysis, possibly involving CFD, should be used to determine the flow coefficent of the spool valve ports. A better understanding of the spool valve flow behaviour can produce more accurate simulations predicting concepts such as engine valve float or pressure fluctuations.

Control of valve timing and duration

Currently, the system can adjust the valve timing and duration. However, there is no scheme behind adjustments, future controller designs should change the valve timing and duration to improve the engine performance and emissions. Such an undertaking will require the use of a fuel injector system and emissions sensors.

6.2.3 Hydraulics Design

Reduce tubing length

The distance between the spool valves and cushion device assemblies should be reduced. The systems could preferably be located beside one another to shink the overall HVVA assembly and reduce the amount of tubing required.

Flexible hoses

In order to phase shift by rotating the spool valve outer casing, the tubing will have

to be flexible. Moreover, flexible tubing can allow greater flexibility in arrangement of parts and further reduce overall size of the setup.

Damping for valve closing speed

Currently, the cushion device provides adequate damping for valve closing speeds. However, the setting can not be adjusted during engine operation and the manufacturing tolerances add considerable complexity to the project. Other methods of damping should be considered, preferably designs with active flow control to adjust cushioning length and coefficient of damping.

Larger accumulator

To reduce fluctuations seen in accumulator pressure, the next design iteration should use a larger accumulator, a lower pre-charge, or both.

References

[1] Anthony Greszler. The role of the internal combustion engine in our energy future. Available at https://energy.gov/sites/prod/files/2014/03/f8/deer11_greszler.pdf, 2014.

[2] Aaron Hula, Amy Bunker, Andrea Maguire, and Jeff Alson. Trends - light-duty automotive technology, carbon dioxide emissions, and fuel economy trends: 1975 through 2016. Technical report, United States Environmental Protection Agency, November 2016. Available at https://www.epa.gov/fuel-economy-trends/trends-report.

[3] how a car works. The engine - how the valves open and close. Available at https://www.howacarworks.com/basics/the-engine-how-the-valves-open-and-close, 2011.

[4] Marlan Davis. Secrets of camshaft power. Available at http://www.hotrod.com/articles/ccrp-9812-secrets-of-camshaft-power/, 1998.

[5] Seinosuke Hara, Seiji Suga, Satoru Watanabe, and Makotot Nakamura. Variable valve actuation systems for environmentally friendly engines. *Hitachi Review*, 58(7), 2009.

[6] Mitsubishi Motors Corporation. Mitsubishi innovative valve timing electronic control system. Available at http://www.mitsubishi-motors.com/en/innovation/technology/library/mivec.html, 2011.

[7] Bimmertips. The basics of bmw vanos variable valve timing system. Available at http://bimmertips.com/basics-bmw-vanos-variable-valve-timing/, 2016.

[8] Division on Engineering National Research Council and Physical Sciences. *Assessment of Fuel Economy Technologies for Light-Duty Vehicles*. National Academies Press, 2010.

[9] Allan Geert Nielsen. Free valve technology. Available at http://www.freevalve.com/technology/freevalve-technology/, 2017.

[10] Tufail Habib. Modeling and investigation of electromechanical valve train actuator at simulated pressure conditions., August 2012.

[11] Mohammad Pournazeri. *Development of a New Fully Flexible Hydraulic Variable Valve Actuation System*. PhD thesis, University of Waterloo, 2012.

[12] Matthew Chermesnok. Hydraulic variable valve timing testing and validation. Master's thesis, University of Waterloo, 2016.

[13] Hydraulics & Pneumatics. More than one good turn. Available at http://www.hydraulicspneumatics.com/fittings-amp-couplings/more-one-good-turn, October 2009.

[14] Jeff Allen and Don Law. Production electro-hydraulic variable valve-train for a new generation of i.c. engines. *SAE Technical Paper*, 2002.

[15] William D. Callister Jr. and David G. Rethwisch. *Materials Science and Engineering: An Introduction*. John Wiley and Sons, eigth edition, 2009.

[16] Richard G. Budynas and J. Keith Nisbett. *Shigley's Mechanical Engineering Design*. McGraw-Hill, eigth edition, 2006.

[17] S. Senhadji, F. Belarifi, and F. Robbe-Valloire. Experimental investigation of friction coefficient and wear rate of brass and bronze under lubrication conditions. *Tribology in Industry*, 38(1):102–107, 2016.

[18] Noah D. Manring. *Hydraulic Control Systems*. John Wiley & Sons, Inc., 2005.

[19] John B. Heywood. *Internal Combustion Engine Fundamentals*. McGraw-Hill, Inc., 1988.

[20] Robert W. Fox, Philip J. Pritchard, and Alan T. McDonald. *Introduction to Fluid Mechanics*. John Wiley & Sons, Inc., seventh edition, 2009.

[21] Mihaela Vlasea. Lecture notes in Fluid Power Control Systems, 2016.

[22] Eaton. ERV1-10 - Proportional Valve. Available at http://www.eaton.com/ecm/groups/public/@pub/@eaton/@hyd/documents/content/pct_273171.pdf, 2009.

[23] MathWorks. Filtering and smoothing data. Available at https://www.mathworks.com/help/curvefit/smoothing-data.html#bq_6ys3-2, 2017.

[24] Richard Stone. *Introduction to Internal Combustion Engines*. Macmillan Publishing Ltd., 1985.

[25] Yangtao Li, Amir Khajepour, Cecile Devaud, and Kaimin Liu. Power and fuel economy optimizations of gasoline engines using hydraulic variable valve actuation system. *Applied Energy*, 206:577–593, 2017.

[26] Microstar Laboratories. Ziegler-nichols tuning rules for PID. Available at http://www.mstarlabs.com/control/znrule.html#Ref2, 2017.

[27] Naomichi Miyashita, Yoshihiro Matsubara, Kazuya Iwata, and Masahiro Ishikawa. Spark plugs for gasoline direct injection engines. *SAE Technical Paper*, March 2001.

[28] Roger Lewis. *Wear of Diesel Engine Inlet Valves and Seats*. PhD thesis, University of Sheffield, 2000.

[29] Peter Forsberg. *Combustion Valve Wear: A Tribological Study of Combustion Valve Sealing Interfaces*. PhD thesis, Uppsala University, 2013.

[30] Mechadyne International Limited. Part load pumping losses in an SI Engine. Available at https://www.mechadyne-int.com/reference/throttle-less-operation/part-load-pumping-losses-in-an-si-engine/, 2017.

[31] Tim Lancefield. The influence of variable valve actuation on the part load fuel economy of a modern light-duty diesel engine. *SAE Technical Paper*, March 2003.

[32] Timing belt theory. Technical report, Gates Mectrol Inc., 2006. Available at http://www.gatesmectrol.com/mectrol/downloads/download_common.cfm?file=Belt_Theory06sm.pdf&folder=brochure.

[33] Nissan Motor Co. Variable valve event and lift system (vvel), 2008.

[34] Karim Nice and Charles W. Bryant. How catalytic converters work, 2000.

[35] Matthew Wright. What is an EGR valve and when it should be repaired?, March 2017.

[36] Jess Benajes, Ernesto Reyes, and Jos M. Lujn. Intake valve pre-lift effect on the performance of a turbocharged diesel engine. *SAE International*, February 1996.

[37] Jacobs Vehicle Systems. How an engine brake works, 2017.

APPENDICES

Appendix A

Matlab Codes and Simulink Models

Matlab Code

The following matlab code is used to initialize the simulation parameters and run through the simulink model.

```
% TEST PARAMETERS
% P_high     (high pressure [psi])
% P_low      (low pressure [psi])
% N          (engine speed [RPM])

% ENGINE/ FUEL THERMODYNAMICS
% Po     (initial atmosphere Pressure [bar])
% k      (thermodynamic concept, k = Cp/Cv)
% R      (Gas constant, Cp = Cv + R [KJ/kg*K])
% Cv         (fuel parameter [KJ/Kg*K])
% Cp         (fuel parameter [KJ/Kg*K])
% Tcyl0      (initial engine cylinder temp [K])
% Pcyl0      (initial engine cylinder Pressure [bar])

% ENGINE DIMENSIONS
% A_piston   (Area of engine pistion [cm^2])
% V_c0       (Volume of eng. cylinder initially [cc])
% r_cs       (radius of carank shaft [mm])
% l_rod      (piston rod length [mm])
```

```
% rv          (valve radius [mm])

% HYDRAULIC FLUID
% Beta        (bulk modulus of hydraulic fluid [bar])
% rho         (density of fluid [kg/m^3])
% mu          (hydraulic fluid viscosity [Ns/m^2])

% HYDRAULIC CYLINDER CHARACTERISTICS
% K           (spring constant [N/mm])
% F_preload   (Preload force from spring [N])
% F_friction  (friction estimate of system [N])
% m           (valve actuator moving mass [g])
% V2o         (hydraulic cylinder dead volume [cc])
% A_p          (hydraulic piston area [mm^2])

% SPOOL VALVE CHARACTERISTICS:
% Cd          (flow coefficient for spool valve [])
% l           {length of spool slot [mm])
% d           (axial leakage distance [mm])
% phi_c     (opening angle for casing port [deg])
% phi_s     (opening angle for spool port [deg])
% r_s         (radius of spool [mm])
% r_c         (radius of casing [mm])

% ENGINE/ FUEL THERMODYNAMICS
%Po = 1.01; % [bar]
Po = 101000; % [bar] to [Pa]
k = 1.4;
R = 0.287 * 1000; % KJ to J
Cv = 0.7175 * 1000; % KJ to J;
Cp = 1.0045 * 1000; % KJ to J;
T_cyl0 = 273 + 100;
%P_cyl0 = 5; % [bar]
P_cyl0 = 500000; % [bar] to [Pa]


% ENGINE DIMENSIONS
A_piston = 0.0064; % 64 cm^2 to m^2
```

```
58 V_c0 = 2.54218e-5; % 56 cc to m^3
59 r_cs = 27/1000; % mm to m (honda gx 200 27 mm)
60 l_rod = 83.8962/1000; % mm to m (honda gx 200 83.8962 mm)
61 rv = 12.5/1000; % mm to m (intake 25 mm dia, exhaust 24 mm dia)
62
63 % HYDRAULIC FLUID
64 %Beta = 17000; % [bar]
65 Beta = 1.7e9; % [bar] to [Pa]
66 rho = 850;
67 mu = 0.051;
68
69 % HYDRAULIC CYLINDER CHARACTERISTICS
70 K_spring = 19930; %N/m -- new on is 19930 N/m with Fmax = 275 N
71 F_preload = 0; % accomodate into F_spring
72 x_preload = 0.003; %mine 0.003-0.003
73 F_friction = 50;
74 m = 0.1; % g to kg
75 V2o = 5.72e-5;
76 A_p = 0.00017355; %173.55 mm^2 to m^2
77
78 % SPOOL VALVE CHARACTERISTICS:
79 Cd = 0.5;
80 l = 8/1000; % mm to m
81 d = 18/1000; % mm to m
82 phi_c = 20;
83 phi_s = 20;
84 r_s = 14.98/1000; % mm to m
85 r_c = 15/1000; % mm to m
86
87 % TEST PARAMETERS
88 d_pipe = (3/8 -2*0.035) * 0.0254;      % 3/8" tube with 0.035"
      thick walls
89 l_pipe = 2.5;                          % 1 m of tubing (
      approximation) + other losses
90
91 P_high_psi = 250; %682 psi = 47 bar
92 P_high = P_high_psi * 6894.76; % Conversion to Pa
93
```

```
P_low_psi = 14.6959; % 1 atm for low pressure
P_low = P_low_psi * 6894.76; % Conversion to Pa

N = 1000;              %engine speed
phaseShifter = 0;      %0 degrees
offset = -100;           %50 degrees offset between HPSV and LPSV

t_4cycles = num2str(2*4*120/N); %time for 4 cycles
```

The code used to test parametric changes, such as varying engine speed, is given below.

```
% Loop for parameter testing
tic
N = 1000; K_spring = 30000;
for i=1:5

    n(i) = N;
    EngineSim(i) = sim('SingleValveSim','StopTime',t_4cycles);

    elementCounter = EngineSim(i).get('x'); % used to get the
       number of elements

    t(1:numel(elementCounter),i) = EngineSim(i).get('time_sim');
    LIFT(1:numel(elementCounter),i) = EngineSim(i).get('lift');
    CA(1:numel(elementCounter),i) = EngineSim(i).get('theta');
    Q_hpsv(1:numel(elementCounter),i) = EngineSim(i).get('Q_hpsv'
       );
    Q_lpsv(1:numel(elementCounter),i) = EngineSim(i).get('Q_lpsv'
       );
    A_hpsv(1:numel(elementCounter),i) = EngineSim(i).get('A_hpsv'
       );
    A_lpsv(1:numel(elementCounter),i) = EngineSim(i).get('A_lpsv'
       );
    F_pressure(1:numel(elementCounter),i) = EngineSim(i).get('
       F_pressure');
    F_spring(1:numel(elementCounter),i) = EngineSim(i).get('
       F_spring');
```

```
20        F_damping(1:numel(elementCounter),i) = EngineSim(i).get('
              F_damping');
21        F_gas(1:numel(elementCounter),i) = EngineSim(i).get('F_gas');
22
23        N = N + 250;
24
25  end
26  toc
```

Simulink Model

The simulation model main page is shown below in Figures A.1 and A.2:

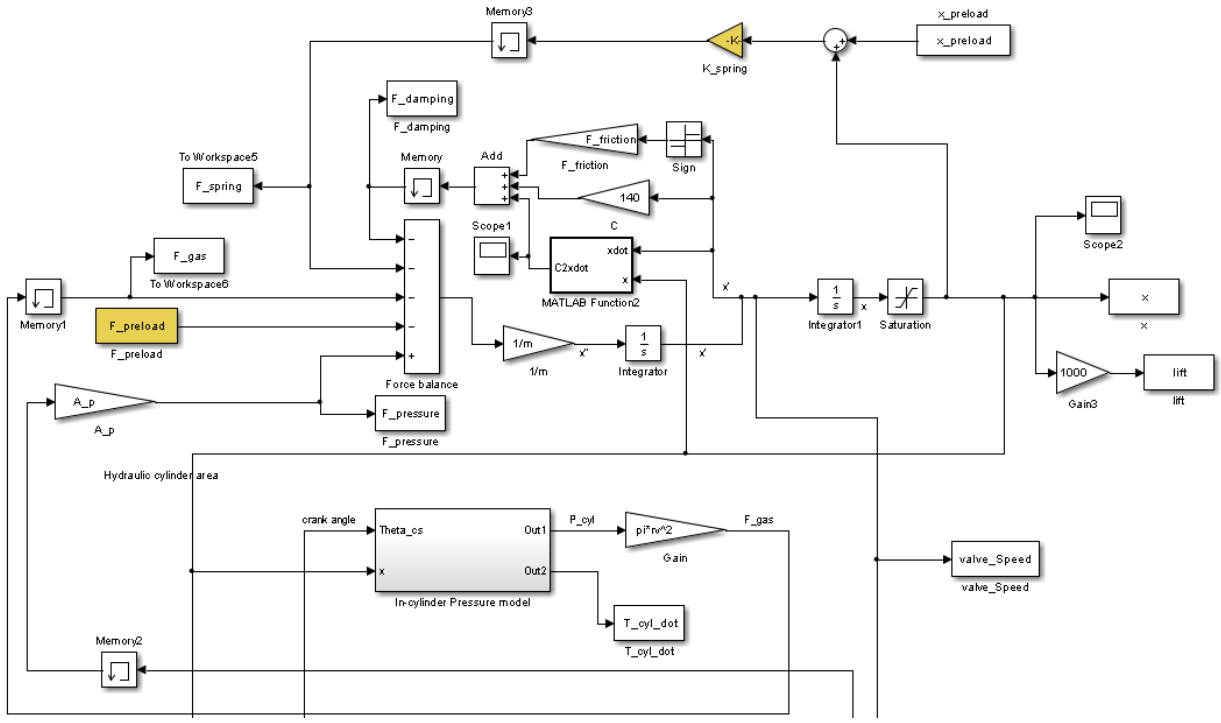

Figure A.1: Simulink model force balance

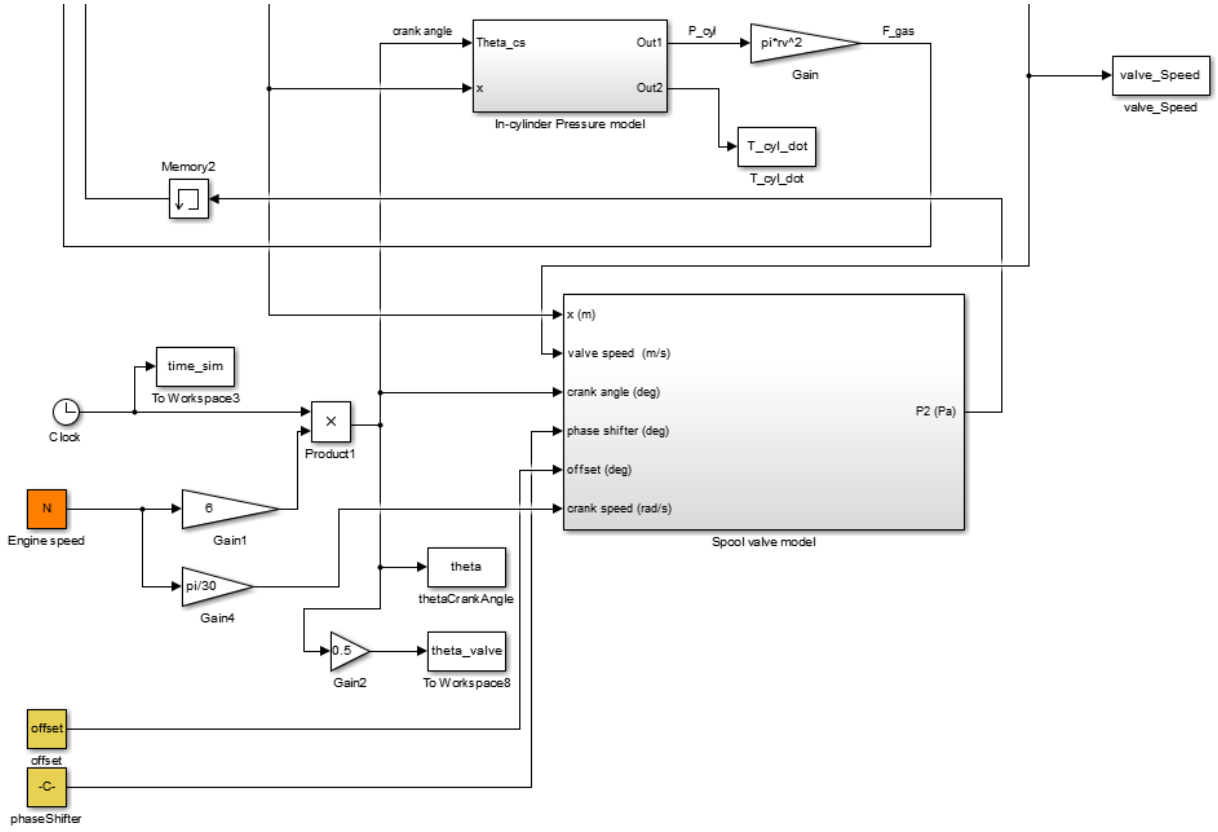

Figure A.2: Simulink model force balance... continued

Appendix B

Hardware Information

B.1 Electrical Components

Given below in Table B.1 is a list of electrical parts used in the HVVA experiments (sensors, encoders, etc).

Table B.1: Electrical Parts List

Part	Supplier	Part #	Description
Spool Valve Encoder	US Digital	S6-10000-250-IE-D-B	Optical encoder: 10000 cycles/rev, index, differential output
Spool Valve Stepper Motor	OMC Stepperonline	23HS41-1804S	Nema 23 CNC Stepper Motor 2.4Nm 1.8A 4.95V
Spool Valve Stepper Motor Drive	OMC Stepperonline	ST-6600	Max 4A Current 40VDC Input 16 Subdivision
Pressure Relief Valve	Wajax	ERV11010.000 12DG	12VDC PWM controlled - Relief at 1000 psi

Table B.1 Electrical Parts . . . Continued from previous page

Part	Supplier	Part #	Description
Valve Displacement Sensor	KSR International	-	Custom made 15mm, 0-5VDC, 2kHz update rate, +/-0.5% full scale accuracy, 4ms delay - induction sensor
Pump Servo	Emerson	DXM-340C	240V, 6.5A, 3000RPM, 1.54Hp Servo Motor
Pump Servo Drive	Emerson	LX-700	96-264 VAC 50/60 Hz
Pump Servo Drive	Emerson	LX-700	96-264 VAC 50/60 Hz
Pressure Sensor	Transducers Direct	TD1000DDG300 0003Q001M	0-3000 psi, 4-28 VDC input, 0-10 VDC output pressure transducer
Crankshaft Encoder	Encoder Products Company	EPC P/N 776-B-H-1024-R-PP-F-9D-A-Y-N	Optical encoder: Slim bore, 1024 cycles/rev, Quadrature A & B with Index

B.2 Hydraulic Components

Given below in Table B.2 is a list of hydraulic parts used in the HVVA experiments (seals, tubing, etc).

Table B.2: Hydraulic Parts List

Part	Supplier	Part #	Description
Pump	McMaster Carr	6296K37	Dispensing Pump 15.9gpm, $1.403 in^3$/rev, 2800 rpm, 3200 psi
Reservoir	McMaster Carr	62945K11	2 Gallon Hydraulic Reservoir
Oil Filter	McMaster Carr	9800K56	10 Micron, 3000 psi, 22 gpm, Hydraulic Oil Filter 3/4"-16

Table B.2 Hydraulic Parts . . . Continued from previous page

Part	Supplier	Part #	Description
Piston Rod U-Seal	McMaster Carr	9505K15	U cup seal 1/8" Wide x 1/8" High, 3/8" ID, 5/8" OD
Piston Rod O-ring Seal	McMaster Carr	9452K17	AS568-009seal 70A durometer
Cushion Device Check Valve	The Lee company	CKFA1876005A	Axial Flow 187 Lee Check Valve
Damping Idle Screw	RC Planet	HPI1474	HPI idle adjustment screw 0.21 BB
Spool Valve O-ring	McMaster Carr	1302N629	Buna-N 3.5 mm Wide, 44.7 mm ID, 51.7 mm OD
Spool Valve Rotary Seal	D&D engineered products	TVM100120-T40S	Turcon Roto Variseal, 2900 psi, 2m/s radial speed, flange seal, ID = 12 mm, OD = 17 mm
Seal Lubricant	McMaster Carr	1204K32	Seal and O-ring Grease Molykote 111
Flexible Tubing	Discount hydraulics	R2-06-ASB	3/8" SAE 100R2AT Hydraulic Hose Assembly - Ends: #4-SAE/ORB Male Swivel, 3/8" Stand Tube
Steel Tubing - Small	Swagelok	SS-T6-S-035-20	316/316L SS Tubing, 3/8 in. OD x 0.035 in. Wall x 20 Feet
Steel Tubing - Large	Swagelok	SS-T8-S-035-20	316/316L SS Tubing, 1/2 in. OD x 0.035 in. Wall x 20 Feet
Engine Head Gasket	eReplacement-Parts	12251-ZL0-003	Honda GX 200 Gasket- Cylinder Head
Engine Carburetor Gasket	eReplacement-Parts	16221-ZH8-801	Gasket- Carburetor for Honda GX 200

Table B.2 Hydraulic Parts ... Continued from previous page

Part	Supplier	Part #	Description
Engine Exhaust Gasket	eReplacement-Parts	16212-ZH8-800	Gasket- Insulator for Honda GX 200
Engine Cover Gasket	McMaster Carr	96165K51	Oil-ResistantCork Gasket between engine head and modified cover

B.3 Mechanical Components

Given below in Table B.3 is a list of important mechanical parts used in the HVVA experiments (springs, pulleys, etc).

Table B.3: Mechanical Parts List

Part	Supplier	Part #	Description
Engine Valve Spring - Light	McMaster Carr	9657K324	Compression Spring - K = 19.93 N/mm, Closed & FlatEnd,1"Long,0.76"ID
Engine Valve Spring - Heavy	McMaster Carr	9657K325	Compression Spring - K = 36.8 N/mm, Closed & FlatEnd,1"Long,0.72"ID, OD 0.97 "
Phase Shifter - Worm gear	SDP/SI	A 1B 6-N24072	Worm Gear 72:1 Gear Ratio, 72 Teeth
Phase Shifter - Worm	SDP/SI	A 1Q55-5N24	Right Hand Worm 24DP / 1 Lead / 0.5P.D., 4.76°lead angle, Ground finish
Crankshaft Pulley	Polytech Design Inc	57XL037	57 tooth aluminum pulley
Spool Valve Pulley	Polytech Design Inc	35XL037	35 tooth aluminum pulley

Table B.3 Mechanical Parts . . . Continued from previous page

Part	Supplier	Part #	Description
Timing Belt	Polytech Design Inc	828XL037	Timing belt 3/8" wide, 0.2" pitch, 414 Tooth, 82.8" Long
Belt Tensioner	Misumi	TNSR10-Y25-F8	Small timing belt tensioning unit
Idler Pulleys	Misumi	AFDF16-40	Idler Pulleys - Backside Tension Type, 10 mm shaft dia
Metal Joining Compound	McMaster Carr	91458A170	High-StrengthRetaining Compound Loctite660,0.2oz.Tube